**Electrochemically Triggered Interfacial Deposition/Assembly of Materials**

by

Md Shamim Iqbal

A dissertation submitted to the Graduate Faculty of
Auburn University
in partial fulfillment of the
requirements for the Degree of
Doctor of Philosophy

Auburn, Alabama
August 08, 2020

Key words: Self-assembled monolayers, ferrocene, electrochemical deposition, polyelectrolytes, colloids, nanomaterials



Approved by

Wei Zhan, Chair, Associate Professor of Chemistry & Biochemistry
German Mills, Professor of Chemistry & Biochemistry
Anne E. V. Gorden, Associate Professor of Chemistry & Biochemistry
William R. Ashurst, Associate Professor of Chemical Engineering

## ABSTRACT

Presented in this Dissertation is a new electrochemical methodology for surface deposition and interfacial assembly of materials. Using ferrocene-terminated self-assembled monolayers to electrochemically recruit polyelectrolytes and colloidal particles on electrode surfaces, I will detail herein the performance, mechanisms and application of this methodology. Specifically –

In Chapter I, a literature survey is given on research topics mostly related to this work: surface-bound electroactive molecular assemblies and interfacial assembly of materials. We find that several powerful and versatile strategies have been developed over the past few decades, enabling such broad applications as electrocatalysis, electrochemical sensors, molecular electronics, actuators, molecular photovoltaics, energy storage, and nanotechnology.

Chapter II describes a novel approach to surface deposition of polyelectrolytes on SAMs surface. This deposition process can be triggered facilely by a potential bias, which oxidizes ferrocene moieties included in the self-assembled monolayer to ferrocenium, whose charge compensation is fulfilled by polyelectrolytes and associated counterions. This approach is quite general, affording quantitative deposition of both polyanions and polycations with a wide range of chemical identities (synthetic polymers, peptides, and DNA) and molecular weights ($10^3$–$10^7$ Da as tested). Conventional layer-by-layer polyelectrolyte deposition can be straightforwardly combined with this method to produce electroactive polymer films. Several techniques, including voltammetry, fluorescence spectroscopy, contact angle analysis,

electrochemical quartz crystal microbalance (EQCM), and atomic force microscopy (AFM) were employed to characterize the deposition processes. A detailed discussion on the involved deposition mechanisms is also presented.

Presented in Chapter III are our findings on employing the same electrochemical trigger, ferrocene oxidation, to achieve interfacial assembly of aqueous-suspended colloid particles. Using carboxylic-terminated polystyrene nano-/microbeads as a model colloid, we confirm first their transfer to and deposition at such redox active surfaces. Key factors involved, including the starting electrode surfaces, colloid size, range/duration of applied potential, and small supporting electrolytes, are examined in detail using voltammetry, EQCM, and confocal laser scanning microscopy. A particularly interesting finding among these is the superior efficiency of the electrochemically triggered assembly compared to the electrically driven process. Taking advantage of this feature, we demonstrate fast, high-fidelity colloid micropattern formation on electrodes at the end.

In Chapter IV, the utility of this new methodology is further extended to other types of materials such as metal and metal oxides nanoparticles, quantum dots, multi walled carbon nanotubes (MWCNTs), and soft materials such as liposomes. We employed atomic force microscopy and confocal laser scanning microscopy to characterize those deposits and/or deposited materials on electrode surfaces. Using liposomes with well-defined surface charge, enabled us to demonstrate mechanistic differences utilizing this approach for deposition of materials with positive, negative and neutral surfaces respectively.

Finally, in Chapter V, I will draw the main conclusions of my studies and offer an outlook of what might be done in the near future along this direction.

TO MY PARENTS

## ACKNOWLEDGMENTS

First & foremost, I would like to offer my sincere gratitude to my research advisor, Professor Wei Zhan for his continuous support, guidance and encouragement. He always made himself available to me and offered his valuable guidance as a mentor. I found him as a patient and positive person, provided constructive remarks during tough times while acted as a source of inspiration. He has maintained high standard in all aspects, and I feel lucky that I received my doctoral training under his supervision. It is Dr. Zhan who taught me to think outside the box and look at things from a different perspective. He has not only helped me to attain a set goal (the degree) but also provided the space required for my personal development.

I'm sincerely grateful to all my advisory committee members including Professor German Mills, Professor Anne E. V. Gorden, Professor William R. Ashurst, and university reader Professor Maria L. Auad for their time and valuable suggestions on this research work. Special thanks are extended to Professor Ashurst for helping me with contact angle measurements in his lab, and to Professor Gorden for allowing me to use the UV-Vis spectrometer in her lab.

I'm thankful to all my lab mates and co-workers including Dr. Mingming Wang, Zening Liu, Jinyan Cui, Hui Jin, Chao Li for their friendship and support. Special thanks to Dr. Wang for his assistance on learning different tools/techniques in our lab. I found him amicable and helpful.

I'm grateful to the Department of Chemistry & Biochemistry, College of Science and Mathematics (COSAM), Graduate School, and Office of International Programs at Auburn University for their support throughout my graduate study at Auburn. I would also like to

mention National Science Foundation (NSF) for their support through a grant (CHE-1808123) which partially supported my research at Auburn.

I'm deeply and genuinely grateful to my family members specially my parents, my wife, my brother Dr. Md Shakil and my sister Shahina Sultana for their love, support and prayers. I would like to specially mention my lovely wife Sayma Afrin Esha for her love, support, encouragement and heartfelt consideration in all situations. I also feel lucky to have two caring and supportive siblings besides me. I'm also thankful to all my friends, relatives and well-wishers for their support. Finally, I solemnly dedicate this dissertation and all achievements in pursuit of PhD degree to my beloved parents, my mother Ibnul Hasnat and my father Dr. Hefazuddin Ahmed (late) for their unconditional love, sacrifices, encouragement, endless support and prayers throughout my life.

## TABLE OF CONTENTS

## LIST OF TABLES

## LIST OF FIGURES

## LIST OF ABBREVIATIONS

| | |
|---|---|
| μCP | Microcontact Printing |
| 1D | One Dimensional |
| 2D | Two dimensional |
| 3D | Three dimensional |
| AFM | Atomic Force Microscopy |
| Au NPs | Gold Nanoparticles |
| Bodipy-Cholesterol | 23-(dipyrrometheneboron difluoride)-24-norcholesterol |
| C12SH | 1-dodecanethiol |
| CCD | Charge-coupled Device |
| CLSM | Confocal Laser Scanning Microscopy |
| CMOS | Complementary Metal Oxide Semiconductor |
| CNTs | Carbon Nanotubes |
| CQDs | Colloidal Quantum Dots |
| CV | Cyclic Voltammetry |
| DNA | Deoxyribonucleic Acid |
| DOTAP | 1,2-dioleoyl-3-trimethylammonium-propane (chloride salt) |
| DSC | Differential Scanning Calorimetry |
| $E_{fwhm}$ | Full-width at Half-maximum |
| EO | Electroosmosis |

| | |
|---|---|
| EOF | Electroosmotic Flow |
| $E_{pa}$ | Peak Oxidation Potential |
| $E_{pc}$ | Peak Reduction Potential |
| EQCM | Electrochemical Quartz Crystal Microbalance |
| Fc | Ferrocene |
| $Fc^{+}$ | Ferrocenium |
| FCA | Ferrocenecarboxaldehyde |
| Fc-C11SH | 11-Ferrocenyl-1-undecanethiol |
| FETs | Field-effect Transistors |
| FTIR | Fourier Transform Infrared |
| GC | Glassy Carbon |
| HOPG | Highly Oriented Pyrolytic Graphite |
| $I_{pa}$ | Anodic Peak Current |
| $I_{pc}$ | Cathodic Peak Current |
| ITO | Indium Tin Oxide |
| IUPAC | International Union of Pure and Applied Chemistry |
| LbL | Layer by Layer |
| LED | Light Emitting Diodes |
| LSV | Linear Sweep Voltammetry or Linear Potential Sweep |
| MWCNTs | Multi-walled Carbon Nanotubes |
| NCs | Nanocrystals |
| NMR | Nuclear Magnetic Resonance |

| | |
|---|---|
| NPs | Nanoparticles |
| OM | Oosawa-Manning |
| PAA | Poly(acrylic acid) or Poly(acrylic acid sodium salt) |
| PDADMAC | Poly(diallyldimethyl ammonium chloride) |
| PDDA | Poly(diallyldimethylammonium chloride) |
| PE | Polyelectrolytes |
| PEI | Poly(ethylenimine) |
| PFcMA | Poly(2-(methacryloyloxy) ethyl ferrocenecarboxylate) |
| PL | Poly(L-lysine hydrochloride) |
| PLL | Poly-L-lysine |
| POPC | 1-palmitoyl-2-oleoyl-glycero-3-phosphocholine |
| POPG | 1-palmitoyl-2-oleoyl-sn-glycero-3-phospho-(1'-rac-glycerol) (sodium salt) |
| PS-COOH | Carboxylate Polystyrene |
| PSS | Poly(styrenesulfonic acid) or Poly(styrene sulfonate) or Poly (styrene sulfate) |
| PVFc | Polyvinylferrocene |
| QCM | Quartz Crystal Microbalance |
| QDs | Quantum Dots |
| $Q_{tot}$ | Total Charge |
| RS· | Thiyl Radical |
| RSA | Random Sequential Adsorption |
| SAMs | Self-Assembled Monolayers |
| SCE | Saturated Calomel Electrode |

| | |
|---|---|
| SCNCs | Colloidal Semiconductor Nanocrystals |
| $SC_nFc$ | Fc-terminated Alkanethiol |
| SEM | Scanning Electron Microscopy |
| SPR | Surface Plasmon Resonance |
| SUVs | Small Unilamellar Vesicles |
| TEM | Transmission Electron Microscopy |
| THF | Tetrahydrofuran |
| TnT | Trigger-and-Trade |
| UHV | Ultrahigh Vacuum |
| VFC | Vinylferrocene |
| XPS | X-ray Photoelectron Spectroscopy |
| XRD | X-ray Diffraction |
| XRR | X-ray Reflectometry |

# CHAPTER 1. INTRODUCTION

Design of surface confined molecular architectures with advanced functionalities offers tailored and controlled chemical, physical, optical and electronic properties.[1] Electroactive molecular assembly have attracted much attention not only because of economic and convenient operations but also offers structure-properties correlation and tunability.[2] Redox modified electrodes with unique and desired properties can be used in electroanalytical and electrochemical sensors, molecular electronics, electrocatalytic energy conversion devices, energy storage, nanotechnology, biology, and so on.[2,3,4] Coadsorbed materials are known to modify the properties of electrode surface by changing the local environment of the redox species.[3] Therefore, a crucial step is to develop devices/methodologies which will not only inherit the advantages of surface confined redox species but also capable of tuning the redox environment to offer improved functionality and controllability.

This chapter starts with redox active surfaces, and their preparation. Following that, redox active self-assembled monolayers (SAMs) will be discussed while putting special emphasis on ferrocene terminated alkanethiols monolayers on gold and its electrochemical properties. After that, interfacial deposition/assembly of polyelectrolytes, water suspended colloids, and other materials will be discussed respectively. This chapter is concluded with the scope of this dissertation *i.e.* what this study intends to accomplish.

## 1.1 Redox active surfaces

Surface modification with electroactive species has been practiced in order to take advantage of

specific properties that such redox species exhibit in solution.[3] Surface-bound redox molecules not only form an optimized surface but also offer improved electrode/electrolyte interfacial properties.[5] Surface confined redox assemblies are superior to solution based redox species because of several reasons: (i) they provide ordered and densely packed arrangements that can lead to stronger and specific interactions which ensures fast responses, (ii) they are compatible with different media, (iii) may offer high sensitivity, and (iv) may ensure reproducibility in responses/results through stable electrochemical responses.[6] Additionally, a small amount of the redox species is required usually for structured surface assembly compared to required concentration in liquid media to attain similar electrochemical activity. Three major factors are important for immobilization of redox species on electrode surfaces: a redox molecule, a substrate or support, and a mode of attachment. The characteristic of the substrate is important in determining the effectiveness of the system while the mode of attachment may lead to changes in the chemical and physical properties of the redox species upon immobilization.[7] Redox species are often part of the integrated chemical entities with functionalities designed and compatible for surface binding either through physical or chemical interaction.

### 1.1.1 Choice of substrate.

Although there are no ideal supports/substrates for the immobilization of redox species, certain characteristic of the matrix such as ability to furnish chemical or physical interaction, mechanical or electrochemical stability, electron transfer kinetics, cost efficiency, etc. are generally considered important during selection of substrates/supports/matrices. Different substrates offer variable properties like hydrophobicity, surface functionality, and their difference in morphology and physiochemical properties can affects activity of redox species. Commonly used substrates are gold[8,9,10], indium tin oxide (ITO) coated surfaces[11,12,13], silicon substrates such as both n-type

and p-type monocrystalline Si(111)[14,4,15,16], glassy carbon (GC)[17,18] electrodes, etc. Substrates like other metal surfaces such as Cu[10,19], Ag, Al[10], silicon microwire arrays[20], mica, carbon-based electrodes such as vitreous carbon, graphite, highly oriented pyrolytic graphite (HOPG)[18,21], etc. are also reported. Each of these electrodes offers advantages or disadvantages. The choice of support is often made based on factors related to the application and the nature of the system. For example, gold as a substrate is easy to obtain in the form of thin films and as a colloid, easy to pattern, conductive, and reasonably inert to atmospheric gases.[2] Thiolate anchored molecular assemblies on gold is one of the most studied platforms that provides a stable, flexible and organized assembly which can be easily characterized with many surface characterization tools. Silicon substrates such as molecularly modified $SiO_x$ substrates can withstand high temperature and are useful in the semiconductor industry. $SiO_x$ substrates like glass and quartz enable optical readout and do not quench fluorescence. ITO coated surfaces, on the other hand, provide highly conductive surfaces like metals while offering electrochemical and spectro-electrochemical detection capabilities.[6]

### 1.1.2 Immobilization methods.

Selection of an appropriate method for immobilization of redox species plays an important role determining the activity and surface bound properties of the redox molecule. Redox species are immobilized on electrode surfaces usually by two main strategies: physical adsorption or chemisorption.[22,23] Physical immobilization methods are characterized by non-covalent interaction such as van der Waals forces, hydrophobicity, electrostatic attractions, hydrogen bonding, etc.[21] Chemical immobilization is largely accomplished by covalent bond formation of integrated redox species with different substrate surface.[24] Chemically modified surfaces with functional groups can react and form covalent bond with redox terminated chemical entities.[25]

### 1.1.2.1 Physical adsorption

Physical adsorption is one of the straightforward methods for reversible attachment of chemical entities terminated with a redox molecule on substrate surface. Adsorption usually can occur through non-specific forces such as van der Waals, hydrophobic interactions, π-interactions, electrostatic interaction and hydrogen bonds.[21]

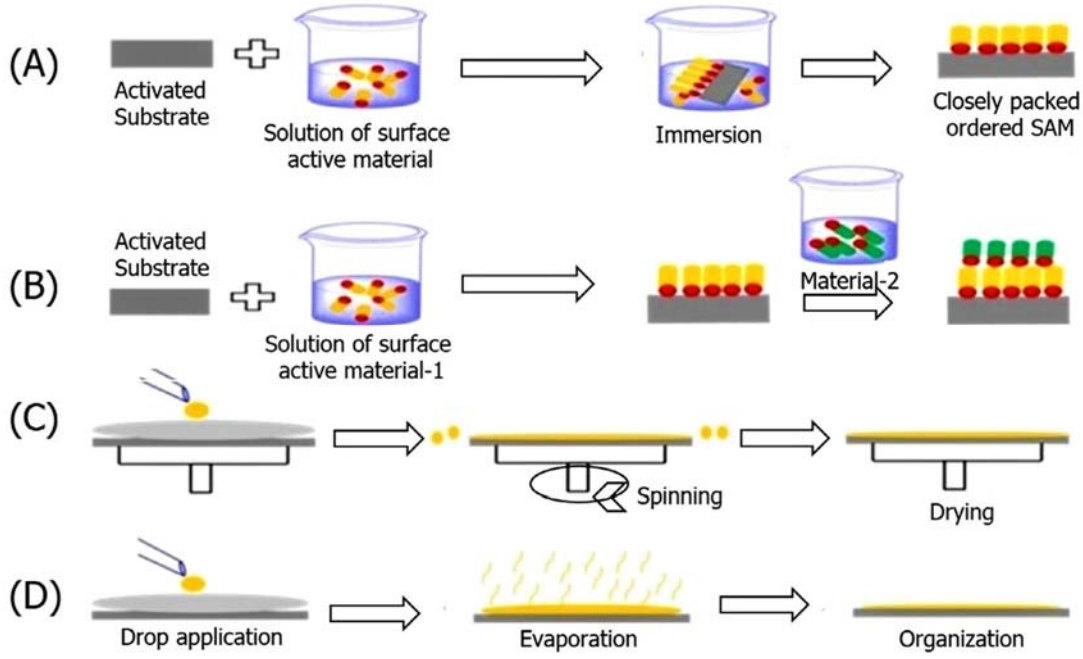


**Figure 1. 1** Schematic representation of various routes for assembly of materials on surface through physical adsorption (A) Incubation, (B) Layer by Layer (LbL) assembly, (C) Spin-coating, and (D) Drop casting. Reprinted with permission from *Coordination Chemistry Reviews*, **2017**, *330*, 144–163. Copyright (2017) Elsevier.

Physical adsorption usually requires soaking or incubation of substrates into a solution containing the redox species or redox containing chemical entities.[7] Other ways are Layer by Layer (LbL) assembly, spin coating, drop casting, patterning of surface by stamping, etc.[6] LbL assembly is obtained starting with a charged surface and subsequent formation of layers by

electrostatic attraction between alternatingly charged materials with brief wash step in between.[26] Drop casting is allowing a solution of redox species to dry on the substrate surface and then wash away non-adsorbed material through rinsing/washing.[6] Spin coating is a method in which thin films of materials are formed on substrate surface by using centrifugal force. It consists of several steps such as dispensing of material containing solution on surface, spin up, stable fluid outflow, spin off, and drying.[27] Patterning of surface with materials of interest involves inking of stamp by materials of interest and then mechanically stamping on substrate surface.[28]

These approaches are often accompanied by drawbacks such as desorption of redox species or leakage of redox species into solution. Substrates/supports/surfaces with physical interaction capabilities are often limited while some form of chemical modification is required to activate the surface for such interaction to take place. However, physical adsorption can be used to form many useful redox active surfaces through a hybrid attachment approach which is a combination of sequential chemical and physical adsorption processes. For example, Yang and co-worker has developed an alternative approach for non-covalent attachment by using hybrid non-covalent attachment of redox species on electrode surfaces. They derivatized a gold electrode with a sulfur-substituted pyrene and then physisorbed a pyrene-terminated ferrocene onto the modified gold electrode.[7] Surfaces produced through such strategy are showed improved electron transfer kinetics compared to reasonably similar systems obtained through covalent bonding of redox active species on surfaces.[29]

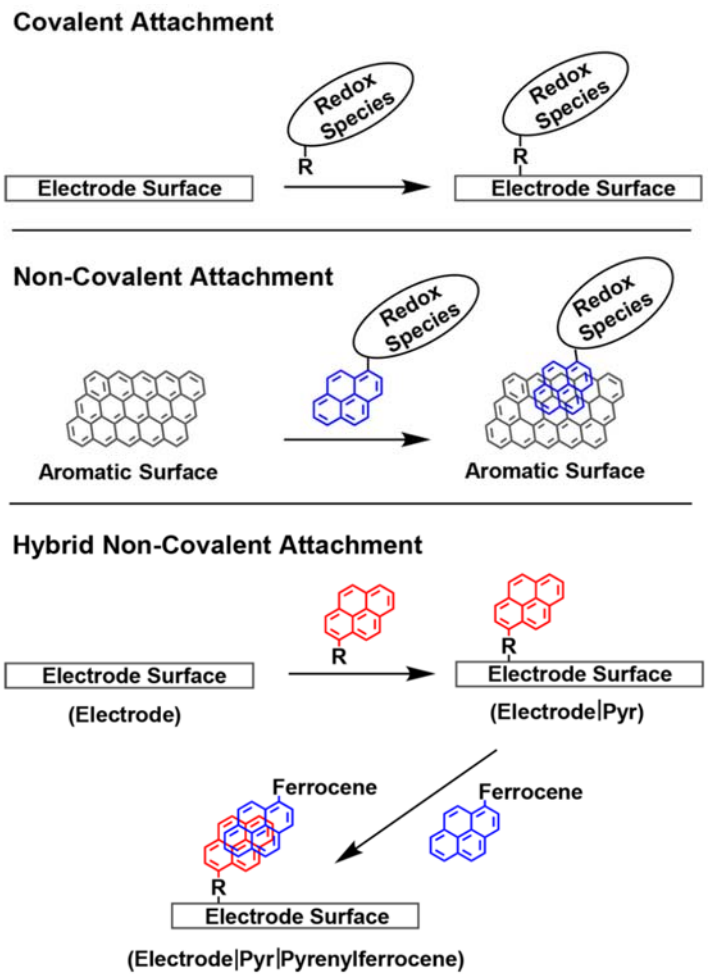


**Figure 1. 2** Methods for molecular attachment to electrode surfaces: conventional attachment vs hybrid non-covalent attachment. Reprinted with permission from *ACS Appl. Mater. Interfaces* **2018**, *10*, 13211−13217. Copyright (2018) American Chemical Society.

### 1.1.2.2 Chemical adsorption

Chemical adsorption of redox species on surface usually involves two major strategies: covalent bonding and cross-linking.[30] Both of these methods involve irreversible immobilization. Formation of a covalent bonds between redox terminated chemical entities and the surface of the substrate is probably the most widely used chemical adsorption strategy. In the 1980's, Murry & co-worker demonstrated chemical modification of metal surfaces with redox active metal

complexes. At that time, they showed covalent attachment through coupling of Ru-complexes- and ferrocene terminated compounds with alkylamine-silanized Pt/PtO-surface.[31,32] This strategy requires silanization of metal surfaces followed by coupling of surface bound amines with -COOH terminated redox containing compounds. In 1990, Chidsey & co-worker showed a simpler strategy for formation of redox active self-assembled monolayers on gold through the co-adsorption of a ferrocene terminated unsubstituted alkanethiol to form a mixed SAMs.[33] Ever since, this kind of metal-thiolate covalent bond formation is one of the most commonly used strategies to confine redox species on surface because this ensures unnecessary interactions between redox centers. There are reports describing formation of SAMs with organosulfur compounds on other metals, such as palladium, silver, copper, and mercury where different metal surfaces demonstrate very different reactivity towards sulfur compounds.[2] Reports on the use of SAMs containing ferrocene terminated alkanethiol on gold, and their use in redox controlled maneuvers will be discussed in a later section.

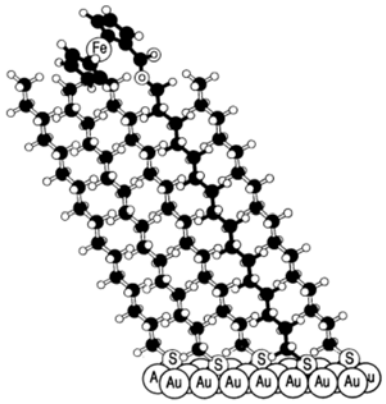


**Figure 1. 3** Inferred structure of the monolayer formed by coadsorption of a ferrocene-terminated alkanethiol and an unsubstituted alkanethiol on Au (111). Reprinted with permission from *Science* **1991**, 251*(4996)*, 919-922. Copyright (1991) American Association for the Advancement of Science.

Scientists around the world choose Si as their substrate of choice because, Si is the second most abundant chemical element on earth, its mass production as high purity crystalline form, and its semiconducting character.[30] Zanoni & co-workers reported immobilization of vinylferrocene (VFC) on Si(100) while studing the SAMs of VFC molecules anchored on Si(100) through Si-C-C-Fc linkages with those of ferrocenecarboxaldehyde (FCA) molecules anchored through Si-O-C-Fc linkages.[34,35] Sugimura & co-worker followed up with similar studies using thermal activation of VFC and FCA molecules with hydrogen-terminated Si(111) substrate to compare their reactivities.[36] Fabre & co-worker showed derivatization of monocrystalline Si (111) surfaces with alkanethiol monolayers terminated by ferrocene. This involves attachment of an amine-substituted ferrocene derivative to a pre-assembled acid-terminated alkyl monolayer using carbodiimide coupling.[14] Tour & co-workers reported surface grafting of ferrocene containing triazene derivatives on Si (100).[15] Gooding & co-worker demonstrated in-situ immobilization of ferrocene derivatives using "click" chemistry of alkyne-terminated alkyl monolayers on highly doped Si(100) surface.[25] Following these reports, many studies were conducted on ferrocene containing compounds with different functionalities immobilized on Si-substrates.[24,16,30] Gallei & co-worker reported immobilization of end-functionalized polyvinylferrocene (PVFc) and poly(2-(methacryloyloxy) ethyl ferrocenecarboxylate) (PFcMA) on $SiO_2$ substrates.[37] Freund and co-workers demonstrated coadsorption of vinylferrocene (VFC) derivatives and non-redox alkyl derivatives on silicon microwire arrays.[20] Reports on chemical immobilization of entities terminated by redox species can also be found on other substrates. The methods discussed involves chemical interaction between redox species or their derivatives and substrates. Moreover, some require secondary activation to activate the surfaces towards useful electrochemical interaction. Therefore, simpler methods for surface modification is desired.

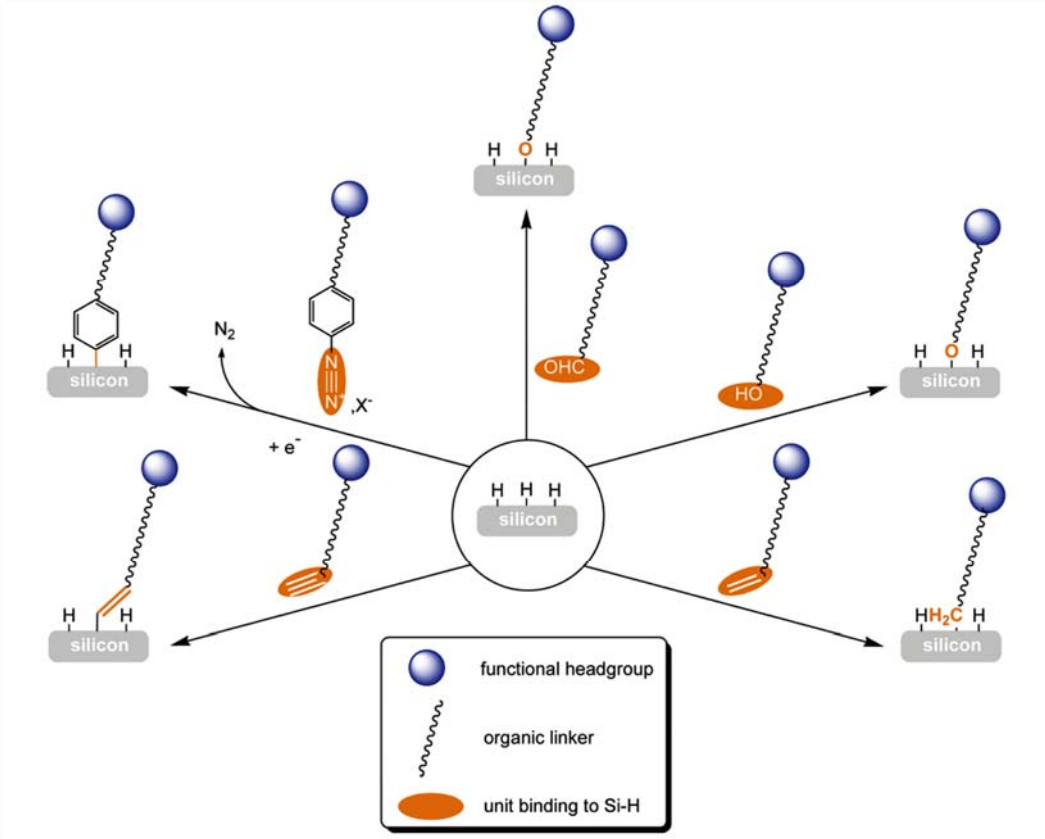


**Figure 1. 4** Direct Covalent Attachment of α,ω-Disubstituted Bifunctional Molecules to Si-H. Reprinted with permission from *Accounts of Chemical Research*, **2010**, *43*, 1509-1518. Copyright (2010) American Chemical Society.

### 1.1.3 Different surface bound redox species.

Due to the stability at higher temperature (up to 400 °C), reactivity as an electrophile, well behaved redox capability, and comparatively easy to derivatize, ferrocene have been used extensively as surface bound redox species.[38] Quinones and their derivatives are organic compounds which experience proton coupled electron transfer.[39] The biological importance of quinones has prompted numerous studies not only analyzing their electrochemical properties but also utilizing them in many redox controlled maneuvers.[40,41] Reports of using surface confined quinone[42,43], hydroquinone[44], and anthraquinone[41,45,46] terminated chemical entities, and other

quinone derivatives[47,48] on different substrates are numerous. Studies of other surface bound redox species especially redox active complexes and catalyst/electrocatalyst, have been reported on various substrates.[49,50]

### 1.2 Ferrocene terminated self-assembled monolayers (SAMs) on gold

Self-assembled monolayers (SAMs) on solid substrates are organic assemblies formed by adsorption of molecular entities onto the surface of solids.[2] Chemical compounds that form SAMs usually have an attached functional group as a head group with specific affinity for a substrate. For example, thiols have special affinity to noble and coinage metals which makes it possible to form well organized assemblies on surfaces of gold, silver, copper, palladium, amongst other.[2]

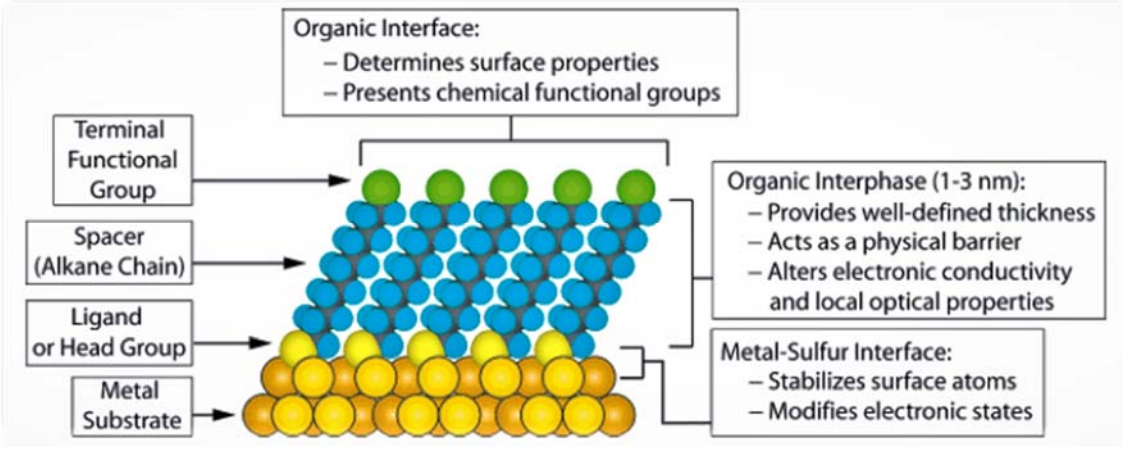


**Figure 1. 5** Schematic diagram of an ideal, single-crystalline SAM of alkanethiolates supported on a gold surface with a (111) texture. The anatomy and characteristics of the SAM are highlighted. Reprinted with permission from *Chemical Reviews*, **2005**, *105*, 1103-1169. Copyright (2005) American Chemical Society.

Among all the platforms discussed in previous sections, self-assembled monolayers (SAMs)

composed of ferrocene containing alkanethiols on gold are probably the most studied platform due to the following reasons: (i) they are easy to prepare *i.e.* do not require in-situ chemical treatment, or other specialized conditions or equipment such as ultrahigh vacuum (UHV) during preparation, (ii) alkanethiols can be easily modified and are available in different chain lengths which offer different electron transfer kinetics to serve as a controlling factor, (iii) they are easily tunable media which link molecular-level structure to interfacial properties, (iv) they are a flexible and simple system that can be easily characterized with surface characterization tools.[2] In this section, self-assembled monolayers (SAMs) formed from ferrocene terminated alkanethiols (and their derivates) on gold, and their associated redox maneuvers will be discussed in brief.

### 1.2.1. Why gold?

Gold is historically the most studied substrate, and gold forms adequate SAMs although this metal is not uniquely good. For many applications Au may not be the substrate of choice but there are many reasons for which gold is a very good substrate to prepare SAMs: (i) gold is easy to obtain in pure form, (ii) thin films and colloids of this metal can be obtained, (iii) the malleable nature of this material enables simple shaping, as well as ease of patterning by lithography or other etching methods, (iv) easy to clean as gold is reasonably inert, and is not attracted by atmospheric gases and most other chemicals, (v) gold binds thiols with reasonably high affinity[51], (vii) gold substrates are very common supports used for a number of characterization methods such as atomic force microscopy (AFM), surface plasmon resonance (SPR), ellipsometry, quartz crystal microbalance (QCM).[52,53]

Other substrates show many of the above mentioned properties exhibited by gold but SAMs formation on those materials have been studied compared to gold. Silver is the second most

studied substrate after gold.[2] Although silver forms simple and high quality SAMs, this metal readily oxidizes under air[54], and is also toxic to some biological materials.[55,56]. Copper can be good choice because this is cheaper metal used in many conductive materials, but Cu is even more susceptible to oxidation than silver.[54] Palladium seems to be a formidable alternative to gold since it has some superior quality than gold such as smaller grain size than gold thin films[57], compatibility with CMOS (complementary metal oxide semiconductor)[58], offers catalytic properties, equal or less than the cost of gold. Although Pd is a competitor to gold as a choice of substrate, the availability of Pd, use in different forms, and compatibility to characterization tools are not as viable as gold.

### 1.2.2 Ferrocene

Ferrocene is the first example of a large class of compounds known as metallocenes, also known as sandwich compounds.[59] Ferrocene consists of two cyclopentadienyl rings sandwiched on opposite sides of a central iron atom. Since first reported in 1951 (discovery in 1940) by Pauson and Kealy[60], ferrocene has become one of the most studied redox species mainly because of several exceptional properties: (i) stability up to 400 °C, well over its melting temperature of 172.5 °C, (ii) reactivity as aromatic nucleophile[61], (iii) exhibits mild and reversible oxidation at around +0.4 V versus the saturated calomel electrode (SCE), and (iv) good stability in air.[38] For all these excellent properties along with the high solubility in many common organic solvents, and a huge number of derivatives synthesized in the last 70 years. For these reasons, ferrocene has become an icon in organometallic chemistry.[38]

Ferrocene owes its stability probably to the existence of two aromatic cyclopentadienyl rings. When one proton is removed from the cyclopentadiene molecule, $C_5H_6$, the resulting anion becomes the aromatic cyclopentadienyl ion, $C_5H_5^-$; giving rise to a situation where instead of ten

electrons holding the ring together via five single carbon–carbon bonds, there are now six extra electrons delocalized above and below the ring. This is very similar to the situation of aromatic systems and thus yield a aroused stability analogous to that observed in the benzene molecule, $C_6H_6$. This similarity to benzene perhaps made Woodward suggest the name ferrocene for $[Fe(C_5H_5)_2]$. This name was quickly accepted by the chemists around the world, and later compounds of the general composition $[M(C_5H_5)_2]$, found their general name as metallocenes.[59]

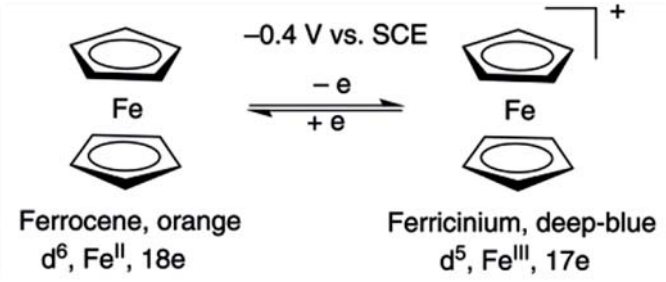


**Figure 1. 6** Reversible oxidation of ferrocene around +0.4 V versus sat. calomel electrode (SCE). Reprinted with permission from *European Journal of Inorganic Chemistry* **2017**, *1*, 6-29. Copyright (2017) John Wiley and Sons.

Mild oxidation of ferrocene by, for example, iodine, $FeCl_3$, etc. yields a stable blue ferricinium salt that can be reduced back to ferrocene with, for example, an acidic aqueous solution of $TiCl_3$, thiosulfate or by other mild reductants.[38] Ferrocene shows reversible single-electron (1e) redox wave upon anodic oxidation at around 0.4 V versus SCE.[62] The actual redox potentials depend on the solvent because the positively charged central ion interact differently with different solvents.[63] Ferrocene has been extensively used for internal standard for redox processes. As this potential really depends on nature of the medium, now-a-days people tend to use decamethylferrocene or other permethylated metallocenes as a more reliable references because, in the latter cases the central ion is protected from interacting with solvents by the cage of ring

methyl groups.[64] Surface bound ferrocene may show a slightly different redox behavior depending on the nature of the substrates, chain length of the alkanethiols or other chemical entities, heterogeneity of the system. Details about the organization and behavior of surface confined ferrocene will be discussed in a later section.

Electrochemical reversibility *i.e.* electron transfer from ferrocene to anode and back transfer between ferrocenium and anode are fast in the time scale of potential scan in cyclic voltammetry (CV).[33] The fast electron transfer process is probably due to no significant structural change (no bond is broken/created during oxidation/reduction) during oxidation, as the structures of ferrocene and ferrocenium are very similar. During oxidation, Fe-C bond lengthening is in the order of 0.1 Å.[65] Fast electron transfer and easy oxidation made ferrocene and its derivatives major candidates in the field of redox catalysis, electrochemical sensing, medicine, and materials science.[38,59]

### 1.2.3. Preparation of ferrocene terminated alkanethiol SAMs on gold

In 1983, Nuzzo and co-workers first demonstrated the formation of self-assembled monolayers of disulfides on gold substrates.[51] In early studies, scientists largely reported adsorption of organosulfur compounds from solution or vapor phase onto gold.[33,52,66,67] Since early 1990, studies on a variety of ligands with limited functionalities have continued to focus on SAMs formed form thiols.[54,68,69] After that, during last two decades scientists have developed technologies to form alkanethiol SAMs on gold with different derivatives of alkanethiols, with various functionalities, and redox capabilities, utilizing different methods. Fabrication of such assemblies can be done by both bottom-up (e.g., self-assembly) or top-down (e.g., micropatterning) methods.

Gold substrates used for SAM formation range from planer surfaces (thin films, foils, single crystals, etc.) to highly curved nanostructures (colloids, nanocrystals, nanorods, etc.). Alkanethiol SAMs on gold surface can be prepared either by adsorption of alkanethiols from solution or from gas phase. In either case, cleanliness of substrate is a must since any contaminants on the surface will affect the kinetics of SAM formation. It is recommended to use the substrates within an hour of preparation or cleaned with strong oxidizing agent such as piranha solution (3:1 of $H_2SO_4$:$H_2O_2$ ) or oxygen plasmas.[2] Purity of thiols are also crucial for the formation of homogeneous and well organized SAMs. Common impurities in thiols are disulfide (which are oxidation products) that are less soluble than the thiol precursors, hence more likely to physisorbed on the surface and alter the physical properties of SAM. Experiments suggest that, <5% of such impurities in thiols do not significantly impact the quality of SAMs.[70,71]

Adsorption of thiols from a solution is very convenient and sufficient for most applications. Usually a number of factors are required to be considered such as solvent, temperature, concentration and immersion time, oxygen in solution. Ethanol is the most used solvent for alkanethiols along with tetrahydrofuran, dimethylformamide, acetonitrile, toluene.[71] While quality of SAMs prepared from these solvents is not much different from one prepared from ethanol but such alcohol is frequently used due to several reasons: (i) $CH_3CH_2OH$ solvates variety of alkanethiols, (ii) it is inexpensive, and available in high purity, and (iii) exhibits low toxicity. Although SAMs are usually prepared at room temperature, studies suggest that preparation of SAMs above 25 °C helps improve the kinetics of formation and reduces the number of defects.[72,73] Concentration and incubation time are inversely related as lower concentration of thiols require longer incubation and vice versa.[74] Concentration required for forming an alkanethiol SAM on gold is minimum of ~1 μM or higher.[51] Although studies suggests that, SAMs prepared using different thiol concentrations differ in physical properties.[71]

In general, SAMs prepared from incubation of substrates in solution with ~1 mM thiol for 12-18 hours results in densely packed well organized assemblies.[2]

### 1.2.4. Gold-thiolate bonds

The foundation to form robust SAMs of alkanethiol, arenethiol and disulfide compounds on gold is provided by the strength of the Au-S bond. Despite of fundamental advances, the dissociative chemistry of the S-H or S-S on gold leading to the formation of the sulfur–gold is still a matter of debate.[2]

It is widely accepted that, covalent interaction at Au-S interface requires formation of gold-thiolate bond.[75] It has long been speculated and, also in some cases experimentally claimed that the formation of an Au-S bond is due to the cleavage of a S-H and S-S bond: the sulfhydryl group (R-SH) is cleaved to form a thiyl radical (RS·).[66] On the other hand, the protonated one *i.e.* SH group can interact with gold only by weak coordination type bond. [65,66] The Au-S bond is suggested to be a strong one -homolytic-[2], and the binding energy of thiolates to the planar gold surfaces is experimentally determined.[76,77,78] However, the fate of the hydrogen of the S-H group has not been decided unambiguously as yet. The possibility that the loss of hydrogen may result in $H_2$ formation has been discussed, and oxidative conversion of hydrogen to water is speculated in presence of oxygen in the reaction media.[2] Kankate & co-workers suggested the release of hydrogen during the formation of SAMs of thiols on gold.[78] On the contrary, in 2019, Inkpen and co-workers claimed that Au-S bond in SAMs prepared from solution deposition of dithiols is free of any chemisorbed character.[79]

Reasonable conclusions are that, the true nature of the dissociation chemistry of S-H and S-S bonds during SAMs formation, and that the actual chemical characterization of Au-S bonds

within the SAMs of thiols on gold are still matter requiring further investigations.

### 1.2.5. Fc-terminated alkanethiol SAMs, their electrochemistry and redox maneuvers

Fc-terminated alkanethiol (in short $SC_nFc$) SAMs serve as model systems to study the redox behavior of immobilized redox species on electrodes. Therefore, the electrochemical behavior of those SAMs in relation to their structure is an important outcome, which has been studied intensively. For a reversible one-step one-electron process, a single and symmetrical redox wave should be observed in cyclic voltammograms.[65] This ideal behavior is observed when redox active species in SAMs do not interact with each other, and electron transfer is fast enough on the experimental time scales. In practice, ideal behavior is rare while non-ideal behavior is ascribed to the inhomogeneity of terminal redox active species in SAMs.[80] In Fc-SAMs, this behavior depends on the electrochemical environments of the Fc-units within the SAMs. The electrochemical environment of the Fc-moiety within SAMs depends on a number of factors including - but not limited to – the packing density of Fc-terminated thiols, the number of carbons (odd or even) in the Fc-terminated alkanethiols, presence of other functional group in Fc-terminated thiol or other thiols within the SAM (in case of mixed SAM), as well as the types of anions in solution, nature of the solvent.

Chidsey and co-workers found a reversible CV responses from mixed SAMs of $FcCO_2(CH_2)_nSH$ and $CH_3(CH_2)_nSH$ when formed at low mole fraction of Fc-thiol ($\chi_{fc} < 0.25$).[33,81] In their investigation they also observed that, increasing the fraction of Fc-thiols make the CV response less symmetric while the anodic peak response shifted to more positive potential vs Ag/AgCI in saturated KCl.[33] The authors ascribed this non-ideal breakdown in this system to a combination of factors such as Fc-Fc interactions and inhomogeneity of Fc-moiety on those sites with increasing Fc-concentration on surface. This kind of peak broadening is also reported by others

as the fraction of Fc-terminated thiol increases in mixed SAMs.[82,83,84] Ju and co-worker reported that, SAMs prepared from a mixture of $Fc(CH_2)_{11}SH$ and $CH_3(CH_2)_{11}SH$ with different proportions displayed different peak shapes and potential separations while the most ideal electrochemical responses were obtained from SAMs prepared from a 50:50 thiol solution.[85] Even the number of carbons in the Fc-terminated alkanethiol chain can impact the outcome or electrochemical behavior, because the tilt angle of the ferrocene group will depend on the number of $-CH_2$ units on the alkane chain.[86,87] Since the Au−S−C bond angle is essentially similar in all SAMs, the angle of the ferrocene function with respect to the surface are different for odd or even number of $-CH_2$ unit within the alkane chain.[88] These so called "odd-even" effects can affect many properties of the SAMs, such as stability[89], wettability[76], and packing density.[90] Moreover, in mixed SAMs, if the number of $-CH_2$ units in the alkanethiol changes while keeping the Fc-thiol fixed, this can alter the surrounding of the redox species and hence the electrochemical response.[91] Creager and co-worker reported mixed SAMs of $Fc(CH_2)_6SH$ and $CH_3(CH_2)_nSH$, where they found that increasing the chain length of the alkanethiol (n = 4 to 12) shifts the redox potential to more positive values.[68] These shifts are predominantly thermodynamic in nature because the anodic and cathodic peak potentials both shifted together.

In pure Fc-SAMs (*i.e.* SAMs constructed with the Fc-CnSH thiol only), varying the values of n can change the supramolecular interactions (i) - (v) depicted in Figure 1.7 by Nijhuis and co-workers.[80] Interplay of these interactions not only determines the structure and composition of the SAMs but also impact the electrochemical behavior of the redox species within SAMs, in this example ferrocene. Nonideal electrochemical responses of ferrocenyl alkanethiolates due to intermolecular interactions within $Fc\text{-}C_nS\text{-}Au$ SAMs were also explained by Yu and co-workers.[92] Moreover, the position of ferrocene within the alkyl chain can impact the electrochemical behavior and properties of SAMs as reported by Nijhuis and co-workers. They

inserted Fc-groups at 14 different positions along the alkyl chain ($FcC_{13-n}SH$, n = 0 -13) and studied them by cyclic voltammetry.[93] Differences in the connector group to which the ferrocene is attached (e.g. $-CH_2$, -C=O, O-C=O, -O=CNH, etc.) in the Fc-terminated alkanethiol can impact the electrochemistry of the SAM as described by Nijhuis and co-worker.[94] This is because the nature of the connector group not only determines the tilt angle of the ferrocene with respect to surface but also impacts the electron donating capability of ferrocene due to the presence of different functional groups. Similar observations were made by Yokota & co-workers where they showed the effect of electron donating connector groups in Fc-SAMs.[95] In mixed Fc-SAMs, alkanethiols modified with hydrophilic functional groups such as -OH, -COOH, $-NH_2$, etc. can impact the composition of SAMs and solvation of the SAMs surface.[91]

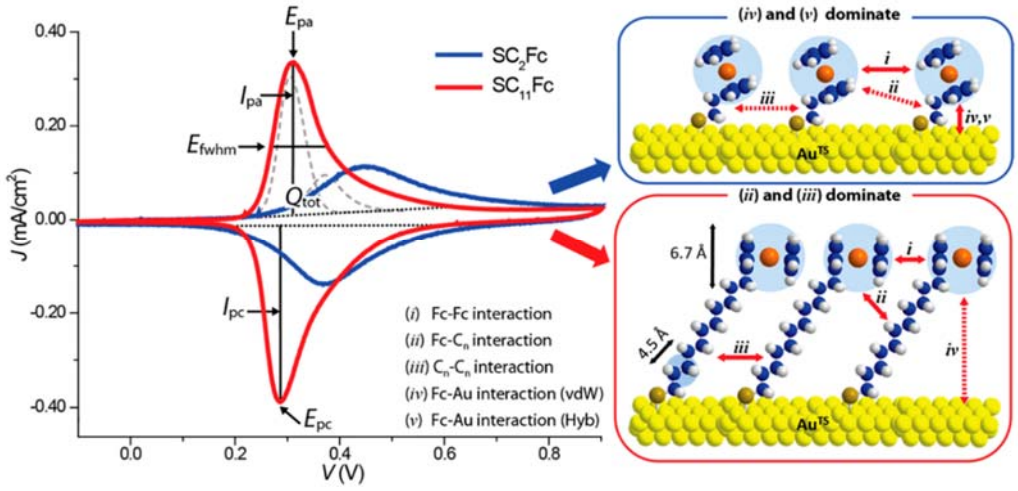


**Figure 1. 7** Schematic illustration of SAMs of Fc-CnSH with n = 2 and 11. The arrows labeled with i to v indicate the supramolecular interactions: (i) Fc-Fc, (ii) Fc-Cn, (iii) Cn-Cn, (iv) Fc-Au (non-covalent), and (v) Fc-Au (covalent). Electrochemical parameters: peak oxidation potential ($E_{pa}$), peak reduction potential ($E_{pc}$), full-width at half-maximum ($E_{fwhm}$), anodic peak current ($I_{pa}$), cathodic peak current ($I_{pc}$), and total charge ($Q_{tot}$). Reprinted with permission from *Journal of Physical Chemistry C* **2015**, *119*, 21978. Copyright (2015) American Chemical Society.

Other factors such as anions in solution can also dictate the outcome of electrochemical behavior of Fc-SAMs. The presence of different inorganic ions in electrolyte solution would provide different electrochemical response of the Fc-SAMs depending on the solvation nature of the anion.[69,68] For instance, hydrophobic anions like $ClO_4^-$ and $BF_4^-$ would ion-pair with ferrocenium ($Fc^+$) because these anions can be transported with almost no associated solvent molecule (e.g. $H_2O$). On the other hand, anions such as $NO_3^-$, $Cl^-$, $SO_4^{2-}$, $HPO_4^{2-}$, $HPO_4^-$, $F^-$, and more hydrophilic anions would interact exclusively with solvent molecule (solvation) which eventually hinders their ability to ion-pair with ferrocenium ($Fc^+$).[85,96] Valincius and co-workers studied the electron transfer rate from the ascorbate to Fc-SAMs and found a more than ten-fold increase in the electrocatalytic oxidation rate constant of ascorbate along the sequence: $PF_6^-$, $ClO_4^-$, $BF_4^-$, $NO_3^-$, $Cl^-$, $SO_4^{2-}$, $NH_2SO_3^-$, and $F^-$.[97] This sequence suggests that, highly hydrated ions promote electrocatalytic electron transfer to Fc-SAMs while poorly hydrating ions inhibit the reaction. Moreover, in CV, the formal potential of Fc- in the SAMs was generally found to shift negatively with increasing anion concentration.[68,98,99]

For Fc-SAMs, both anodic and cathodic peak currents were found to increase with increasing scan rate, as is expected for surface bound redox species in reversible electrode processes.[33,65,82,85] The shape and general features of the voltammogram remain independent of scan rate (<100 $mVs^{-1}$) with little peak separation.[33,68,85,100] However, higher scan rates induce the positive and negative current peaks to split apart substantially indicating that the scan rate becomes comparable to the rates of electron transfer.[81,84,98]

When an external potential is applied to Fc-SAMs in the positive direction, the conversion of Fc to $Fc^+$ causes electrostatic repulsion between neighboring Fc-molecules, whereas $Fc^+$ also interacting with counter ions. Consequently, the SAMs rearranges. This rearrangement has to

happen to minimize the electrostatic repulsion and to allow ingress of counterions to neutralize the excess surface charge.[98] The Fc-SAMs was reported to reorient to a more upright position upon oxidation as shown in Figure 1.8.[101,102] Since the distance between the $Fc^+$ and gold electrode is smaller than the distance between counter ion and gold electrode, the repulsion between gold electrode and terminal $Fc^+$ continue to dominate. Hence the monolayer changes orientation to more perpendicular position with respect to the electrode surface.[101] Interaction of the counterions with $Fc^+$ also play an important role in the process. Norman and co-workers studied electroactuation dynamics of gold coated microcantilevers modified with Fc-$C_{11}$S-Au SAMs.[103] They postulated that redox-induced deflection of the microcantilever is caused by volume expansion of the monolayer resulting from collective re-orientational motions induced by the complexation of counter ions (perchlorate) to the ferroceniums. A similar demonstration was provided by Badia and co-worker.[104] Something similar was also found by ellipsometry and surface plasmon resonance studies that, thickness of Fc-SAMs increases upon oxidation.[105,106,107]

Electrodes coated with electroactive self-assembled molecular films was demonstrated as molecular switch towards integration of electronic application.[108] Marchante and co-worker demonstrated the use of Fc-$C_{11}$S-Au SAMs probed with an ionic gel as electrolyte to produce a solid-state device capable of functioning as electrochemical switch.[109] Oxidation of Fc to $Fc^+$ also induce a wettability change to the SAMs surface *i.e.* transition from a pristine hydrophobic SAMs to hydrophilic SAMs upon oxidation.[110] Smart surfaces with surface wettability switching properties can find applications as self-cleaning surfaces, lab-on-chip systems, microfluidic devices, and thin film sensors.[37]

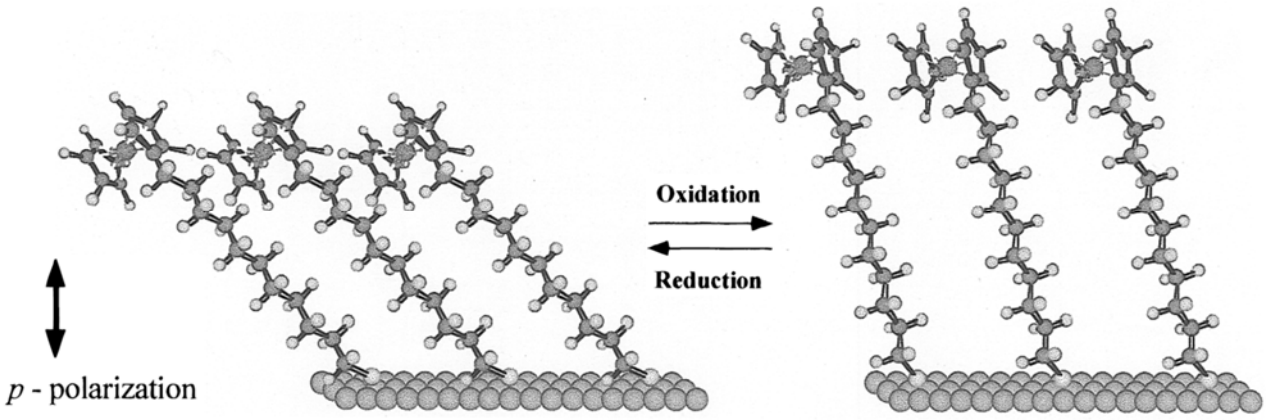


**Figure 1. 8** Schematic model for the orientation change of the Fc-C11SH monolayer: left side, monolayer terminated with ferrocene; right side, monolayer terminated with oxidized ferrocene, *i.e.*, ferricenium cation. Reprinted with permission from *Langmuir* **1997**, *13*, 3157-3161. Copyright (1997) American Chemical Society.

### 1.3. Surface deposition of polyelectrolytes

#### 1.3.1 Polyelectrolytes and their properties

Polyelectrolytes are macromolecular species with ionizable repeating functional groups, that when placed in water or other ionizing solvent dissociate into highly charged polymers. Such dissociation typically takes place by releasing counter ions into the solution, leaving charges on polymer chains.[111,112] Depending on the charges present in the polymeric backbones, polyelectrolytes types include cationic (polycations), anionic (polyanions), and zwitterionic (polyampholytes).[113] Polyelectrolytes can also be classified into strongly and weakly charged ones. 'Strong polyelectrolytes' are the ones that completely dissociate in solution throughout the pH range whereas 'weak polyelectrolytes' exhibit has a dissociation constant ($pK_a$ or $pK_b$) in the range of ~2–10, hence there will be partial dissociation at intermediate pH values.[111]

Numerous properties of polyelectrolytes *i.e.* charged polymers differ considerably compared to

their electroneutral counterparts (uncharged polymers) such as excellent water solubility *i.e.* their natural tendency to swell and bind large amounts of water, and their ability to interact strongly with oppositely charged surfaces and other charged species.[114] These unique properties of polyelectrolytes are being widely exploited in many technological and industrial fields.[115] The physical properties of polyelectrolyte solutions are strongly affected by degree of dissociation. During the dissociation of polyelectrolytes, the counterions are released into the solution which affect the ionic strength of the solution. In a solution with low ionic strength, polyelectrolytes tend to exist in their most extended or uncoiled form due to repulsion between the unscreened charges in the polymeric backbone. On the other hand, as the ionic strength of solution increases, polyelectrolytes tend to be more coiled due to screening effect from the polymeric charges by the presence of salt counterions in higher concentrations as shown in Figure 1.9. The ionic strength of the polyelectrolyte solution will thus affect the conformation of the polymeric chain in solution.[116]

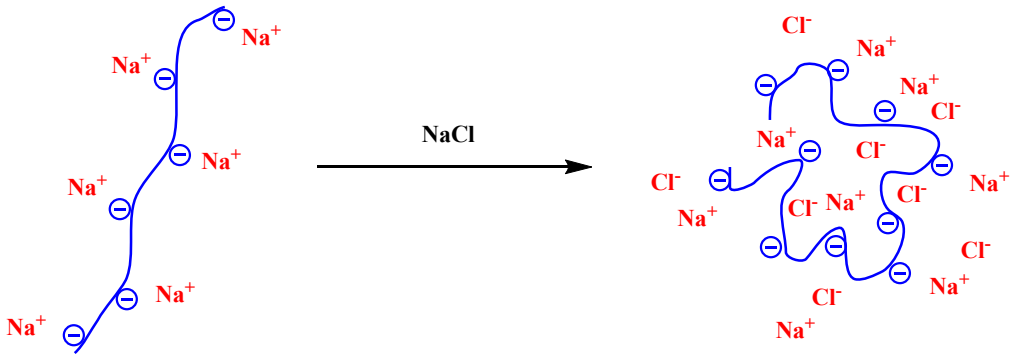


**Figure 1. 9** Ionic strength effect on polyelectrolyte conformation in solution.

The solution behavior of polyelectrolytes is not well understood because, from an experimental point of view, there are too many variables that contribute to the polyelectrolyte phenomena. Often those variables are non-linearly coupled, and end results can be confusing.[117] While a

number of other parameters can influence the behavior of polyelectrolytes, perhaps the most common are linear charge density of the chain, chain length (molecular weight), salt concentration, and pH of the solution.[116,117]

### 1.3.2 Methods for physical deposition of polyelectrolytes

Different methods have been developed for deposition of polyelectrolytes on surface. Polyelectrolytes can be adsorbed onto oppositely charged surface simply from solution, by spin casting, by solvent evaporation, by spray coating, etc. as shown in Figure 1.10.[27] In all these cases, the adhesion is mainly obtained through a collective van der Walls interaction between the charges in the polymer backbone with oppositely charged substrate surface. Because of large surface area, these log-chain charged polymers do not desorb like smaller molecules.[27]

There are other methods such as covalent grafting where polyelectrolytes can be grafted into a surface through chemical interaction between reactive groups within a polymeric chain and functional groups in a substrate.[118] In this dissertation, the investigations are solely related to physical deposition of polyelectrolytes hence deposition through chemical interactions will not be discussed.

#### 1.3.2.1 Dip coating

Adsorption of polyelectrolytes through dip coating method was first demonstrated by Decher and co-workers in the 1990s.[26] In this method, a charged substrate is dipped or immersed in a solution of polyelectrolyte of opposite charge usually for 5 - 20 minutes, and then rinsed with deionized water to provide a layer of polyelectrolyte on surface. This technique is applicable for various types of substrates regardless of shapes and morphology.[27] This method is time consuming because the deposition involved diffusion, adsorption and rearrangement of

polyelectrolyte chains. However, the procedure has certain advantages to offer such as low consumption of materials from solution hence the same polyelectrolyte solution can be used for several deposition steps. The thickness and roughness of the resulting layer on the surface usually depends on immersion time, ionic strength of polyelectrolyte solution, pH, temperature.[27]

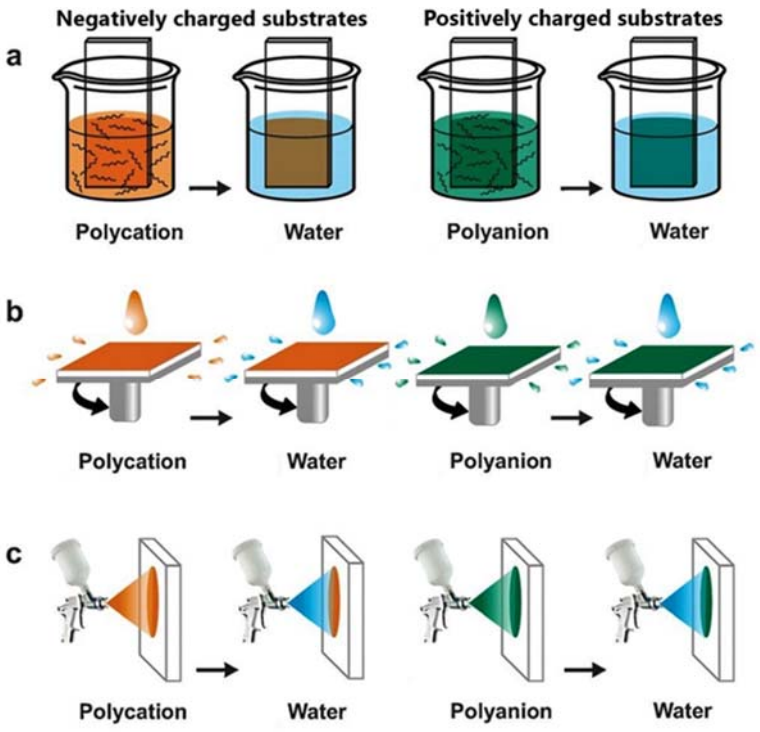


**Figure 1. 10** Schematic representation of physical deposition processes of polyelectrolytes: (a) Dip-coating, (b) Spin-coating. (c) Spray-coating. Reprinted with slight modification with permission from *Chemical Society Review* **2012**, *41*, 5998-6009. Chemistry (2012) The Royal Society of Chemistry.

### 1.3.2.2 Spin-coating

Spin assisted polyelectrolytes assembly is used as an alternative to dip-coating assembly to accelerate the deposition process. This process was introduced in 2001, almost concurrently by three groups, Hong and co-worker[119], Char and co-worker[120] and Wang and co-workers.[121] In

this process, a substrate is placed in an automated spin coater, and then the polyelectrolyte solution is introduced on substrate surface. The spin coater is then accelerated rapidly at a certain speed. Due to centrifugal force, the solution disperses throughout the surface while the excess solution is ejected off the substrate which provides a uniform layer of polyelectrolytes film. The resultant film is then rinsed with water and spin dried. This process is quicker, and film thickness can be controlled through variation of speed, and by changing the viscosity of the polyelectrolyte solution.[121] There are also some disadvantages e.g. this process doesn't work well in non-planner surfaces and generation of uniform films is difficult on substrates with large surface areas. Therefore, a flat surface with reasonable size is required.

#### 1.3.2.3 Spray-coating

Polyelectrolyte films can be fabricated by spraying an aqueous solution of polyelectrolyte onto an oppositely charged surface.[122,123] In 2000, Schlenoff and co-workers demonstrated the use of spray coating where they reported formation of LbL films by alternative spraying of a solution of poly(diallyldimethylammonium chloride) (PDDA) and another solution of poly(styrenesulfonic acid) (PSS) on surface.[122] They found that the produced films exhibit similar morphology and composition compared to the one produced with a conventional dip-coating method. In spray-coating, the polyelectrolyte solution is sprayed on a vertically held substrate by using an air-pump-driven spray can containing the liquid.[123] The air pump ensures that a constant flow is achieved throughout the spraying process while the vertically oriented substrate act as gravity-driven drainage of the excess solution driven by gravity. Deposition is followed by rinsing with water to remove physically adsorbed polyelectrolyte molecules producing an uniform film.[122] The advantages of spray coating are fast fabrication of film and ability to cover larger surface areas. However, this requires large amount of polyelectrolyte solution, and solution drained in

the process is not reusable. Spraying time, spraying distance, solution flow rate, concentration and pH of the polyelectrolyte solution can influence the film thickness. A combination of techniques, such as spray- and spin- assisted formation of LbL, has also been used as means to optimize the deposition process.[123,124]

### 1.3.3 Layer-by-layer (LbL) assembly of polyelectrolytes

Self-assembled film formation is usually based on covalent, coordination, hydrogen bonding, host/guest interaction, and hydrophobic/hydrophilic interaction chemistry, etc. These interactions are often restricted to certain classes of compounds depending on the nature of interaction. For macromolecules such as polyelectrolytes, electrostatic attraction between oppositely charged entities is an obvious alternative as a driving force for multilayer buildup. In addition, other secondary interactions are possible such as hydrophobic/hydrophilic effects, hydrogen bonding, van der Waals interactions, etc.[117] Even the electrostatic adsorption from solution is not straightforward in case of polyelectrolytes due to their complex properties in solution and many factors affecting adsorption onto a surface. Theoretical studies on deposition of polyelectrolytes form solution onto oppositely charged surfaces have been reported since 1970s.[125,126] The first experimental observation was reported in 1985 by Cosgrove and co-workers who investigated the deposition of poly(styrene sulfonate) on both positively and negatively charged latex polystyrene.[127] Since then a combination of theoretical and experimental works were reported to correlate experimental evidence with theoretical observations. The concept of layer-by-layer assembly was introduced first by Iler in 1966, when he reported fabrication of multilayers by alternative deposition of positively and negatively charged colloid particles[128]. However, the first multilayer formation of polyelectrolytes on flat surface was reported in 1990s by Decher and co-workers.[129,116] This process generally involved deposition of polyelectrolytes from solution onto

an oppositely charged substrate, and then building up layers of oppositely charged polyelectrolytes towards multilayer formation as demonstrated in Figure 1.11.[26] A rinsing step is usually employed after each polyelectrolyte deposition to remove the chains that are not adsorbed or weakly adsorbed. This process can be repeated until the formation of film with desired thickness.[130]

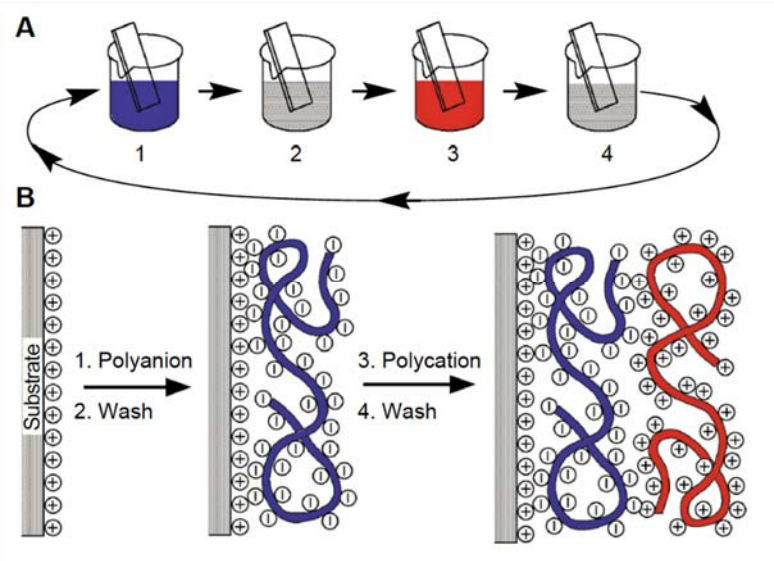


**Figure 1. 11** (A) Schematic of the film deposition process. Steps 1 and 3 represent the adsorption of a polyanion and polycation, respectively, and steps 2 and 4 are washing steps. The four steps are the basic buildup sequence for the simplest film architecture. (B) Simplified molecular picture of the first two adsorption steps, depicting film deposition starting with a positively charged substrate. Counterions are omitted for clarity. Reprinted with permission from Science **1997**, 277 *(5330)*, 1232-1237. Copyright (1997) American Association for the Advancement of Science.

LbL assembly of thin polyelectrolyte films this process has received intense and growing interest.[130,131] Although dip-coating is the most used method for LbL assembly, other methods such as spin-coating, spray-coating, perfusion are widely used.[131] These methods have their

advantages and disadvantages while spin and spray-methods are often applied for industrial applications mainly due to their low-cost and time-effectiveness.[132,133,134] However, other nonconventional methods including hydrodynamic-dip-coating[135], high-gravity field-[136], inkjet/3D printing-assisted[137,138,139], electrodeposition[140] are also reported for LbL assembly of polyelectrolytes.

Almost any type of charged substrates or substrates with proper surface functionalities are suitable for LbL assembly of polyelectrolytes such as planar, porous, colloidal particles, and cylindrical structures regardless of size and shape. By immersing a charged substrate into dilute solutions containing an oppositely charged polyelectrolyte followed by repeating immersion in alternatively charged polyelectrolytes leads to multilayer film formation. This kind of LbL assembly based on electrostatic interaction can lead to multilayer films of well-controlled composition, structure and thickness.[130] Nevertheless, when using purely electrostatic interactions, changes in external stimuli such as ionic strength[141,142,143], pH[144,145,146], applied electric field[147,148,149], light[150,151], temperature[143,152] may influence the adsorption of polyelectrolytes and the properties of the adsorbed layers; these factors might even induce desorption. Moreover, there is no general growth mechanism of LbL films as they are found to grow linearly, exponentially, or mixtures of the two types of growth depending on polyelectrolytes pair and deposition conditions. When two strong polyelectrolytes are used in the formation of LbL, liner growth is usually observed due to charge overcompensation.[153,154,155] On the other hand, polyelectrolyte pairs consisting of at least one polypeptide or polysaccharide are found to show exponential growth which is more rapid compared to linear growth.[156,157,158,159,160] The mechanism of exponential growth is not fully understood yet, but may be related to fast diffusion of both polyelectrolytes involved in layer formation.[161] Podsiadlo and co-workers showed a comparison of linear vs exponential growth where they incorporated an inorganic

sheet, $Na^+$-montmorillonite (MTM) in combination with poly(ethylenimine) (PEI) and poly(acrylic acid) (PAA) to form a tricomponent film, shown in Figure 1.12.[162]

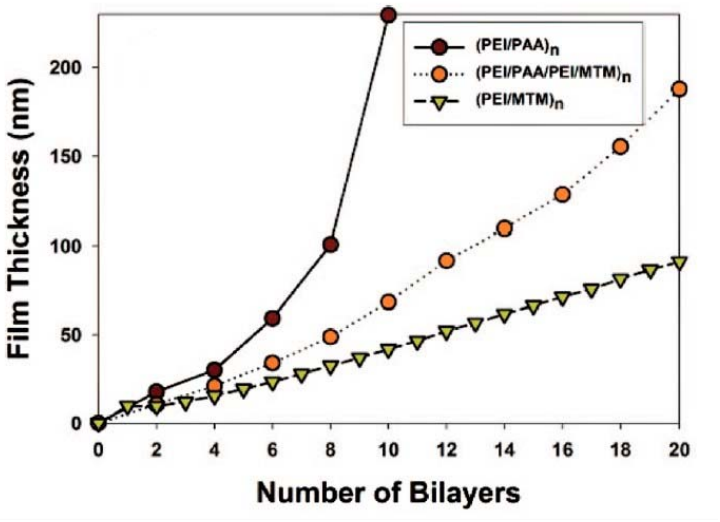


**Figure 1. 12** Comparison of linear and exponential LbL film growth on a silicon wafer with thickness measured through ellipsometry. The "exponential" upswing of the growth curve for $(PEI/PAA/PEI/MTM)_n$ can be clearly seen. The deposition interval was 2 minutes for e-LBL films, and 5 minutes for the $(PEI/MTM)_n$ films. Reprinted with permission from *Nano Lett*er **2008**, *6*, 1762-1770. Copyright (2008) American Chemical Society.

LbL assembly is relatively cheap, can be done at room temperature, allows integration of biomaterials (polypeptides, polysaccharides, proteins, polynucleotides, DNAs, etc.) in films, and can be achieved under mild conditions compared to other bottom up approach. Several techniques are employed for characterization of the properties of LbL polyelectrolyte film assemblies including UV−visible spectroscopy, Fourier transform infrared (FTIR) spectroscopy, quartz crystal microbalance (QCM), surface plasmon resonance (SPR) spectroscopy, ellipsometry, differential scanning calorimetry (DSC), nuclear magnetic resonance (NMR), X-ray diffraction (XRD), X-ray reflectometry (XRR), X-ray photoelectron spectroscopy (XPS),

dual polarization interferometry, atomic force microscopy (AFM), scanning electron microscopy (SEM), transmission electron microscopy (TEM), confocal laser scanning microscopy (CLSM).[131] Due to fast formation, cost-effectiveness, possible integration of wide ranges of materials, and convenient characterization, LbL films have found applications in various fields including sensing and bioelectronics[163,164,165,166], drug delivery[167,168,169], protein adsorption, cell adhesion[170,171], tissue engineering and regenerative medicine[172,173], separation technology[174,175], energy storage and conversion.[176]

### 1.3.4 Polyelectrolytes deposition on thiol SAMs surfaces

Polyelectrolyte thin film formation was first reported in the 1980s when polyelectrolytes containing terminal thiol groups were self-assembled on metal surfaces.[177] In the early 1990s, adsorption of charged biomolecules such as proteins on thiol SAMs was reported.[178,179] However, surface deposition of a polyelectrolyte from an aqueous solution onto functionalized thiol SAMs was introduced in 1994 by Corn and co-workers.[180] They demonstrated electrostatic deposition of the cationic polypeptide poly-L-lysine (PLL) onto a carboxylic acid-terminated alkanethiol monolayer on gold. In 1996, Kaifer and co-workers reported adsorption of viologen-containing polyelectrolytes on the surface of carboxylate-terminated SAMs. They indicated that, while carboxyl terminated SAMs enhances the adsorption, the hydrophobic character of the viologen polyelectrolyte was an important component of the overall driving force. In late 1990s, self-assembly of polyelectrolytes from aqueous solution on to patterned carboxylate-terminated alkanethiol SAMs generated through microcontact printing was reported by several groups.[156,181] In 2004, Gaub and co-workers studied adsorption and desorption of poly(acrylic acid) (PAA) covalently attached in an AFM cantilever, on/from alkanethiol SAMs with different terminal groups (-$CH_3$, -OH, -COOH).[182] Later, polyelectrolyte multilayer formation or LbL assembly on

SAMs were reported.[183,184] Tiraferri and co-workers in 2014, investigated deposition of anionic sodium poly(styrene sulfonate) (PSS) and cationic poly(diallyldimethyl ammonium chloride) (PDADMAC) on SAMs of alkanethiols terminated with different functional groups (-$CH_3$, -OH, -COOH, -$NH_2$).[185] Their study not only elaborated the role of surface chemistry on polyelectrolytes adsorption but also demonstrated the importance of other factors such as ionic strength, hydrophobicity, etc. It also suggests the likelihood of adsorption of polyelectrolytes on like charged substrates in the presence of small counter ions. The same group in 2015 further presented a comparative study of adsorption of cationic, anionic, and neutral polymers on both positively and negatively charged modified alkanethiols SAMs surface.[186] Overall, tunable properties of SAMs offers the flexibility to control surface charges through wide range of functional groups attached at their distal end. This allows to control the amount of polyelectrolytes adsorption on surface.[185]

### 1.4. Surface deposition/assembly of aqueous suspended colloids

According to the IUPAC (International Union of Pure and Applied Chemistry) definition, a colloidal system "...refers to a state of subdivision, implying that the molecules or polymolecular particles dispersed in a medium have at least in one direction a dimension roughly between 1 nm and 1 μm, or that in a system discontinuities are found at distances of that order."[187] Colloidal particles may be considered as building blocks for materials with properties of technological interest. Due to the broad definition of colloidal particles, a wide range of structures can be generated though colloidal assembly. Colloidal assembly is considered as a model system for studying fundamental physics of the atomic world, and also found applications in photonic devices, nanoscale electronics, energy migration, energy-conversion, energy-storage, bio-sensors, drug/gene delivery, hierarchically structured catalysts, etc.[188,189] Strategies for colloidal

assembly are usually of two types: the physical approach governed by "top-down" methodologies, and complementary chemically inspired "bottom-up" strategies. The resulting structures after assembly on a surface can be 1D (one dimensional), 2D (two dimensional), and 3D (three dimensional). In this part of the discussion, 1 D and 2D colloidal assembly on a substrate through physical approaches especially electrostatic self-assembly and electrically driven assemblies will be discussed because, these are more related to the work presented in this dissertation.

Two-dimensional colloid assemblies on a solid substrate are generally termed as colloidal monolayers. This monolayer formation is usually subdivided into two types: closed packed and non-closed packed structures.[190] Our selection for the discussion of electrostatic self-assembly and electrically driven assemblies will fall under the closed packed category. A brief overview of methods for closed packed 2D colloidal monolayers are showed in Table 1.[190]

### 1.4.1. Electrostatic self-assembly

Charged colloidal particles can be adsorbed into an oppositely charged surface using electrostatic attraction. However, electrostatic interactions between objects must not be too strong, otherwise it might lead to random aggregation due to irreversible bindings. When a dispersion of charged particles is allowed to deposit into an oppositely charged substrate, there is a competition between attraction of colloids and substrate and interparticle repulsions. Random deposition of particles onto surfaces is believed to be driven by such competitive forces, and the adsorption mechanism is described by the random sequential adsorption (RSA) theory.[191] Once immobilized on the surface, the particles will no longer be able to move laterally across the surface. Moreover, any space between already adsorbed particles that is smaller than the average particle size becomes inaccessible for further adsorption of particles. Thus resulting disordered assembly

on surface are usually found to have a surface coverage of less than 50%.[190]

**Table 1. 1** Overview of 2D crystallization methods for close-packed colloidal monolayers. Reprinted with permission from *Chemical Reviews* **2015**, *115*, 6265-6311. Copyright (2015) American Chemical Society.

| *Method* | *Schematic* | *Remarks* |
|---|---|---|
| **Direct Assembly Methods** | | |
| **Controlled Evaporation** | 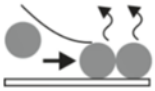 | Extremely simple process; meniscus pinning and coffee-stain effects prevent large area patterning and long-range order; risk of multilayer formation; limited substrates. |
| **Vertical Deposition (Convective Assembly)** | 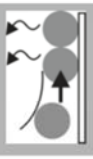 | Requires tight control of parameters; slow process; meniscus pinning; risk of multilayer formation; limited substrates. |
| **Horizontal Deposition** | 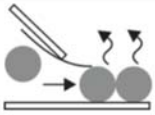 | Requires tight control of parameters; slow process; meniscus pinning; risk of multilayer formation; tunable deposition conditions by a microscope;limited substrates. |
| **Spin-Coating** | 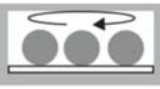 | Fast process; waste of some dispersion; shear forces limit high order; limited substrates, risk of multilayer formation. |
| **Sedimentation** | 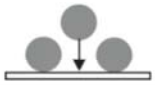 | Sophisticated cell design to prevent multilayer formation. |
| **Electrostatic Deposition** | 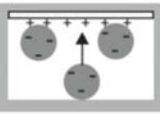 | Attraction prevents high order; can be circumvented by sophisticated processes; suitable for patterning. |
| **Electrophoretic Deposition** | 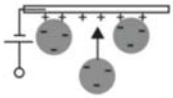 | Higher order in AC-fields, suitable for patterning; complex pattern formation. |
| **Liquid Interface-Mediated Methods** | | |
| **Langmuir-Type** |  | Good control and high order; manipulation of subphase possible; arbitrary substrates; large areas; experimentally complex, slow. |
| **Floating** | 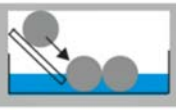 | Experimentally simple and fast; arbitrary substrates; large areas; heteromonolayers possible; high order. |
| **Direct Assembly** |  | Experimentally simple and fast; large areas; arbitrary substrates; high order. |

Electrostatic interactions can cause particles to self-assemble into crystalline or non-crystalline arrays. Electrostatic attractions between particles may be manipulated to control or direct particles adsorption towards a desired structured assembly. Surface charges on the particles can be maneuvered by varying functional groups on the surface and altering their density on the particle surface. The magnitude of electrostatic attraction or repulsion can also be tuned by changing the pH of the dispersion medium, by altering the ionic strength of the medium via adding small ions, etc.

Electrostatic adsorption of charged particles on to an oppositely charged solid surface was shown by Iler in 1960s, who reported preparation of both monolayer[192] and multilayers[128] of particles on interface based on electrostatic adsorption. Preparation and characterization of mono- and multilayers using Iler's technique was employed by several groups in the 1990s.[193] In 2000, Hammond and co-workers reported self-organization of sub-micron sized colloid particles on a substrate.[194] They first developed polyelectrolyte multilayer on chemically patterned surfaces followed by colloidal particle deposition onto patterned polyelectrolytes templates. After their report, controlled and patterned self-assembly of particles became popular due to promising potential applications in microelectronic devices. In 2002, Jonas and co-workers reported site-selective assembly of colloidal polymer particles to generate molecularly mixed monolayers which allowed particle adsorption and photoactivation within the same monolayer.[195] In 2010, Zhang and co-workers showed colloidal crystal formation based on electrostatic self-assembly where they formed a 2D poly(styrene sulfate) (PSS) colloidal crystal onto a positively charged substrate. Their unique strategy consists of two steps: formation of 3D PSS crystal in ethanol where electrostatic attraction is absent, which results in high quality colloidal crystals. A subsequent wash with water results in well-packed PSS colloidal monolayers tightly linked to the surface due to electrostatic interactions.[196]

### 1.4.2. Electrically driven assembly of colloids

Like electrostatic assembly, electrically driven processes for example, electrophoretic deposition also take the advantage of electrostatic attractions to immobilize charged colloidal particles onto an oppositely charged substrate.[197] In case of electrostatic assembly processes, charges are fixed on a substrate. On the other hand, a variable external electric field can generate either positive or negatively charges on the surface of a conductive substrate. In electrophoretic deposition, an applied electric field generates charges on the electrode surface which should induce a strong electrostatic attraction if probed with oppositely charged colloids. Like electrostatic self-assembly, this attraction should impede ordering of colloidal particles on electrode surfaces resulting in random adsorption. However, in case of colloidal assembly under an electric field, ordering of particles has been observed due to interparticle attractive forces which lead to formation of crystalline monolayers.[198,199] This kind of interparticle attraction between similarly charged colloids is not easy to explain only in terms of classical colloidal forces.[190] In the usual sense, there should be repulsions between similarly charged colloid particles, and between the ion clouds around the colloids and the electrode. The unexpected attractive force between similarly charged colloids during formation of crystalline monolayer has been attributed to one or combination of the following phenomena: electrophoresis[199], electroosmosis[200,201,202], and electrohydrodynamic motion of ions.[203,204,197]

When a dc electric field is applied, the dominating effect observed is electroosmotic flow, first observed by Bohmer[205] and later elaborated by Anderson & co-workers.[200,201] As the oppositely charged colloids are attracted towards the electrode, the counterion cloud of the colloids will contain charges of similar sign as those on the electrode. Therefore, ions are repelled from the electrode, subsequently drawing fluid across the electrode to maintain mass balance. This flow

pulls fluid towards the particle and is directed away from electrode. Attraction is observed when a second particle is dragged towards the first particle by this flow. In case of ac fields, usually electrohydrodynamic forces dominates.[204,197,206] Here, ions produced upon water electrolysis are attracted towards oppositely charged electrodes to form a concentration gradient at each electrode. Any nearby colloids will disrupt the concentration gradient and initiate an ion flow towards the electrode. This convective flow will sweep particles toward each other across the electrode surface resulting in particles interaction.

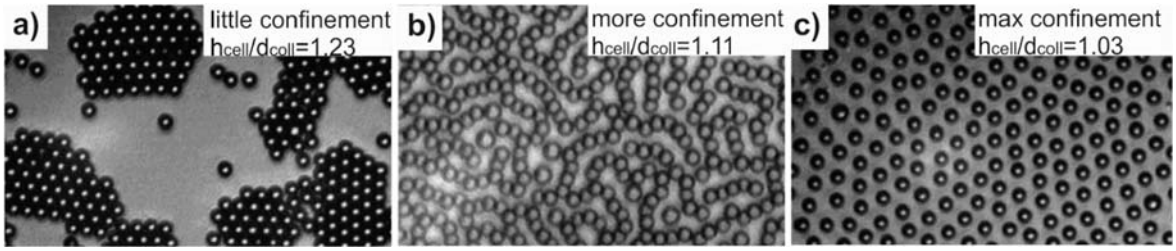


**Figure 1. 13** Two-dimensional colloid assembly structures created by electrohydrodynamic flow on an electrode surface under varying confinement, which was characterized by the ratio of colloid diameter over cell gap dimension, as reported by Marr's group[207]. With decreasing cell height, attractive electrohydrodynamic flows are decreased, leading to stronger contributions of repulsive dipole−dipole interactions. This causes a change in the assembly structures from close-packed (a) to chain-like (b) and non-close-packed (c). Reprinted with permission from *Chemical Reviews* **2015**, *115*, 6265-6311. Copyright (2015) American Chemical Society.

Compared to a single electrode, introduction of a second electrode creates another confining wall in a colloid system under an electrode field. Two-electrode confinement can decrease the fluid flow and overlap of the flow field is now possible. As a result, the particles can experience a diminished attraction between each other. This particle confinement can have a dramatic effect on the assembly of colloids, as demonstrated by Marr and co-workers. They showed that,

variation of the nature of electric field and degree of confinement can induce formation of different structures due to various degrees of attraction and repulsion. They demonstrated such effect for 4 μm polystyrene (PS) colloidal assembly under various confinement conditions, shown in Figure 1.13.[207]

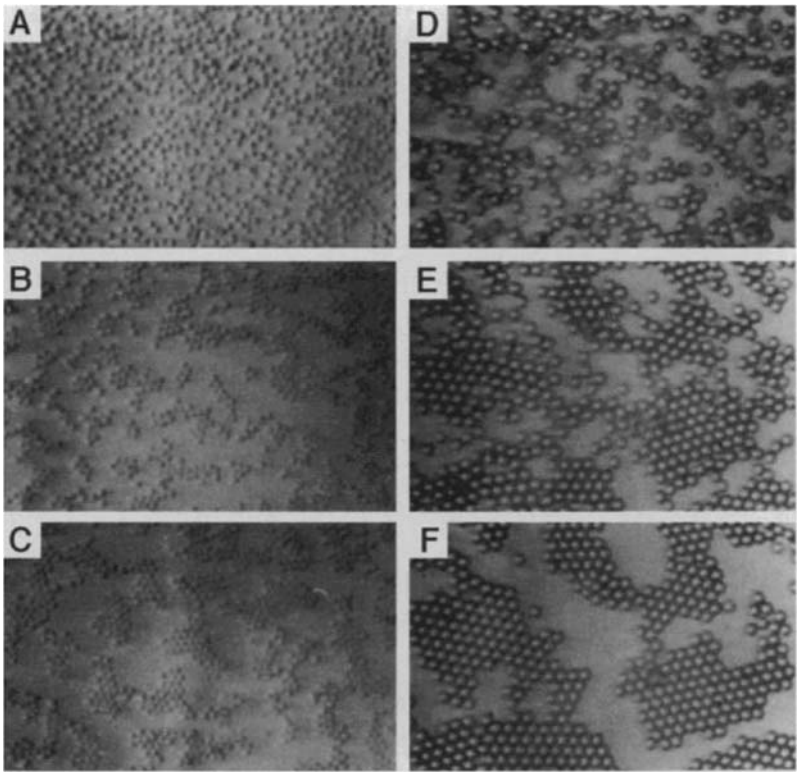


**Figure 1. 14** (A to C) Silica particles 900 nm in diameter electrophoretically deposited onto the transparent anode with a controlled applied voltage (from 0 to 2 V) to maintain a constant current of 40 μA $cm^{-2}$. (D to F) PS particles 2 μm in diameter deposited by application of a constant voltage (2 V). The time elapsed between successive frames is ~15 s. No field was applied in (A) and (D). Reprinted with permission from *Science* **1996**, 272(*5262*), 706-709. Copyright (1996) American Association for the Advancement of Science.

Electrophoretic assembly of colloids are often achieved using alternating electric fields.[208,209]

Alternating voltage allows manipulation of particles virtually in any type of media and also offers the advantage of attaining high voltages without causing water electrolysis or electroosmotic currents which can impact particle ordering.[210] Liu and co-worker reported the formation of highly ordered monolayers by applying alternating fields which improved controlling the nucleation rate of ordered patches as compared to the case of a constant electric field.[208] Formation of superstructures is also possible through pattern formation on electrode surfaces using electrophoretic assembly.[211,212]

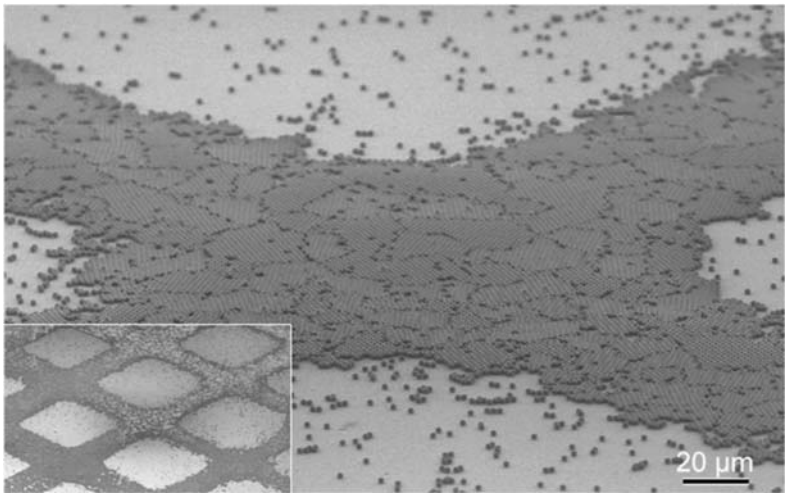


**Figure 1. 15** Scanning electron microscope (SEM) image of a pattern produced by an applied electric field followed by concurrent UV illumination. Dense packing of particles results in crystalline (ordered) domains that vary in size (10±20 mm). The inset (600mm wide) shows the overall appearance of the pattern. Reprinted with permission from *Nature* **2000**, *404*, 56-59. Copyright (2000) Nature Publishing Group.

Velev and co-workers demonstrated directed orientation of crystals by using two electrodes deposited on the same surface with a wide gap between them.[210] The same group later reported an evaporative assembly process in combination with an applied ac field where they

demonstrated an electrowetting-on-dielectrics phenomenon introduced by the applied field to attain a more uniform coating with large crystallite domains.[213]

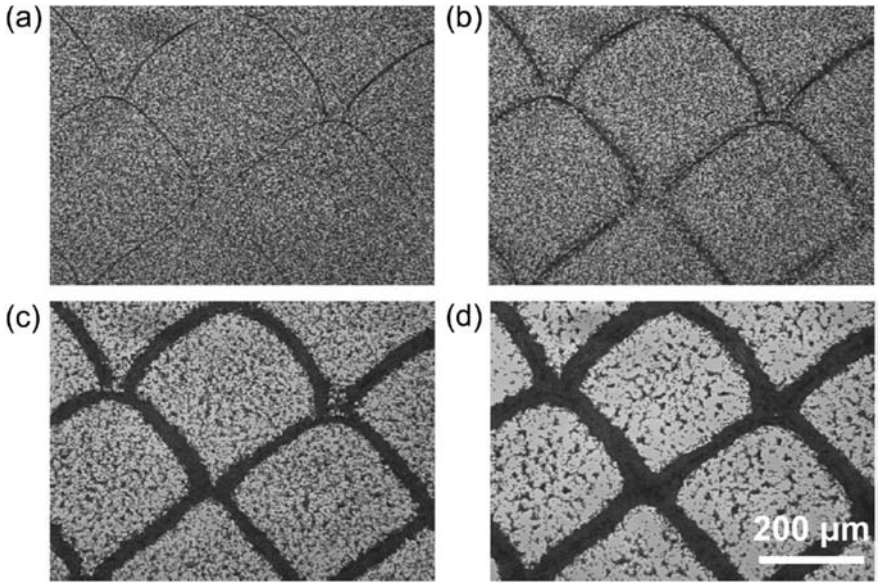


**Figure 1. 16** Time snapshots of large-area epitaxial crystallization and oriented patterning of a 2D colloidal crystal using a colloidal line network as a template, under the alternating electric field of frequency f = 400 Hz and field strength E = $4.0 \times 10^4$ V/m. (a) 0 s, (b) 2.0 s, (c) 5.0 s, (d) 10.0 s. Reprinted with permission from *Journal of the American Chemical Society* **2009**, *131*, 4976-4982. Copyright (2009) American Chemical Society.

Aksay and co-workers attained different 2D colloid phases (showed in Figure 1.14) by manipulating current density changes which ultimately control the magnitude of lateral attraction between colloidal particles at the electrode surface.[204] As shown in Figure 1.14, the applied electric field restricts particles movement to two-dimensions across the electrode surface while long-range attractive forces accumulates particles resulting in a 2D crystal formation. The same group later reported a combined method of application of electric field followed by UV-illumination to create ordered arrays of colloidal particles with tunable patterns showed in Figure

1.15.[214] This optical tunability offers many possibilities for orchestrating electrophoretic deposition while allowing convenient control of the intensity and location of the photon flux.

Liu and co-workers utilized predefined one-dimensional colloidal lines as an epitaxial template to initiate site specific 2D colloidal crystallization while the crystal growth can be manipulated by an external alternating electric field, shown in Figure 1.15.[215] Zamborini and co-workers recently demonstrated redox mediated size selective electrophoretic deposition of gold nanoparticles.[216] They utilized the proton coupled oxidation of hydroquinone to electrophoretically deposit citrate stabilized gold nanoparticles on glass/indium-tin-oxide (ITO) electrodes. An interesting find was that, oxidation on smaller particles occurred faster than larger particles which allowed deposition of 4 nm particles at a potential about 300-400 mV more negative than needed for 15 nm diameter particles, enabling to realize selective deposition.

### 1.5 The scope of this dissertation

The motivation of this dissertation is to utilize a redox-active surface to recruit different chemical entities to the surface which will provide the surface a new identity where variety of chemistry can be launched. We focused on developing a general method for electrochemical deposition of various materials such as polyelectrolytes, water suspended colloids, metal & metal oxide nanoparticles, carbon nanotubes, quantum dots, soft materials (liposomes), biomaterials (peptides, DNA), etc. utilizing the same platform, and novel integration of the thus produced technology.

In Chapter 2, we demonstrated an electrochemical approach for surface deposition of polyelectrolytes. We used a ferrocene terminated alkanethiol SAMs on gold to initiate the deposition process by applying an external electric field while probed the SAMs surface with

polyelectrolytes solutions. We demonstrated deposition of both polyanions and polycations with wide range of molecular weight ($10^3$-$10^7$ Da as tested) on the same surface. We characterized deposition processes by using voltammetry, fluorescence spectroscopy, contact angle analysis, electrochemical quartz crystal microbalance, and atomic force microscopy. We presented a detailed mechanism of deposition processes for both polyanion and polycation. At the end, we reported the formation of electroactive layer-by-layer (LbL) polyelectrolytes film utilizing the deposition method while characterized the film formation by using UV-vis spectroscopy.

In Chapter 3, we extended the utilization of the same redox-active surface to electrochemically deposit/assemble colloidal particles suspended in water, in this case carboxylated polystyrene nano-/micro-spheres. We studied in detail a couple of key factors involved in the process including the starting electrode surfaces, colloid size, range/duration of applied potential, and effects of small supporting electrolytes. In the process we used voltammetry, electrochemical quartz crystal microbalance, and confocal laser scanning microscopy to characterize the deposition process and study the key factors involved. We were able to demonstrate the superior efficiency of the electrochemically triggered assembly compared to the electrically driven process. We further demonstrated fast, high-fidelity colloid micropattern formation on electrodes at the end.

In chapter 4, we further extended the deposition platform for various types of functionalized materials including metal & metal oxide nanoparticles, quantum dots, multi-walled carbon nanotubes (MWCNTs), liposomes, etc. We characterized depositions for materials of respective types by using atomic force microscopy and confocal laser scanning microscopy. We also compared deposition processes for materials containing negative and positive charge with the one with no charge, while using liposomes as model materials. This study provides us with a

better understanding of the forces and factors involved in the deposition process.

In chapter 5, we have made general conclusion on our work. Here, we also discussed the usefulness, applications, and probable future directions of our research utilizing our developed deposition technique.

**References**


(1) Gallei, M.; Rüttiger, C. Recent Trends in Metallopolymer Design: Redox-Controlled Surfaces, Porous Membranes, and Switchable Optical Materials Using Ferrocene-Containing Polymers. *Chem. - A Eur. J.* **2018**, *24* (40), 10006–10021. https://doi.org/10.1002/chem.201800412.

(2) Love, J. C.; Estroff, L. A.; Kriebel, J. K.; Nuzzo, R. G.; Whitesides, G. M. *Self-Assembled Monolayers of Thiolates on Metals as a Form of Nanotechnology*; 2005; Vol. 105. https://doi.org/10.1021/cr0300789.

(3) Wayu, M. B.; Pannell, M. J.; Labban, N.; Case, W. S.; Pollock, J. A.; Leopold, M. C. Functionalized Carbon Nanotube Adsorption Interfaces for Electron Transfer Studies of Galactose Oxidase. *Bioelectrochemistry* **2019**, *125*, 116–126. https://doi.org/10.1016/j.bioelechem.2018.10.003.

(4) Hauquier, F.; Ghilane, J.; Fabre, B.; Hapiot, P. Conducting Ferrocene Monolayers on Nonconducting Surface. *J. Am. Chem. Soc.* **2008**, *130* (9), 2748–2749. https://doi.org/10.1021/ja711147f.

(5) Takahashi, S.; Anzai, J. Recent Progress in Ferrocene-Modified Thin Films and Nanoparticles for Biosensors. *Materials (Basel).* **2013**, *6* (12), 5742–5762. https://doi.org/10.3390/ma6125742.

(6) Singh, V.; Mondal, P. C.; Singh, A. K.; Zharnikov, M. Molecular Sensors Confined on SiOx Substrates. *Coord. Chem. Rev.* **2017**, *330*, 144–163. https://doi.org/10.1016/j.ccr.2016.09.015.

(7) Lydon, B. R.; Germann, A.; Yang, J. Y. Chemical Modification of Gold Electrodes: Via Non-Covalent Interactions. *Inorg. Chem. Front.* **2016**, *3* (6), 836–841. https://doi.org/10.1039/c6qi00010j.

(8) Watcharinyanon, S.; Moons, E.; Johansson, L. S. O. Mixed Self-Assembled Monolayers of Ferrocene-Terminated and Unsubstituted Alkanethiols on Gold: Surface Structure and Work Function. *J. Phys. Chem. C* **2009**, *113* (5), 1972–1979. https://doi.org/10.1021/jp808938d.

(9) Chen, C. P.; Luo, W. R.; Chen, C. N.; Wu, S. M.; Hsieh, S.; Chiang, C. M.; Dong, T. Y. Redox-Active π-Conjugated Organometallic Monolayers: Pronounced Coulomb Blockade Characteristic at Room Temperature. *Langmuir* **2013**, *29* (9), 3106–3115. https://doi.org/10.1021/la303796r.

(10) Berger, J.; Kośmider, K.; Stetsovych, O.; Vondráček, M.; Hapala, P.; Spadafora, E. J.; Švec, M.; Jelínek, P. Study of Ferrocene Dicarboxylic Acid on Substrates of Varying Chemical Activity. *J. Phys. Chem. C* **2016**, *120* (38), 21955–21961. https://doi.org/10.1021/acs.jpcc.6b05978.

(11) Zotti, G.; Schiavon, G.; Zecchin, S.; Berlin, A.; Pagani, G.; Canavesi, A. Self-Assembly of Pyrrolyl- and Cyclopentadithiophene-4-Yl-n-Hexylferrocene on ITO Electrodes and Their Anodic Coupling to Polyconjugated Polymer Layers. *Langmuir* **1997**, *13* (10), 2694–2698. https://doi.org/10.1021/la960745b.

(12) Zotti, G.; Schiavon, G.; Zecchin, S.; Berlin, A.; Pagani, G. Adsorption of Ferrocene

Compounds on Indium-Tin-Oxide Electrodes. Enhancement of Adsorption by Decomposition of Ferrocenium Molecules by Oxygen. *Langmuir* **1998**, *14* (7), 1728–1733. https://doi.org/10.1021/la971092h.

(13) Kim, B.; Ratcliff, E. L.; Armstrong, N. R.; Kowalewski, T.; Pyun, J. Ferrocene Functional Polymer Brushes on Indium Tin Oxide via Surface-Initiated Atom Transfer Radical Polymerization. *Langmuir* **2010**, *26* (3), 2083–2092. https://doi.org/10.1021/la902590u.

(14) Fabre, B.; Hauquier, F. Single-Component and Mixed Ferrocene-Terminated Alkyl Monolayers Covalently Bound to Si(111) Surfaces. *J. Phys. Chem. B* **2006**, *110* (13), 6848–6855. https://doi.org/10.1021/jp055698n.

(15) Lu, M.; He, T.; Tour, J. M. Surface Grafting of Ferrocene-Containing Triazene Derivatives on Si(100). *Chem. Mater.* **2008**, *20* (23), 7352–7355. https://doi.org/10.1021/cm8007182.

(16) Fabre, B.; Pujari, S. P.; Scheres, L.; Zuilhof, H. Micropatterned Ferrocenyl Monolayers Covalently Bound to Hydrogen-Terminated Silicon Surfaces: Effects of Pattern Size on the Cyclic Voltammetry and Capacitance Characteristics. *Langmuir* **2014**, *30* (24), 7235–7243. https://doi.org/10.1021/la501330j.

(17) Jouikov, V.; Simonet, J. Novel Method for Grafting Alkyl Chains onto Glassy Carbon. Application to the Easy Immobilization of Ferrocene Used as Redox Probe. *Langmuir* **2012**, *28* (1), 931–938. https://doi.org/10.1021/la204028u.

(18) Tanaka, M.; Sawaguchi, T.; Sato, Y.; Yoshioka, K.; Niwa, O. Surface Modification of GC and HOPG with Diazonium, Amine, Azide, and Olefin Derivatives. *Langmuir* **2011**, *27* (1), 170–178. https://doi.org/10.1021/la1035757.

(19) Ormaza, M.; Abufager, P.; Bachellier, N.; Robles, R.; Verot, M.; Le Bahers, T.; Bocquet,

M. L.; Lorente, N.; Limot, L. Assembly of Ferrocene Molecules on Metal Surfaces Revisited. *J. Phys. Chem. Lett.* **2015**, *6* (3), 395–400. https://doi.org/10.1021/jz5026118.

(20) Kang, O. S.; Bruce, J. P.; Herbert, D. E.; Freund, M. S. Covalent Attachment of Ferrocene to Silicon Microwire Arrays. *ACS Appl. Mater. Interfaces* **2015**, *7* (48), 26959–26967. https://doi.org/10.1021/acsami.5b07814.

(21) Bullock, R. M.; Das, A. K.; Appel, A. M. Surface Immobilization of Molecular Electrocatalysts for Energy Conversion. *Chem. - A Eur. J.* **2017**, *23* (32), 7626–7641. https://doi.org/10.1002/chem.201605066.

(22) Ghafari, M. T.; Varmaghani, F.; Karimi, B.; Khakyzadeh, V. Robust Non-Covalent and Covalent Anchored: N, N, N ′, N'-Tetramethyl-p-Phenylenediamine Derivative on Electrode Surface via Spontaneous Physical Immobilization and in Situ Generated Aryldiazonium Ion Electro-Grafting: Implication for on-Surface Chemistry . *Analyst* **2020**, *145* (2), 596–606. https://doi.org/10.1039/c9an01628g.

(23) Mohamad, N. R.; Marzuki, N. H. C.; Buang, N. A.; Huyop, F.; Wahab, R. A. An Overview of Technologies for Immobilization of Enzymes and Surface Analysis Techniques for Immobilized Enzymes. *Biotechnol. Biotechnol. Equip.* **2015**, *29* (2), 205–220. https://doi.org/10.1080/13102818.2015.1008192.

(24) Fabre, B. Bound to Hydrogen-Terminated Silicon Surfaces . Communication Devices. *Acc. Chem. Res.* **2010**, *43* (12), 1509–1518. https://doi.org/10.1021/ar100085q.

(25) Ciampi, S.; Eggers, P. K.; Le Saux, G.; James, M.; Harper, J. B.; Gooding, J. J. Silicon (100) Electrodes Resistant to Oxidation in Aqueous Solutions: An Unexpected Benefit of Surface Acetylene Moieties. *Langmuir* **2009**, *25* (4), 2530–2539. https://doi.org/10.1021/la803710d.

(26) G, D. Fuzzy Nanoassemblies: Toward Layered Polymeric Multicomposites. *Science (80-. ).* **1997**, *277* (August), 1232–1237.

(27) Li, Y.; Wang, X.; Sun, J. Layer-by-Layer Assembly for Rapid Fabrication of Thick Polymeric Films. *Chem. Soc. Rev.* **2012**, *41* (18), 5998–6009. https://doi.org/10.1039/c2cs35107b.

(28) Iqbal, M. S.; Zhan, W. Electrochemically Triggered Interfacial Deposition/Assembly of Aqueous-Suspended Colloids. *ChemElectroChem* **2020**, *7* (5), 1097–1106. https://doi.org/10.1002/celc.201902143.

(29) Hanna, C. M.; Sanborn, C. D.; Ardo, S.; Yang, J. Y. Interfacial Electron Transfer of Ferrocene Immobilized onto Indium Tin Oxide through Covalent and Noncovalent Interactions. *ACS Appl. Mater. Interfaces* **2018**, *10* (15), 13211–13217. https://doi.org/10.1021/acsami.8b01219.

(30) Fontanesi, C.; Como, E. Da; Vanossi, D.; Montecchi, M.; Cannio, M.; Mondal, P. C.; Giurlani, W.; Innocenti, M.; Pasquali, L. Redox-Active Ferrocene Grafted on H-Terminated Si(111): Electrochemical Characterization of the Charge Transport Mechanism and Dynamics. *Sci. Rep.* **2019**, *9* (1), 1–7. https://doi.org/10.1038/s41598-019-45448-w.

(31) Abruna, H. D.; Meyer, T. J.; Murray, R. W. Chemical and Electrochemical Properties of 2, 2'-Bipyiridyl Complexes of Ruthenium Covalently Bound to Platinum Oxide Electrodes. *Inorg. Chem.* **1979**, *18* (11), 3233–3240. https://doi.org/10.1021/ic50201a058.

(32) Murray, R. W. Chemically Modified Electrodes. *Acc. Chem. Res.* **1980**, *13* (5), 135–141. https://doi.org/10.1021/ar50149a002.

(33) Chidsey, C. E. D.; Bertozzi, C. R.; Putvinski, T. M.; Mujsce, A. M. Coadsorption of

Ferrocene-Terminated and Unsubstituted Alkanethiols on Gold: Electroactive Self-Assembled Monolayers. *J. Am. Chem. Soc.* **1990**, *112* (11), 4301–4306. https://doi.org/10.1021/ja00167a028.

(34) Zanoni, R.; Cattaruzza, F.; Coluzza, C.; Dalchiele, E. A.; Decker, F.; Di Santo, G.; Flamini, A.; Funari, L.; Marrani, A. G. An AFM, XPS and Electrochemical Study of Molecular Electroactive Monolayers Formed by Wet Chemistry Functionalization of H-Terminated Si(1 0 0) with Vinylferrocene. *Surf. Sci.* **2005**, *575* (3), 260–272. https://doi.org/10.1016/j.susc.2004.11.023.

(35) Dalchiele, E. A.; Aurora, A.; Bernardini, G.; Cattaruzza, F.; Flamini, A.; Pallavicini, P.; Zanoni, R.; Decker, F. XPS and Electrochemical Studies of Ferrocene Derivatives Anchored on N- and p-Si(1 0 0) by Si-O or Si-C Bonds. *J. Electroanal. Chem.* **2005**, *579* (1), 133–142. https://doi.org/10.1016/j.jelechem.2005.02.002.

(36) Tajimi, N.; Sano, H.; Murase, K.; Lee, K. H.; Sugimura, H. Thermal Immobilization of Ferrocene Derivatives on (111) Surface of n-Type Silicon: Parallel between Vinylferrocene and Ferrocenecarboxaldehyde. *Langmuir* **2007**, *23* (6), 3193–3198. https://doi.org/10.1021/la062674e.

(37) Elbert, J.; Gallei, M.; Rüttiger, C.; Brunsen, A.; Didzoleit, H.; Stühn, B.; Rehahn, M. Ferrocene Polymers for Switchable Surface Wettability. *Organometallics* **2013**, *32* (20), 5873–5878. https://doi.org/10.1021/om400468p.

(38) Astruc, D. Why Is Ferrocene so Exceptional? *Eur. J. Inorg. Chem.* **2017**, *2017* (1), 6–29. https://doi.org/10.1002/ejic.201600983.

(39) Son, E. J.; Kim, J. H.; Kim, K.; Park, C. B. Quinone and Its Derivatives for Energy Harvesting and Storage Materials. *J. Mater. Chem. A* **2016**, *4* (29), 11179–11202.

https://doi.org/10.1039/c6ta03123d.

(40) Quan, M.; Sanchez, D.; Wasylkiw, M. F.; Smith, D. K. Voltammetry of Quinones in Unbuffered Aqueous Solution: Reassessing the Roles of Proton Transfer and Hydrogen Bonding in the Aqueous Electrochemistry of Quinones. *J. Am. Chem. Soc.* **2007**, *129* (42), 12847–12856. https://doi.org/10.1021/ja0743083.

(41) Abhayawardhana, A. D.; Sutherland, T. C. Heterogeneous Proton-Coupled Electron Transfer of an Aminoanthraquinone Self-Assembled Monolayer. *J. Phys. Chem. C* **2009**, *113* (12), 4915–4924. https://doi.org/10.1021/jp807287p.

(42) Dey, R. S.; Gupta, S.; Paira, R.; Raj, C. R. Electrochemically Derived Redox Molecular Architecture: A Novel Electrochemical Interface for Voltammetric Sensing. *ACS Appl. Mater. Interfaces* **2010**, *2* (5), 1355–1360. https://doi.org/10.1021/am1000213.

(43) He, X.; Wang, X.; Jin, X.; Zhou, H.; Shi, X.; Chen, G.; Long, Y. Epimeric Monosaccharide-Quinone Hybrids on Gold Electrodes Protein Recognitions. *J. Am. Chem. Soc.* **2011**, 3649–3657.

(44) Curreli, M.; Li, C.; Sun, Y.; Lei, B.; Gundersen, M. A.; Thompson, M. E.; Zhou, C. Selective Functionalization of In2O3 Nanowire Mat Devices for Biosensing Applications. *J. Am. Chem. Soc.* **2005**, *127* (19), 6922–6923. https://doi.org/10.1021/ja0503478.

(45) Batchelor-Mcauley, C.; Kozub, B. R.; Menshykau, D.; Compton, R. G. Voltammetric Responses of Surface-Bound and Solution-Phase Anthraquinone Moieties in the Presence of Unbuffered Aqueous Media. *J. Phys. Chem. C* **2011**, *115* (3), 714–718. https://doi.org/10.1021/jp1096585.

(46) Hanna, C. M.; Luu, A.; Yang, J. Y. Proton-Coupled Electron Transfer at Anthraquinone Modified Indium Tin Oxide Electrodes. *ACS Appl. Energy Mater.* **2019**, *2* (1), 59–65.

https://doi.org/10.1021/acsaem.8b01568.

(47) Zhang, Q. D.; March, G.; Noel, V.; Piro, B.; Reisberg, S.; Tran, L. D.; Hai, L. V.; Abadia, E.; Nielsen, P. E.; Sola, C.; et al. Label-Free and Reagentless Electrochemical Detection of PCR Fragments Using Self-Assembled Quinone Derivative Monolayer: Application to Mycobacterium Tuberculosis. *Biosens. Bioelectron.* **2012**, *32* (1), 163–168. https://doi.org/10.1016/j.bios.2011.11.048.

(48) Abhayawardhana, A. D.; Sutherland, T. C. Heterogeneous Proton-Coupled Electron Transfer of a Hydroxy-Anthraquinone Self-Assembled Monolayer. *J. Electroanal. Chem.* **2011**, *653* (1–2), 50–55. https://doi.org/10.1016/j.jelechem.2011.01.009.

(49) Kang, D.; Ricci, F.; White, R. J.; Plaxco, K. W. Survey of Redox-Active Moieties for Application in Multiplexed Electrochemical Biosensors. *Anal. Chem.* **2016**, *88* (21), 10452–10458. https://doi.org/10.1021/acs.analchem.6b02376.

(50) Barsan, M. M.; Ghica, M. E.; Brett, C. M. A. Electrochemical Sensors and Biosensors Based on Redox Polymer/Carbon Nanotube Modified Electrodes: A Review. *Anal. Chim. Acta* **2015**, *881*, 1–23. https://doi.org/10.1016/j.aca.2015.02.059.

(51) Nuzzo, R. G.; Allara, D. L. Adsorption of Bifunctional Organic Disulfides on Gold Surfaces. *J. Am. Chem. Soc.* **1983**, *105* (13), 4481–4483. https://doi.org/10.1021/ja00351a063.

(52) Porter, M. D.; Bright, T. B.; Allara, D. L.; Chidsey, C. E. Spontaneously Organized Molecular Assemblies. 4. Structural Characterization of n-Alkyl Thiol Monolayers on Gold by Optical Ellipsometry, Infrared Spectroscopy, and Electrochemistry. *J. Am. Chem. Soc.* **1987**, *109* (12), 3559–3568. https://doi.org/10.1021/ja00246a011.

(53) Iqbal, M. S.; Zhan, W. Electrochemically Triggered Surface Deposition of

Polyelectrolytes. *Langmuir* **2018**, *34* (43), 12776–12786. https://doi.org/10.1021/acs.langmuir.8b02671.

(54) Laibinis, P. E.; Whitesides, G. M.; Aliara, D. L.; Tao, Y. T.; Parikh, A. N.; Nuzzo, R. G. Comparison of the Structures and Wetting Properties of Self-Assembled Monolayers of n-Alkanethiols on the Coinage Metal Surfaces, Cu, Ag, Au. *J. Am. Chem. Soc.* **1991**, *113* (19), 7152–7167. https://doi.org/10.1021/ja00019a011.

(55) Dowling, D. P.; Donnelly, K.; McConnell, M. L.; Eloy, R.; Arnaud, M. N. Deposition of Anti-Bacterial Silver Coatings on Polymeric Substrates. *Thin Solid Films* **2001**, *398* (399), 602–606. https://doi.org/10.1016/S0040-6090(01)01326-8.

(56) Poon, V. K. M.; Burd, A. In Vitro Cytotoxity of Silver: Implication for Clinical Wound Care. *Burns* **2004**, *30* (2), 140–147. https://doi.org/10.1016/j.burns.2003.09.030.

(57) Carvalho, A.; Geissler, M.; Schmid, H.; Michel, B.; Delamarche, E. Self-Assembled Monolayers of Eicosanethiol on Palladium and Their Use in Microcontact Printing. *Langmuir* **2002**, *18* (6), 2406–2412. https://doi.org/10.1021/la015596y.

(58) Stanley Wolf, R. N. T. *Silicon Processing for the VLSI Era*; Sunset Beach, CA. : Lattice Press, c1986., 1986.

(59) Werner, H. At Least 60 Years of Ferrocene: The Discovery and Rediscovery of the Sandwich Complexes. *Angew. Chemie - Int. Ed.* **2012**, *51* (25), 6052–6058. https://doi.org/10.1002/anie.201201598.

(60) KEALY, T. J.; PAUSON, P. L. A New Type of Organo-Iron Compound. *Nature* **1951**, *168* (4285), 1039–1040. https://doi.org/10.1038/1681039b0.

(61) Woodward, R. B.; Rosenblum, M.; Whiting, M. C. A NEW AROMATIC SYSTEM. *J. Am. Chem. Soc.* **1952**, *74* (13), 3458–3459. https://doi.org/10.1021/ja01133a543.

(62) Connelly, N. G.; Geiger, W. E. Chemical Redox Agents for Organometallic Chemistry. *Chem. Rev.* **1996**, *96* (2), 877–910. https://doi.org/10.1021/cr940053x.

(63) Yokota, Y.; Yamada, T.; Kawai, M. Ion-Pair Formation between Ferrocene-Terminated Self-Assembled Monolayers and Counteranions Studied by Force Measurements. *J. Phys. Chem. C* **2011**, *115* (14), 6775–6781. https://doi.org/10.1021/jp2001404.

(64) Noviandri, I.; Brown, K. N.; Fleming, D. S.; Gulyas, P. T.; Lay, P. A.; Masters, A. F.; Phillips, L. The Decamethylferrocenium/Decamethylferrocene Redox Couple: A Superior Redox Standard to the Ferrocenium/Ferrocene Redox Couple for Studying Solvent Effects on the Thermodynamics of Electron Transfer. *J. Phys. Chem. B* **1999**, *103* (32), 6713–6722. https://doi.org/10.1021/jp991381+.

(65) Bard, A. J.; Faulkner, L. R. *Electrochemical Methods: Fundamentals and Applications*, 2nd ed.; Willey: New York, 2001.

(66) Dubois, L. H.; Nuzzo, R. G. Synthesis, Structure, and Properties of Model Organic Surfaces. *Annu. Rev. Phys. Chem.* **1992**, *43* (1), 437–463. https://doi.org/10.1146/annurev.pc.43.100192.002253.

(67) Bain, C. D.; Whitesides, G. M. Molecular-Level Control over Surface Order in Self-Assembled Monolayer Films of Thiols on Gold. *Science* **1988**, *240* (4848), 62–63. https://doi.org/10.1126/science.240.4848.62.

(68) Rowe, G. K.; Creager, S. E. Redox and Ion-Pairing Thermodynamics in Self-Assembled Monolayers. *Langmuir* **1991**, *7* (10), 2307–2312. https://doi.org/10.1021/la00058a055.

(69) Uosaki, K.; Sato, Y.; Kita, H. Electrochemical Characteristics of a Gold Electrode Modified with a Self-Assembled Monolayer of Ferrocenylalkanethiols. *Langmuir* **1991**, *7* (7), 1510–1514. https://doi.org/10.1021/la00055a038.

(70) Christopher Love, J.; Wolfe, D. B.; Haasch, R.; Chabinyc, M. L.; Paul, K. E.; Whitesides, G. M.; Nuzzo, R. G. Formation and Structure of Self-Assembled Monolayers of Alkanethiolates on Palladium. *J. Am. Chem. Soc.* **2003**, *125* (9), 2597–2609. https://doi.org/10.1021/ja028692+.

(71) Bain, C. D.; Troughton, E. B.; Tao, Y. T.; Evall, J.; Whitesides, G. M.; Nuzzo, R. G. Formation of Monolayer Films by the Spontaneous Assembly of Organic Thiols from Solution onto Gold. *J. Am. Chem. Soc.* **1989**, *111* (1), 321–335. https://doi.org/10.1021/ja00183a049.

(72) Yamada, R.; Wano, H.; Uosaki, K. Effect of Temperature on Structure of the Self-Assembled Monolayer of Decanethiol on Au(111) Surface. *Langmuir* **2000**, *16* (13), 5523–5525. https://doi.org/10.1021/la991394e.

(73) Kawasaki, M.; Sato, T.; Tanaka, T.; Takao, K. Rapid Self-Assembly of Alkanethiol Monolayers on Sputter-Grown Au(111). *Langmuir* **2000**, *16* (4), 1719–1728. https://doi.org/10.1021/la990310z.

(74) Bensebaa, F.; Voicu, R.; Huron, L.; Ellis, T. H.; Kruus, E. Kinetics of Formation of Long-Chain n-Alkanethiolate Monolayers on Polycrystalline Gold. *Langmuir* **1997**, *13* (20), 5335–5340. https://doi.org/10.1021/la970052a.

(75) Häkkinen, H. The Gold–Sulfur Interface at the Nanoscale. *Nat. Chem.* **2012**, *4* (6), 443–455. https://doi.org/10.1038/nchem.1352.

(76) Nuzzo, R. G.; Zegarski, B. R.; DuBois, L. H. Fundamental Studies of the Chemisorption of Organosulfur Compounds on Au( 111). Implications for Molecular Self-Assembly on Gold Surfaces. *J. Am. Chem. Soc.* **1987**, *109* (3), 733–740. https://doi.org/10.1021/ja00237a017.

(77) Castner, D. G.; Hinds, K.; Grainger, D. W. X-Ray Photoelectron Spectroscopy Sulfur 2p Study of Organic Thiol and Bisulfide Binding Interactions with Gold Surfaces. *Langmuir* **1996**, *12* (21), 5083–5086. https://doi.org/10.1021/la960465w.

(78) Kankate, L.; Turchanin, A.; Gölzhäuser, A. On the Release of Hydrogen from the S-H Groups in the Formation of Self-Assembled Monolayers of Thiols. *Langmuir* **2009**, *25* (18), 10435–10438. https://doi.org/10.1021/la902168u.

(79) Inkpen, M. S.; Liu, Z. –F; Li, H.; Campos, L. M.; Neaton, J. B.; Venkataraman, L. Non-Chemisorbed Gold–Sulfur Binding Prevails in Self-Assembled Monolayers. *Nat. Chem.* **2019**, *11* (4), 351–358. https://doi.org/10.1038/s41557-019-0216-y.

(80) Nerngchamnong, N.; Thompson, D.; Cao, L.; Yuan, L.; Jiang, L.; Roemer, M.; Nijhuis, C. A. Nonideal Electrochemical Behavior of Ferrocenyl-Alkanethiolate SAMs Maps the Microenvironment of the Redox Unit. *J. Phys. Chem. C* **2015**, *119* (38), 21978–21991. https://doi.org/10.1021/acs.jpcc.5b05137.

(81) Chidsey, C. E. D. Free Energy and Temperature Dependence of Electron Transfer at the Metal-Electrolyte Interface. *Science (80-. ).* **1991**, *251* (4996), 919 LP – 922. https://doi.org/10.1126/science.251.4996.919.

(82) Auletta, T.; Veggel, F. C. J. M. Van; Reinhoudt, D. N. Self-Assembled Monolayers on Gold of Ferrocene-Terminated Thiols and Hydroxyalkanethiols. **2002**, No. d, 1288–1293. https://doi.org/10.1021/la011474u.

(83) Lee, L. Y. S.; Sutherland, T. C.; Rucareanu, S.; Lennox, R. B. Ferrocenylalkylthiolates as a Probe of Heterogeneity in Binary Self-Assembled Monolayers on Gold. *Langmuir* **2006**, *22* (9), 4438–4444. https://doi.org/10.1021/la053317r.

(84) Guo, Y.; Zhao, J.; Zhu, J. Study on the Intermolecular Interactions between the Functional

Moieties in Ferrocene-Terminated Alkanethiol Self-Assembled Monolayer on Gold. *Thin Solid Films* **2008**, *516* (10), 3051–3057. https://doi.org/10.1016/j.tsf.2007.12.092.

(85) Ju, H.; Leech, D. Effect of Electrolytes on the Electrochemical Behaviour of 11-(Ferrocenylcarbonyloxy)Undecanethiol SAMs on Gold Disk Electrodes. *Phys. Chem. Chem. Phys.* **1999**, *1* (7), 1549–1554. https://doi.org/10.1039/a809754b.

(86) Nerngchamnong, N.; Wu, H.; Sotthewes, K.; Yuan, L.; Cao, L.; Roemer, M.; Lu, J.; Loh, K. P.; Troadec, C.; Zandvliet, H. J. W.; et al. Supramolecular Structure of Self-Assembled Monolayers of Ferrocenyl Terminated n -Alkanethiolates on Gold Surfaces. *Langmuir* **2014**, *30* (44), 13447–13455. https://doi.org/10.1021/la503493x.

(87) Feng, Y.; Dionne, E. R.; Toader, V.; Beaudoin, G.; Badia, A. Odd-Even Effects in Electroactive Self-Assembled Monolayers Investigated by Electrochemical Surface Plasmon Resonance and Impedance Spectroscopy. *J. Phys. Chem. C* **2017**, *121* (39), 24626–24640. https://doi.org/10.1021/acs.jpcc.7b08053.

(88) Tao, F.; Bernasek, S. L. Understanding Odd-Even Effects in Organic Self-Assembled Monolayers. *Chem. Rev.* **2007**, *107* (5), 1408–1453. https://doi.org/10.1021/cr050258d.

(89) Colorado, R.; Villazana, R. J.; Lee, T. R. Self-Assembled Monolayers on Gold Generated from Aliphatic Dithiocarboxylic Acids. *Langmuir* **1998**, *14* (22), 6337–6340. https://doi.org/10.1021/la9804381.

(90) Heister, K.; Rong, H. T.; Buck, M.; Zharnikov, M.; Grunze, M.; Johansson, L. S. O. Odd-Even Effects at the S-Metal Interface and in the Aromatic Matrix of Biphenyl-Substituted Alkanethiol Self-Assembled Monolayers. *J. Phys. Chem. B* **2001**, *105* (29), 6888–6894. https://doi.org/10.1021/jp010180e.

(91) Creager, S. E.; Rowe, G. K. Solvent and Double-Layer Effects on Redox Reactions in

Self-Assembled Monolayers of Ferrocenyl-Alkanethiolates on Gold. *J. Electroanal. Chem.* **1997**, *420* (1–2), 291–299. https://doi.org/10.1016/S0022-0728(96)04785-7.

(92) Tian, H.; Dai, Y.; Shao, H.; Yu, H. Z. Modulated Intermolecular Interactions in Ferrocenylalkanethiolate Self-Assembled Monolayers on Gold. *J. Phys. Chem. C* **2013**, *117* (2), 1006–1012. https://doi.org/10.1021/jp310012v.

(93) Duffin, T. J.; Nerngchamnong, N.; Thompson, D.; Nijhuis, C. A. Direct Measurement of the Local Field within Alkyl-Ferrocenyl-Alkanethiolate Monolayers: Importance of the Supramolecular and Electronic Structure on the Voltammetric Response and Potential Profile. *Electrochim. Acta* **2019**, *311*, 92–102. https://doi.org/10.1016/j.electacta.2019.04.041.

(94) Song, P.; Yuan, L.; Roemer, M.; Jiang, L.; Nijhuis, C. A. Supramolecular vs Electronic Structure: The Effect of the Tilt Angle of the Active Group in the Performance of a Molecular Diode. *J. Am. Chem. Soc.* **2016**, *138* (18), 5769–5772. https://doi.org/10.1021/jacs.6b02208.

(95) Yokota, Y.; Mino, Y.; Kanai, Y.; Utsunomiya, T.; Imanishi, A.; Wolak, M. A.; Schlaf, R.; Fukui, K. I. Comparative Studies of Photoelectron Spectroscopy and Voltammetry of Ferrocene-Terminated Self-Assembled Monolayers Possessing Different Electron-Donating Abilities. *J. Phys. Chem. C* **2014**, *118* (20), 10936–10943. https://doi.org/10.1021/jp5023899.

(96) Rudnev, A. V.; Zhumaev, U.; Utsunomiya, T.; Fan, C.; Yokota, Y.; Fukui, K. I.; Wandlowski, T. Ferrocene-Terminated Alkanethiol Self-Assembled Monolayers: An Electrochemical and in Situ Surface-Enhanced Infra-Red Absorption Spectroscopy Study. *Electrochim. Acta* **2013**, *107* (3), 33–44. https://doi.org/10.1016/j.electacta.2013.05.134.

(97) Valincius, G.; Niaura, G.; Kazakevičiene, B.; Talaikyte, Z.; Kažemekaite, M.; Butkus, E.; Razumas, V. Anion Effect on Mediated Electron Transfer through Ferrocene-Terminated Self-Assembled Monolayers. *Langmuir* **2004**, *20* (16), 6631–6638. https://doi.org/10.1021/la0364800.

(98) Cruanes, M. T.; Drickamer, H. G.; Faulkner, L. R. Characterization of Charge Transfer Processes in Self-Assembled Monolayers by High-Pressure Electrochemical Techniques. *Langmuir* **1995**, *11* (10), 4089–4097. https://doi.org/10.1021/la00010a074.

(99) Redepenning, J.; Flood, J. M. Influence of Electrolyte Activity on Formal Potentials Measured for Ferrocenylhexanethiol Monolayers on Gold: Indistinguishable Responses in Aqueous Solutions of HClO4 and NaClO4. *Langmuir* **1996**, *12* (2), 508–512. https://doi.org/10.1021/la950715t.

(100) Chambers, R. C.; Inman, C. E.; Hutchison, J. E. Electrochemical Detection of Nanoscale Phase Separation in Binary Self-Assembled Monolayers. *Langmuir* **2005**, *21* (10), 4615–4621. https://doi.org/10.1021/la050104t.

(101) Ye, S.; Sato, Y.; Uosaki, K. Redox-Induced Orientation Change of a Self-Assembled Monolayer of 11-Ferrocenyl-1-Undecanethiol on a Gold Electrode Studied by in Situ FT-IRRAS. *Langmuir* **1997**, *13* (12), 3157–3161. https://doi.org/10.1021/la9700432.

(102) Shimazu, K.; Ye, S.; Sato, Y.; Uosaki, K. Simultaneous Detection of Structural Change and Mass Transport Accompanying the Redox of a Ferrocenylundecanethiol Monolayer with the Novel FT-IR Reflection Absorption Spectroscopy/Electrochemical Quartz Crystal Microbalance Combined System. *J. Electroanal. Chem.* **1994**, *375* (1–2), 409–413. https://doi.org/10.1016/0022-0728(94)03601-2.

(103) Norman, L. L.; Badia, A. Redox Actuation of a Microcantilever Driven by a Self-

Assembled Ferrocenylundecanethiolate Monolayer : An Investigation of the Origin of the Micromechanical Motion and Surface Stress. **2009**, No. 5, 2328–2337.

(104) Dionne, E. R.; Toader, V.; Badia, A. Microcantilevers Bend to the Pressure of Clustered Redox Centers. *Langmuir* **2014**, *30* (3), 742–752. https://doi.org/10.1021/la403551c.

(105) Ohtsuka, T.; Sato, Y.; Uosaki, K. Dynamic Ellipsometry of a Self-Assembled Monolayer of a Ferrocenylalkanethiol during Oxidation-Reduction Cycles. *Langmuir* **1994**, *10* (10), 3658–3662. https://doi.org/10.1021/la00022a045.

(106) Yao, X.; Wang, J.; Zhou, F.; Wang, J.; Tao, N. Quantification of Redox-Induced Thickness Changes of 11- Ferrocenylundecanethiol Self-Assembled Monolayers by Electrochemical Surface Plasmon Resonance. *J. Phys. Chem. B* **2004**, *108* (22), 7206–7212. https://doi.org/10.1021/jp049651y.

(107) Uematsu, T.; Kuwabata, S. In Situ Surface Plasmon Resonance Measurements of Self-Assembled Monolayers of Ferrocenylalkylthiols under Constant Potentials. *Anal. Sci.* **2008**, *24* (3), 307–312. https://doi.org/10.2116/analsci.24.307.

(108) Periyasamy, G.; Levine, R. D.; Remacle, F. Redox-Executed Logic Operations through the Reversible Voltammetric Response Characteristics of Electroactive Self-Assembled Monolayers. *Aust. J. Chem.* **2010**, *63* (2), 173–183. https://doi.org/10.1071/CH09504.

(109) Marchante, E.; Crivillers, N.; Buhl, M.; Veciana, J.; Mas-Torrent, M. An Electrically Driven and Readable Molecular Monolayer Switch Based on a Solid Electrolyte. *Angew. Chemie - Int. Ed.* **2016**, *55* (1), 368–372. https://doi.org/10.1002/anie.201508449.

(110) Abel, A.; Wu, Y.; Bachmann, J. Stimulus-Responsive Nanoporous System Based on a Redox-Active Molecular Self-Assembled Monolayer. *Langmuir* **2017**, *33* (33), 8289–8294. https://doi.org/10.1021/acs.langmuir.7b01918.

(111) Banerjee, S.; Tyagi, A. K.; Hassan, P. A.; Verma, G.; Ganguly, R. Soft Materials — Properties and Applications. *Funct. Mater*. **2012**, 1–59. https://doi.org/10.1016/B978-0-12-385142-0.00001-5.

(112) Jayasuriya, A. C. Production of Micro- and Nanoscale Chitosan Particles for Biomedical Applications. *Chitosan Based Biomater. Vol. 1* **2017**, 185–209. https://doi.org/10.1016/B978-0-08-100230-8.00008-X.

(113) Schanze, K. S.; Shelton, A. H. Functional Polyelectrolytes. *Langmuir* **2009**, *25* (24), 13698–13702. https://doi.org/10.1021/la903785g.

(114) Stuart, M. C.; de Vries, R.; Lyklema, H. Polyelectrolytes. *Fundam. Interface Colloid Sci.* **2005**, *5*, 2.1-2.84. https://doi.org/10.1016/S1874-5679(05)80006-6.

(115) Zhang, W.; Zhao, Q.; Yuan, J. Porous Polyelectrolytes: The Interplay of Charge and Pores for New Functionalities. *Angew. Chemie - Int. Ed.* **2018**, *57* (23), 6754–6773. https://doi.org/10.1002/anie.201710272.

(116) Decher, G.; Hong, J. D.; Schmitt, J. Buildup of Ultrathin Multilayer Films by a Self-Assembly Process: III. Consecutively Alternating Adsorption of Anionic and Cationic Polyelectrolytes on Charged Surfaces. *Thin Solid Films* **1992**, *210–211* (PART 2), 831–835. https://doi.org/10.1016/0040-6090(92)90417-A.

(117) Muthukumar, M. 50th Anniversary Perspective: A Perspective on Polyelectrolyte Solutions. *Macromolecules* **2017**, *50* (24), 9528–9560. https://doi.org/10.1021/acs.macromol.7b01929.

(118) Mévellec, V.; Roussel, S.; Tessier, L.; Chancolon, J.; Mayne-L'Hermite, M.; Deniau, G.; Viel, P.; Palacin, S. Grafting Polymers on Surfaces: A New Powerful and Versatile Diazonium Salt-Based One-Step Process in Aqueous Media. *Chem. Mater.* **2007**, *19* (25),

6323–6330. https://doi.org/10.1021/cm071371i.

(119) Lee, S. S.; Hong, J. D.; Kim, C. H.; Kim, K.; Koo, J. P.; Lee, K. B. Layer-by-Layer Deposited Multilayer Assemblies of Ionene-Type Polyelectrolytes Based on the Spin-Coating Method [2]. *Macromolecules* **2001**, *34* (16), 5358–5360. https://doi.org/10.1021/ma0022304.

(120) Cho, J.; Char, K.; Hong, J. D.; Lee, K. B. Fabrication of Highly Ordered Multilayer Films Using a Spin Self-Assembly Method. *Adv. Mater.* **2001**, *13* (14), 1076–1078. https://doi.org/10.1002/1521-4095(200107)13:14<1076::AID-ADMA1076>3.0.CO;2-M.

(121) Chiarelli, P. A.; Johal, M. S.; Casson, J. L.; Roberts, J. B.; Robinson, J. M.; Wang, H. L. Controlled Fabrication of Polyelectrolyte Multilayer Thin Films Using Spin-Assembly. *Adv. Mater.* **2001**, *13* (15), 1167–1171. https://doi.org/10.1002/1521-4095(200108)13:15<1167::AID-ADMA1167>3.0.CO;2-A.

(122) Schlenoff, J. B.; Dubas, S. T.; Farhat, T. Sprayed Polyelectrolyte Multilayers. *Langmuir* **2000**, *16* (26), 9968–9969. https://doi.org/10.1021/la001312i.

(123) Schaaf, P.; Voegel, J. C.; Jierry, L.; Boulmedais, F. Spray-Assisted Polyelectrolyte Multilayer Buildup: From Step-by-Step to Single-Step Polyelectrolyte Film Constructions. *Adv. Mater.* **2012**, *24* (8), 1001–1016. https://doi.org/10.1002/adma.201104227.

(124) Merrill, M. H.; Sun, C. T. Fast, Simple and Efficient Assembly of Nanolayered Materials and Devices. *Nanotechnology* **2009**, *20* (7). https://doi.org/10.1088/0957-4484/20/7/075606.

(125) Hesselink, F. T. On the Adsorption of Polyelectrolyte Macromolecules on a Flat Interface. An Approximate Theory for Low Potentials. *J. Electroanal. Chem.* **1972**, *37* (1), 317–325. https://doi.org/10.1016/S0022-0728(72)80236-5.

(126) Hesselink, F. T. On the Theory of Polyelectrolyte Adsorption to the Adsorption Free Energy. *J. Colloid Interface Sci.* **1977**, *60* (7), 448–466.

(127) Cosgrove, T. Obey, T. M. Vincent, B. The Configuration of Sodium Poly(Styrene Sulfonate) at Polystyrene/Solution Interfaces. *J. Colloid Interface Sci.* **1986**, *111* (2), 409–418.

(128) R. K. Iler. Multilayers of Colloidal Particles. *J. Colloid Interface Sci.* **1966**, *21* (6), 569–594.

(129) Decher, G.; Hong, J. -D. Buildup of Ultrathin Multilayer Films by a Self-assembly Process, 1 Consecutive Adsorption of Anionic and Cationic Bipolar Amphiphiles on Charged Surfaces. *Makromol. Chemie. Macromol. Symp.* **1991**, *46* (1), 321–327. https://doi.org/10.1002/masy.19910460145.

(130) Richardson, J. J.; Cui, J.; Björnmalm, M.; Braunger, J. A.; Ejima, H.; Caruso, F. Innovation in Layer-by-Layer Assembly. *Chem. Rev.* **2016**, *116* (23), 14828–14867. https://doi.org/10.1021/acs.chemrev.6b00627.

(131) Borges, J.; Mano, J. F. Molecular Interactions Driving the Layer-by-Layer Assembly of Multilayers. *Chem. Rev.* **2014**, *114* (18), 8883–8942. https://doi.org/10.1021/cr400531v.

(132) Krogman, K. C.; Zacharia, N. S.; Schroeder, S.; Hammond, P. T. Automated Process for Improved Uniformity and Versatility of Layer-by-Layer Deposition. *Langmuir* **2007**, *23* (6), 3137–3141. https://doi.org/10.1021/la063085b.

(133) Krogman, K. C.; Lowery, J. L.; Zacharia, N. S.; Rutledge, G. C.; Hammond, P. T. Spraying Asymmetry into Functional Membranes Layer-by-Layer. *Nat. Mater.* **2009**, *8* (6), 512–518. https://doi.org/10.1038/nmat2430.

(134) Kim, S. Y.; Hong, J.; Kavian, R.; Lee, S. W.; Hyder, M. N.; Shao-Horn, Y.; Hammond, P.

T. Rapid Fabrication of Thick Spray-Layer-by-Layer Carbon Nanotube Electrodes for High Power and Energy Devices. *Energy Environ. Sci.* **2013**, *6* (3), 888–897. https://doi.org/10.1039/c2ee23318e.

(135) Kim, H. J.; Lee, K.; Kumar, S.; Kim, J. Dynamic Sequential Layer-by-Layer Deposition Method for Fast and Region-Selective Multilayer Thin Film Fabrication. *Langmuir* **2005**, *21* (18), 8532–8538. https://doi.org/10.1021/la0511182.

(136) Ma, L.; Cheng, M.; Jia, G.; Wang, Y.; An, Q.; Zeng, X.; Shen, Z.; Zhang, Y.; Shi, F. Layer-by-Layer Self-Assembly under High Gravity Field. *Langmuir* **2012**, *28* (25), 9849–9856. https://doi.org/10.1021/la301553w.

(137) Wang, T. C.; Chen, B.; Rubner, M. F.; Cohen, R. E. Selective Electroless Nickel Plating on Polyelectrolyte Multilayer Platforms. *Langmuir* **2001**, *17* (21), 6610–6615. https://doi.org/10.1021/la010755z.

(138) Andres, C. M.; Kotov, N. A. Inkjet Deposition of Layer-by-Layer Assembled Films. *J. Am. Chem. Soc.* **2010**, *132* (41), 14496–14502. https://doi.org/10.1021/ja104735a.

(139) Suntivich, R.; Shchepelina, O.; Choi, I.; Tsukruk, V. V. Inkjet-Assisted Layer-by-Layer Printing of Encapsulated Arrays. *ACS Appl. Mater. Interfaces* **2012**, *4* (6), 3102–3110. https://doi.org/10.1021/am3004544.

(140) Richardson, J. J.; Ejima, H.; Lörcher, S. L.; Liang, K.; Senn, P.; Cui, J.; Caruso, F. Preparation of Nano- and Microcapsules by Electrophoretic Polymer Assembly. *Angew. Chemie - Int. Ed.* **2013**, *52* (25), 6455–6458. https://doi.org/10.1002/anie.201302092.

(141) Dubas, S. T.; Schlenoff, J. B. Swelling and Smoothing of Polyelectrolyte Multilayers by Salt. *Langmuir* **2001**, *17* (25), 7725–7727. https://doi.org/10.1021/la0112099.

(142) Dubas, S. T.; Schlenoff, J. B. Polyelectrolyte Multilayers Containing a Weak Polyacid:

Construction and Deconstruction. *Macromolecules* **2001**, *34* (11), 3736–3740. https://doi.org/10.1021/ma001720t.

(143) Büscher, K.; Graf, K.; Ahrens, H.; Helm, C. A. Influence of Adsorption Conditions on the Structure of Polyelectrolyte Multilayers. *Langmuir* **2002**, *18* (9), 3585–3591. https://doi.org/10.1021/la011682m.

(144) Dubas, S. T.; Farhat, T. R.; Schlenoff, J. B. Multiple Membranes from "True" Polyelectrolyte Multilayers [11]. *J. Am. Chem. Soc.* **2001**, *123* (22), 5368–5369. https://doi.org/10.1021/ja015774+.

(145) Chung, A. J.; Rubner, M. F. Methods of Loading and Releasing Low Molecular Weight Cationic Molecules in Weak Polyelectrolyte Multilayer Films. *Langmuir* **2002**, *18* (4), 1176–1183. https://doi.org/10.1021/la010873m.

(146) Delcea, M.; Möhwald, H.; Skirtach, A. G. Stimuli-Responsive LbL Capsules and Nanoshells for Drug Delivery. *Adv. Drug Deliv. Rev.* **2011**, *63* (9), 730–747. https://doi.org/10.1016/j.addr.2011.03.010.

(147) Shi, L.; Lu, Y.; Sun, J.; Zhang, J.; Sun, C.; Liu, J.; Shen, J. Site-Selective Lateral Multilayer Assembly of Bienzyme with Polyelectrolyte on ITO Electrode Based on Electric Field-Induced Directly Layer-by-Layer Deposition. *Biomacromolecules* **2003**, *4* (5), 1161–1167. https://doi.org/10.1021/bm030003e.

(148) Yamauchi, F.; Kato, K.; Iwata, H. Layer-by-Layer Assembly of Poly(Ethyleneimine) and Plasmid DNA onto Transparent Indium-Tin Oxide Electrodes for Temporally and Spatially Specific Gene Transfer. *Langmuir* **2005**, *21* (18), 8360–8367. https://doi.org/10.1021/la0505059.

(149) Boulmedais, F.; Tang, C. S.; Keller, B.; Vörös, J. Controlled Electrodissolution of

Polyelectrolyte Multilayers: A Platform Technology towards the Surface-Initiated Delivery of Drugs. *Adv. Funct. Mater.* **2006**, *16* (1), 63–70. https://doi.org/10.1002/adfm.200400406.

(150) Wang, Y.; Han, P.; Wu, G.; Xu, H.; Wang, Z.; Zhang, X. Selectively Erasable Multilayer Thin Film by Photoinduced Disassembly. *Langmuir* **2010**, *26* (12), 9736–9741. https://doi.org/10.1021/la1004648.

(151) Bédard, M. F.; De Geest, B. G.; Skirtach, A. G.; Möhwald, H.; Sukhorukov, G. B. Polymeric Microcapsules with Light Responsive Properties for Encapsulation and Release. *Adv. Colloid Interface Sci.* **2010**, *158* (1–2), 2–14. https://doi.org/10.1016/j.cis.2009.07.007.

(152) Tan, H. L.; McMurdo, M. J.; Pan, G.; Van Patten, P. G. Temperature Dependence of Polyelectrolyte Multilayer Assembly. *Langmuir* **2003**, *19* (22), 9311–9314. https://doi.org/10.1021/la035094f.

(153) Sukhorukov, G. B.; Möhwald, H.; Decher, G.; Lvov, Y. M. Assembly of Polyelectrolyte Multilayer Films by Consecutively Alternating Adsorption of Polynucleotides and Polycations. *Thin Solid Films* **1996**, *284–285* (95), 220–223. https://doi.org/10.1016/S0040-6090(95)08309-X.

(154) Caruso, F.; Niikura, K.; Furlong, D. N.; Okahata, Y. 2. Assembly of Alternating Polyelectrolyte and Protein Multilayer Films for Imiminosensing. *Langmuir* **1997**, *13* (13), 3427–3433. https://doi.org/10.1021/la9608223.

(155) Schoeler, B.; Kumaraswamy, G.; Caruso, F. Investigation of the Influence of Polyelectrolyte Charge Density on the Growth of Multilayer Thin Films Prepared by the Layer-by-Layer Technique. *Macromolecules* **2002**, *35* (3), 889–897.

https://doi.org/10.1021/ma011349p.

(156) Clark, S. L.; Montague, M.; Hammond, P. T. Selective Deposition in Multilayer Assembly: SAMs as Molecular Templates. *Supramol. Sci.* **1997**, *4* (1–2), 141–146. https://doi.org/10.1016/S0968-5677(96)00055-7.

(157) Elbert, D. L.; Herbert, C. B.; Hubbell, J. A. Thin Polymer Layers Formed by Polyelectrolyte Multilayer Techniques on Biological Surfaces. *Langmuir* **1999**, *15* (16), 5355–5362. https://doi.org/10.1021/la9815749.

(158) Ruths, J.; Essler, F.; Decher, G.; Riegler, H. Polyelectrolytes. I: Polyanion/Polycation Multilayers at the Air/Monolayer/Water Interface as Elements for Quantitative Polymer Adsorption Studies and Preparation of Hetero-Superlattices on Solid Surfaces. *Langmuir* **2000**, *16* (23), 8871–8878. https://doi.org/10.1021/la000257a.

(159) Picart, C.; Mutterer, J.; Richert, L.; Luo, Y.; Prestwich, G. D.; Schaaf, P.; Voegel, J. C.; Lavalle, P. Molecular Basis for the Explanation of the Exponential Growth of Polyelectrolyte Multilayers. *Proc. Natl. Acad. Sci. U. S. A.* **2002**, *99* (20), 12531–12535. https://doi.org/10.1073/pnas.202486099.

(160) Halthur, T. J.; Elofsson, U. M. Multilayers of Charged Polypeptides as Studied by in Situ Ellipsometry and Quartz Crystal Microbalance with Dissipation. *Langmuir* **2004**, *20* (5), 1739–1745. https://doi.org/10.1021/la035475t.

(161) Lavalle, P.; Vivet, V.; Jessel, N.; Decher, G.; Voegel, J. C.; Mesini, P. J.; Schaaf, P. Direct Evidence for Vertical Diffusion and Exchange Processes of Polyanions and Polycations in Polyelectrolyte Multilayer Films. *Macromolecules* **2004**, *37* (3), 1159–1162. https://doi.org/10.1021/ma035326h.

(162) Podsiadlo, P.; Michel, M.; Lee, J.; Verploegen, E.; Kam, N. W. S.; Ball, V.; Lee, J.; Qi,

Y.; Hart, A. J.; Hammond, P. T.; et al. Exponential Growth of LBL Films with Incorporated Inorganic Sheets. *Nano Lett.* **2008**, *8* (6), 1762–1770. https://doi.org/10.1021/nl8011648.

(163) Wang, Y.; Tang, Z.; Podsiadlo, P.; Elkasabi, Y.; Lahann, J.; Kotov, N. A. Mirror-like Photoconductive Layer-by-Layer Thin Films of Te Nanowires: The Fusion of Semiconductor, Metal, and Insulator Properties. *Adv. Mater.* **2006**, *18* (4), 518–522. https://doi.org/10.1002/adma.200501465.

(164) Wang, Y.; Angelatos, A. S.; Caruso, F. Template Synthesis of Nanostructured Materials via Layer-by-Layer Assembly. *Chem. Mater.* **2008**, *20* (3), 848–858. https://doi.org/10.1021/cm7024813.

(165) De Geest, B. G.; De Koker, S.; Sukhorukov, G. B.; Kreft, O.; Parak, W. J.; Skirtach, A. G.; Demeester, J.; De Smedt, S. C.; Hennink, W. E. Polyelectrolyte Microcapsules for Biomedical Applications. *Soft Matter* **2009**, *5* (2), 282–291. https://doi.org/10.1039/b808262f.

(166) Tong, W.; Song, X.; Gao, C. Layer-by-Layer Assembly of Microcapsules and Their Biomedical Applications. *Chem. Soc. Rev.* **2012**, *41* (18), 6103–6124. https://doi.org/10.1039/c2cs35088b.

(167) Boudou, T.; Crouzier, T.; Ren, K.; Blin, G.; Picart, C. Multiple Functionalities of Polyelectrolyte Multilayer Films: New Biomedical Applications. *Adv. Mater.* **2010**, *22* (4), 441–467. https://doi.org/10.1002/adma.200901327.

(168) Zhang, Y.; Yu, J.; Bomba, H. N.; Zhu, Y.; Gu, Z. Mechanical Force-Triggered Drug Delivery. *Chem. Rev.* **2016**, *116* (19), 12536–12563. https://doi.org/10.1021/acs.chemrev.6b00369.

(169) Correa, S.; Dreaden, E. C.; Gu, L.; Hammond, P. T. Engineering Nanolayered Particles for Modular Drug Delivery. *J. Control. Release* **2016**, *240*, 364–386. https://doi.org/10.1016/j.jconrel.2016.01.040.

(170) Dierendonck, M.; De Koker, S.; De Rycke, R.; De Geest, B. G. Just Spray It-LbL Assembly Enters a New Age. *Soft Matter* **2014**, *10* (6), 804–807. https://doi.org/10.1039/c3sm52202d.

(171) Correia, C. R.; Reis, R. L.; Mano, J. F. Multilayered Hierarchical Capsules Providing Cell Adhesion Sites. *Biomacromolecules* **2013**, *14* (3), 743–751. https://doi.org/10.1021/bm301833z.

(172) Itoh, Y.; Matsusaki, M.; Kida, T.; Akashi, M. Locally Controlled Release of Basic Fibroblast Growth Factor from Multilayered Capsules. *Biomacromolecules* **2008**, *9* (8), 2202–2206. https://doi.org/10.1021/bm800321w.

(173) Nishiguchi, A.; Yoshida, H.; Matsusaki, M.; Akashi, M. Rapid Construction of Three-Dimensional Multilayered Tissues with Endothelial Tube Networks by the Cell-Accumulation Technique. *Adv. Mater.* **2011**, *23* (31), 3506–3510. https://doi.org/10.1002/adma.201101787.

(174) Zhao, J.; Pan, F.; Li, P.; Zhao, C.; Jiang, Z.; Zhang, P.; Cao, X. Fabrication of Ultrathin Membrane via Layer-by-Layer Self-Assembly Driven by Hydrophobic Interaction towards High Separation Performance. *ACS Appl. Mater. Interfaces* **2013**, *5* (24), 13275–13283. https://doi.org/10.1021/am404268z.

(175) Joseph, N.; Ahmadiannamini, P.; Hoogenboom, R.; Vankelecom, I. F. J. Layer-by-Layer Preparation of Polyelectrolyte Multilayer Membranes for Separation. *Polym. Chem.* **2014**, *5* (6), 1817–1831. https://doi.org/10.1039/c3py01262j.

(176) Xiang, Y.; Lu, S.; Jiang, S. P. Layer-by-Layer Self-Assembly in the Development of Electrochemical Energy Conversion and Storage Devices from Fuel Cells to Supercapacitors. *Chem. Soc. Rev.* **2012**, *41* (21), 7291–7321. https://doi.org/10.1039/c2cs35048c.

(177) Stouffer, J. M.; McCarthy, T. J. Polymer Monolayers Prepared by the Spontaneous Adsorption of Sulfur-Functionalized Polystyrene on Gold Surfaces1. *Macromolecules* **1988**, *21* (5), 1204–1208. https://doi.org/10.1021/ma00183a003.

(178) Prime, K. L.; Whitesides, G. M. Self-Assembled Organic Monolayers: Model Systems for Studying Adsorption of Proteins at Surfaces. *Science (80-. ).* **1991**, *252* (5009), 1164–1167. https://doi.org/10.1126/science.252.5009.1164.

(179) Collinson, M.; Bowden, E. F.; Tarlov, M. J. Voltammetry of Covalently Immobilized Cytochrome c on Self-Assembled Monolayer Electrodes. *Langmuir* **1992**, *8* (5), 1247–1250. https://doi.org/10.1021/la00041a004.

(180) Jordan, C. E.; Frey, B. L.; Kornguth, S.; Com, R. M. Characterization of Poly-L-Lysine Adsorption onto Alkanethiol-Modified Gold Surfaces with Polarization-Modulation Fourier Transform Infrared Spectroscopy and Surface Plasmon Resonance Measurements. *Langmuir* **1994**, *10* (10), 3642–3648. https://doi.org/10.1021/la00022a043.

(181) Yan, L.; Huck, W. T. S.; Zhao, X. M.; Whitesides, G. M. Patterning Thin Films of Poly(Ethylene Imine) on a Reactive SAM Using Microcontact Printing. *Langmuir* **1999**, *15* (4), 1208–1214. https://doi.org/10.1021/la980818m.

(182) Friedsam, C.; Del Campo Bécares, A.; Jonas, U.; Seitz, M.; Gaub, H. E. Adsorption of Polyacrylic Acid on Self-Assembled Monolayers Investigated by Single-Molecule Force Spectroscopy. *New J. Phys.* **2004**, *6*. https://doi.org/10.1088/1367-2630/6/1/009.

(183) Vercelli, B.; Zotti, G.; Berlin, A.; Grimoldi, S. Polypyrrole Self-Assembled Monolayers and Electrostatically Assembled Multilayers on Gold and Platinum Electrodes for Molecular Junctions. *Chem. Mater.* **2006**, *18* (16), 3754–3763. https://doi.org/10.1021/cm060802e.

(184) Kett, P. J. N.; Casford, M. T. L.; Yang, A. Y.; Lane, T. J.; Johal, M. S.; Davies, P. B. Structural Changes in a Polyelectrolyte Multilayer Assembly Investigated by Reflection Absorption Infrared Spectroscopy and Sum Frequency Generation Spectroscopy. *J. Phys. Chem. B* **2009**, *113* (6), 1559–1568. https://doi.org/10.1021/jp807453w.

(185) Maroni, P.; Montes Ruiz-Cabello, F. J.; Tiraferri, A. Studying the Role of Surface Chemistry on Polyelectrolyte Adsorption Using Gold-Thiol Self-Assembled Monolayer with Optical Reflectivity. *Soft Matter* **2014**, *10* (46), 9220–9225. https://doi.org/10.1039/c4sm02093f.

(186) Maroni, P.; Montes Ruiz-Cabello, F. J.; Cardoso, C.; Tiraferri, A. Adsorbed Mass of Polymers on Self-Assembled Monolayers: Effect of Surface Chemistry and Polymer Charge. *Langmuir* **2015**, *31* (22), 6045–6054. https://doi.org/10.1021/acs.langmuir.5b01103.

(187) Everett, D. H. Manual of Symbols and Terminology for Physicochemical Quantities and Units. *Pure Appl. Chem.* **1972**, *31* (4), 577–638. https://doi.org/10.1351/pac197231040577.

(188) Ozin, G. A.; Hou, K.; Lotsch, B. V.; Cademartiri, L.; Puzzo, D. P.; Scotognella, F.; Ghadimi, A.; Thomson, J. Nanofabrication by Self-Assembly. *Mater. Today* **2009**, *12* (5), 12–23. https://doi.org/10.1016/S1369-7021(09)70156-7.

(189) Li, F.; Josephson, D. P.; Stein, A. Colloidal Assembly: The Road from Particles to

Colloidal Molecules and Crystals. *Angew. Chemie - Int. Ed.* **2011**, *50* (2), 360–388. https://doi.org/10.1002/anie.201001451.

(190) Vogel, N.; Retsch, M.; Fustin, C. A.; Del Campo, A.; Jonas, U. Advances in Colloidal Assembly: The Design of Structure and Hierarchy in Two and Three Dimensions. *Chem. Rev.* **2015**, *115* (13), 6265–6311. https://doi.org/10.1021/cr400081d.

(191) Evans, J. W. Random and Cooperative Sequential Adsorption. *Rev. Mod. Phys.* **1993**, *65* (4), 1281–1329. https://doi.org/10.1103/RevModPhys.65.1281.

(192) Iler, R. K. Adsorption of Colloidal Silica on Alumina and of Colloidal Alumina on Silica. *J. Am. Ceram. Soc.* **1964**, *47* (4), 194–198. https://doi.org/10.1111/j.1151-2916.1964.tb14391.x.

(193) Fulda, K. U.; Kampes, A.; Krasemann, L.; Tieke, B. Self-Assembled Mono- and Multilayers of Monodisperse Cationic and Anionic Latex Particles. *Thin Solid Films* **1998**, *327–329* (1–2), 752–757. https://doi.org/10.1016/S0040-6090(98)00780-9.

(194) Chen, K. M.; Jiang, X.; Kimerling, L. C.; Hammond, P. T. Selective Self-Organization of Colloids on Patterned Polyelectrolyte Templates. *Langmuir* **2000**, *16* (20), 7825–7834. https://doi.org/10.1021/la000277c.

(195) Jonas, U.; Del Campo, A.; Krüger, C.; Glasser, G.; Boos, D. Colloidal Assemblies on Patterned Silane Layers. *Proc. Natl. Acad. Sci. U. S. A.* **2002**, *99* (8), 5034–5039. https://doi.org/10.1073/pnas.082634799.

(196) Zhang, X.; Zhang, J.; Zhu, D.; Li, X.; Zhang, X.; Wang, T.; Yang, B. A Universal Approach to Fabricate Ordered Colloidal Crystals Arrays Based on Electrostatic Self-Assembly. *Langmuir* **2010**, *26* (23), 17936–17942. https://doi.org/10.1021/la103778m.

(197) Trau, M.; Saville, D. A.; Aksay, I. A. Assembly of Colloidal Crystals at Electrode

Interfaces. *Langmuir* **1997**, *13* (24), 6375–6381. https://doi.org/10.1021/la970568u.

(198) Richetti, P.; Prost, J.; Barois, P. Two-Dimensional Aggregation and Crystallization of a Colloidal Suspension of Latex Spheres. *J. Phys. Lettres* **1984**, *45* (23), 1137–1143. https://doi.org/10.1051/jphyslet:0198400450230113700.

(199) Giersig, M.; Mulvaney, P. Preparation of Ordered Colloid Monolayers by Electrophoretic Deposition. *Langmuir* **1993**, *9* (12), 3408–3413. https://doi.org/10.1021/la00036a014.

(200) Solomentsev, Y.; Böhmer, M.; Anderson, J. L. Particle Clustering and Pattern Formation during Electrophoretic Deposition: A Hydrodynamic Model. *Langmuir* **1997**, *13* (23), 6058–6061. https://doi.org/10.1021/la970294a.

(201) Solomentsev, Y.; Guelcher, S. A.; Bevan, M.; Anderson, J. L. Aggregation Dynamics for Two Particles during Electrophoretic Deposition under Steady Fields. *Langmuir* **2000**, *16* (24), 9208–9216. https://doi.org/10.1021/la0005199.

(202) Prieve, D. C.; Sides, P. J.; Wirth, C. L. 2-D Assembly of Colloidal Particles on a Planar Electrode. *Curr. Opin. Colloid Interface Sci.* **2010**, *15* (3), 160–174. https://doi.org/10.1016/j.cocis.2010.01.005.

(203) O'Brien, R. W.; White, L. R. Electrophoretic Mobility of a Spherical Colloidal Particle. *J. Chem. Soc. Faraday Trans. 2 Mol. Chem. Phys.* **1978**, *74*, 1607–1626. https://doi.org/10.1039/F29787401607.

(204) Trau, M.; Saville, D. A.; Aksay, I. A. Field-Induced Layering of Colloidal Crystals. *Science (80-. ).* **1996**, *272* (5262), 706 LP – 709. https://doi.org/10.1126/science.272.5262.706.

(205) Böhmer, M. In Situ Observation of 2-Dimensional Clustering during Electrophoretic Deposition. *Langmuir* **1996**, *12* (24), 1994–1997. https://doi.org/10.1021/la960183w.

(206) Sides, P. J. Electrohydrodynamic Particle Aggregation on an Electrode Driven by an Alternating Electric Field Normal to It. *Langmuir* **2001**, *17* (19), 5791–5800. https://doi.org/10.1021/la0105376.

(207) Gong, T.; Wu, D. T.; Marr, D. W. M. Two-Dimensional Electrohydrodynamically Induced Colloidal Phases. *Langmuir* **2002**, *18* (26), 10064–10067. https://doi.org/10.1021/la026241x.

(208) Zhang, K. Q.; Liu, X. Y. In Situ Observation of Colloidal Monolayer Nucleation Driven by an Alternating Electric Field. *Nature* **2004**, *429* (6993), 739–743. https://doi.org/10.1038/nature02630.

(209) Abe, M.; Yamamoto, A.; Orita, M.; Ohkubo, T.; Sakai, H.; Momozawa, N. Control of Particle Alignment in Water by an Alternating Electric Field. *Langmuir* **2004**, *20* (17), 7021–7026. https://doi.org/10.1021/la0490801.

(210) Lumsdon, S. O.; Kaler, E. W.; Velev, O. D. Two-Dimensional Crystallization of Microspheres by a Coplanar AC Electric Field. *Langmuir* **2004**, *20* (6), 2108–2116. https://doi.org/10.1021/la035812y.

(211) Kumacheva, B. E.; Golding, R. K. Colloid Crystal Growth on Mesoscopically Patterned Surfaces: Effect of Confinement. **2002**, *4* (3), 221–224.

(212) Dziomkina, N. V.; Vancso, G. J. Colloidal Crystal Assembly on Topologically Patterned Templates. *Soft Matter* **2005**, *1* (4), 265–279. https://doi.org/10.1039/b503145c.

(213) Kleinert, J.; Kim, S.; Velev, O. D. Electric-Field-Assisted Convective Assembly of Colloidal Crystal Coatings. *Langmuir* **2010**, *26* (12), 10380–10385. https://doi.org/10.1021/la100119m.

(214) Hayward, R. C.; Saville, D. A.; Aksay, I. A. Electrophoretic Assembly of Colloidal

Crystals with Optically Tunable Micropatterns. *Nature* **2000**, *404* (6773), 56–59. https://doi.org/10.1038/35003530.

(215) Xie, R.; Liu, X. Y. Controllable Epitaxial Crystallization and Reversible Oriented Patterning of Two-Dimensional Colloidal Crystals. *J. Am. Chem. Soc.* **2009**, *131* (13), 4976–4982. https://doi.org/10.1021/ja900049r.

(216) Allen, S. L.; Zamborini, F. P. Size-Selective Electrophoretic Deposition of Gold Nanoparticles Mediated by Hydroquinone Oxidation. *Langmuir* **2019**, *35* (6), 2137−2145. https://doi.org/10.1021/acs.langmuir.8b03904.

# CHAPTER 2. ELECTROCHEMICALLY TRIGGERED SURFACE DEPOSITION OF POLYELECTROLYTES*

## 2.1 Introduction

This article reports a new approach to polyelectrolyte deposition on self-assembled monolayer (SAM) surfaces that can be triggered facilely by a potential bias. When applied, this bias drives the oxidation of ferrocene (Fc) moieties on the SAM to ferrocenium ($Fc^+$), whose charge compensation in this particular case is fulfilled by polyelectrolytes and associated counterions present in the surroundings. This approach is quite general, enabling quantitative deposition of both polyanions and polycations with a wide range of chemical identities (synthetic polymers, peptides, and DNA) and molecular weights ($10^3$-$10^7$ Da). Besides its practical implications, this work also illustrates the possibility and potential benefits of conducting electrochemical processes under unconventional conditions-here, use of polyelectrolytes in place of small ions to maintain interfacial charge balance.

Like many other truly useful technologies, gold-anchored alkanethiol SAMs[1] are simple to operate and yet rich in offering. Through their distal end, a variety of functionalities can be attached to these alkanethiols, which, when similarly assembled, yield well-defined surfaces on which diverse chemistries can be launched. Among these are ferrocene-terminated SAMs, which have served not only as an invaluable model system for probing fundamental electron transfer processes[2-4] but also a flexible platform for biosensing,[5,6] electroactuation,[7] and molecular photovoltaics.[8,9] On the other hand, alkanethiols terminated with amine and carboxylic groups readily afford charged SAMs, which, among other possibilities, provide



*This chapter is copied from a published paper (*Langmuir* **2018**, *34*, 12776 -12786) with minor modification.

excellent starting surfaces for layer-by-layer polyelectrolyte deposition.[10,11] This fruitful integration has led to electroactive polymer/protein films displaying robust electrochemical communication,[12,13] as well as redox-doped polyelectrolyte multilayers whose thickness and mechanical properties can be electrochemically manipulated.[14,15]

This work introduces a new type of SAM/polyelectrolyte integration that is electrochemically initiated and controlled. In relation to existing systems, this approach combines the following features: (1) facile polymer deposition that can be accomplished in a matter of seconds; (2) quantitative deposition, according to ferrocene density prepared into the SAMs; (3) broad applicability, to both anionic and cationic polyelectrolytes, either synthetic or natural, in a wide molecular weight range; and (4) ready coupling to conventional layer-by-layer polyelectrolyte deposition to yield electroactive polymer composite films. All these features, importantly, can be obtained from the same starting surfaces-ferrocene-terminated SAMs. Several techniques, including voltammetry, fluorescence spectroscopy, contact angle analysis, electrochemical quartz crystal microbalance, and atomic force microscopy, were employed to characterize the deposition processes. A detailed discussion on the involved deposition mechanisms is also presented.

## 2.2 Experimental Section

### 2.2.1 Reagents

11-Ferrocenyl-1-undecanethiol (Fc-C11SH), 1-dodecanethiol (C12SH), poly(acrylic acid sodium salt), poly(allylamine hydrochloride), poly(fluorescein isothiocyanate allylamine hydrochloride) with a polymer to fluorophore mole ratio of 50:1, DNA sodium salt from calf thymus, and sodium perchlorate hydrate (99.99% trace metal basis) were products of Sigma-

Aldrich (St. Louis, MO). Poly(L-lysine hydrochloride) and poly(L-glutamic acid sodium salt) were obtained from Alamanda Polymers (Huntsville, AL). 5′- Fluorescein-labeled poly(adenine) 25-mer was obtained from Integrated DNA Technologies, Inc. (Coralville, IA). The structure and molecular weight of these polymers are listed in Table 2.1. Deionized water of 18.2 MΩ·cm (Millipore) was used in preparing all aqueous solutions as well as in all rinsing steps.

**Table 2. 1** Polyelectrolytes Investigated in This Study and Their Structure and Molecular Weight (Da).

| Polymer | Structure | Polymer | Structure |
|---|---|---|---|
| Poly(acrylic acid sodium salt)<br><br>2100<br>8000<br>15000 | 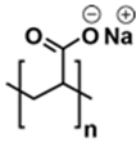 | DNA sodium salt from calf thymus<br><br>10-15 x $10^6$ | not shown |
| Poly(L-glutamic acid sodium salt)<br><br>3000<br>7500<br>15000 | 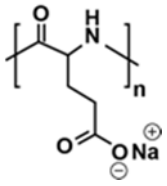 | Poly(fluorescein isothiocyanate allylamine HCl)<br><br>16200<br>17500[a] | 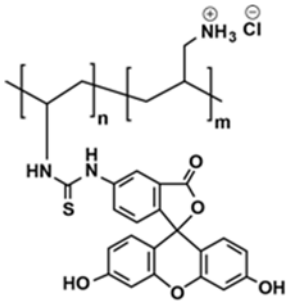 <br>5′-fluorescein-$(A)_{25}$-3′ |
| Poly(L-lysine HCl)<br><br>3300<br>8200<br>16000 | 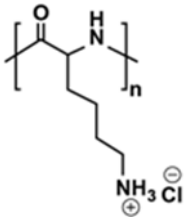 | 5′-fluorescein-labeled poly(adenine) 25-mer<br><br>8300 | 5′-fluorescein-(A)25-3′ |

[a]Poly(allylamine HCl) only.

### 2.2.2 Formation of Self-Assembled Monolayers

Self-assembled monolayers (SAMs) of Fc-C11SH, either pure or mixed 1:1 (mole ratio) with C12SH, were formed on three types of gold-coated substrates depending on the intended use. For voltammetric and water contact angle characterization, the substrates were prepared in-house by sputtering gold onto chromium-coated silicon wafers (Au thickness: ∼1000 nm). The other two substrates were commercially obtained: semitransparent gold-coated microscope slides (Au thickness: 10 nm, Sigma-Aldrich) for fluorescence spectroscopy and atomic force microscopy and gold-coated quartz crystal wafers with a Cr adhesion layer (diameter: 1 in., Stanford Research System, Sunnyvale, CA) for quartz crystal microbalance. Right before their incubation in thiol solutions, these substrates were immersed in a piranha solution (3:1 v/v mixture of concentrated $H_2SO_4$ and $H_2O_2$ 30 wt % aqueous solution) for either 15 (for the gold-coated Si wafers) or 3 min (for the other two substrates), thoroughly rinsed with deionized water and ethanol, and then dried under N2. Thus, cleaned dry substrates were immediately immersed in an ethanol solution dissolved either with 0.5 mM Fc-C11SH and C12SH each (for mixed Fc SAMs) or with 1.0 mM Fc-C11SH alone (for pure Fc SAMs). The incubation was allowed to proceed for 16−18 h in the dark, after which the substrates were thoroughly rinsed with methanol to remove excess thiols on surface, then rinsed with deionized water, and finally dried under $N_2$. These freshly prepared SAMs are immediately subjected to their next treatments as specified below.

### 2.2.3 Electrochemical Treatments and Characterization

Cyclic voltammetry (CV) and linear sweep voltammetry (LSV) were used in this work to (1) initiate polyelectrolyte deposition on Fc SAMs and (2) electrochemically characterize the Fc SAMs before/after the deposition step. These measurements were performed in homemade

Teflon cells housing SAM-covered gold substrates as the working electrode, a platinum wire as the counter electrode, and Ag/AgCl in saturated KCl solution as the reference electrode and are operated by a PC-controlled potentiostat (CHI 910B, CH Instruments, Austin, TX) with a potential scan rate of 100 mV/s. In the order of operation, a given SAM is typically treated with three separate voltammetric scans: (1) a CV scan in 0.1 M $NaClO_4$, (2) an LSV or a CV scan in a 1.0 mM (polymer concentration) aqueous solution of a polyelectrolyte, and (3) another CV scan back in 0.1M $NaClO_4$. In between scans, the solution occupying the electrochemical cell was thoroughly exchanged out first with deionized water and then with the medium intended for the next scan. To ensure reproducibility, it is critical to keep the SAM immersed in liquid during the entire time of these voltammetric runs.

### 2.2.4 Water Contact Angle Measurement

A Ramé-Hart model 200 automated goniometer (Succasunna, NJ) was used to measure the water contact angles of Fc-C11SH/C12SH mixed SAMs at room temperature. The Ramé-Hart DROPimage Standard software was used to collect images and analyze the obtained angles. Prior to a measurement, a SAM was first LSV-treated in either DI water alone or a 1.0 mM polyelectrolyte aqueous solution, thoroughly washed with deionized water, and then dried under $N_2$. In each case, a measurement was promptly taken after a 4 μL deionized water droplet was gently placed onto the SAM.

### 2.2.5 Electrochemical Quartz Crystal Microbalance (EQCM)

EQCM measurements were carried out on a Stanford Research Systems QCM analyzer with a 5 MHz crystal oscillator (Model: QCM25, Sunnyvale, CA) at room temperature. The quartz crystals used here are polished quartz wafers of 1 in. diameter with circular gold electrodes

coated on both sides, which are first grafted with a 1:1 Fc-C11SH/C12SH mixed SAM as described above. The SAM-coated crystal was subsequently mounted on the QCM crystal holder, and its solution-facing electrode was used as the working electrode in a three electrode configuration together with a Pt-wire counter electrode and a Ag/AgCl reference electrode (in saturated KCl). To do so, a PC controlled potentiostat (CHI 910B, CH Instruments) was connected to the QCM crystal holder via the crystal face bias connector of the QCM25 crystal controller. This setup enables simultaneous monitoring of the QCM frequency shift and current on the working electrode (crystal) as a function of the applied potential. The potential is fed by the potentiostat in the form of 10 consecutive CV scans between 0.1 and 0.8 V; scan rate: 100 mV/s.

### 2.2.6 Fluorescence Spectroscopy

Fluorescence emission spectra of fluorescein-conjugated polyelectrolytes deposited on semitransparent gold-coated microscope slides were acquired on a PI Acton spectrometer (Spectra Pro SP 2356, Acton, NJ) equipped with a CCD (Charge-coupled device) camera (PI Acton PIXIS: 400B, Acton, NJ). This spectrometer is connected to the side port of an epifluorescence microscope (Nikon TE-2000 U, Japan), which provides light selection (excitation: 470 ± 11 nm; dichroic: 484 nm long pass; emission: 496 nm long pass) and holds the sample cells. For sample preparation, the gold-coated microscope slides were first grafted with 1:1 Fc-C11SH/C12SH mixed SAMs, which were then subjected to an LSV (or a CV) scan either in a 1.0mM aqueous solution of poly(fluorescein isothiocyanate allylamine hydrochloride) or in a 10 μM aqueous solution of 5′-fluorescein-labeled poly(adenine) 25-mer; potential scan rate: 100 mV/s. Following the electrochemical treatment, the SAMs were thoroughly rinsed with deionized water to remove unbound polyelectrolytes. The resulting films

remain immersed in deionized water during the entire course of fluorescence acquisition.

### 2.2.7 Atomic Force Microscopy (AFM)

AFM characterization of cleaned gold coated substrate, SAMs treated in deionized water, and polymer-modified SAMs was carried out using a Bruker MultiMode 8 atomic force microscope (Bruker, USA) in air and at room temperature. Silicon nitride probes (Model: ScanAsyst AIR, Bruker) used in these measurements have a force constant of 0.4 N/m, a resonant frequency of 70 kHz, and a nominal tip radius of 2 nm and are operated in Scanasyst Air mode with a scan rate of 1 Hz and a resolution of 512 × 512 pixels. The substrates used are semitransparent gold-coated microscope slides, on which ferrocene SAMs were first formed as described above. For deposition of polyelectrolytes, these SAMs were then subjected to a linear potential sweep from 0.1 to 0.8 V vs Ag/AgCl at 100 mV/s in the following aqueous solutions: 1.0 mM poly(acrylic acid sodium salt), MW ~ 15 kDa, and poly(L-lysine hydrochloride), MW~ 16 kDa, and 0.1 μMDNA from calf thymus. Thus, treated SAMs were thoroughly rinsed with deionized water and then dried under $N_2$ before AFM scanning. All AFM images presented in this work are original with no graphical touchup.

### 2.2.8 Layer-by-Layer Polyelectrolyte Deposition

Pure Fc-C11SH SAMs deposited with poly(acrylic acid sodium salt) were used as the starting surfaces to build layer-by-layer polyelectrolyte films. These Fc- C11SH SAMs were formed on semitransparent gold-coated microscope slides, on which poly(acrylic acid sodium salt) (PAA, MW ~ 15 kDa) was deposited by a linear potential sweep from 0.1 to 0.8 V vs Ag/AgCl at a scan rate of 100 mV/s in a 1.0 mM aqueous solution of PAA. The resulting films were thoroughly rinsed with deionized water and then incubated in a 1.0 mM aqueous solution of

poly(fluorescein isothiocyanate allylamine hydrochloride) for 15 min. Four additional rounds of 15 min incubation were given alternately in 1.0 mM PAA and poly(fluorescein isothiocyanate allylamine hydrochloride) so they reached a total of 10 layers at the end of the deposition. In each round, a UV−vis absorption spectrum of the resultant film was taken with a UV−visible spectrophotometer (Cary 50 Bio, Varian).

## 2.3 Results and Discussion

### 2.3.1 Electrochemical Treatments and Characterization

We initially hypothesized the following "trigger-and-trade" (TnT) scheme to electrostatically deposit polyanions, $M^+Poly^-$, where $M^+$ refers to the counterions, onto ferrocene-containing SAMs:

$$\text{Fc-SAM} - e^- \rightarrow \text{Fc}^+\text{-SAM} \qquad (1)$$

$$\text{Fc}^+\text{-SAM} + M^+Poly^- \rightarrow Poly^-\text{Fc}^+\text{-SAM} + M^+ \qquad (2)$$

To test this hypothesis, we first carried out cyclic voltammetry (CV) on 1:1 Fc-C11SH/C12SH mixed SAMs in poly(acrylic acid sodium salt) (PAA, MW 8000 Da) aqueous solutions. To diagnose the impact of such treatments on the SAMs, we also ran separate CV scans on the same SAMs in 0.1 M $NaClO_4$ before and after each given treatment. As expected, the initial scan returns a symmetrical, bell-shaped voltammogram that is typical for electrode-bound ferrocenes probed in perchlorate (Figure 2.1 a). Compared to this standard response, the CV scan in PAA obtained afterward displays moderately sluggish ferrocene oxidation with its peak lagging the former by about 30 mV (CV in red, Figure 2.1 a). This result confirms that 1mM PAA, i.e., polymer plus its associated $Na^+$, can sustain ferrocene oxidation sufficiently and, in

addition, reveals PAA's lower tendency to ion pair with ferrocenium ($Fc^+$) as compared to perchlorate. By stabilizing the reaction product, such ion pairing effectively improves the kinetics of and lowers the driving force required for ferrocene oxidation.[16,17] This effect is clearly shown by the significantly more sluggish oxidation profile obtained in $Cl^-$, a poor ion-pairing agent18 to $Fc^+$ (CV in gray, Figure 2.1 a).

When this PAA/CV-treated Fc-SAM was rescanned in 0.1 M $NaClO_4$, a ~14% decrease in the amount of electron transfer was observed (CV in dashed line, Figure 2.1 a). Two processes may potentially be responsible for this decrease: (1) ferrocene loss from the SAM and (2) the intended polymer deposition. In the first case, it is well documented that Fc SAMs probed in hydrophilic small ions such as $Cl^-$ often suffer from electroactivity decays[18-20] upon extended potential bias, pointing to the susceptibility of ferrocenium ($Fc^+$) to secondary reactions[21,22] such as nucleophilic attacks when not properly protected, e.g., via ion pairing. To better gauge the contribution of this mechanism to the observed decay, we then examined fresh Fc-C11SH/C12SH mixed SAMs under more stringent conditions. Subjected to 10 consecutive CV scans in PAA, the SAM displays progressively decreasing ferrocene redox features, with the largest decrease occurring during the first scan (Figure 2.1 b). Upon completion, this treatment registers a ~45% decrease in redox activity of the SAM when probed in 0.1 M $NaClO_4$, which is comparable to the level of decrease obtained from SAMs similarly treated in 0.1 M NaCl (data not shown). In comparison, no appreciable loss was observed from SAMs similarly treated in 0.1 M $NaClO_4$. These results thus point to the likely occurrence of ferrocene loss from the SAM when oxidized in polyanion aqueous solutions. To minimize such losses, therefore, it is preferable to subject these Fc SAMs only to a short period of potential bias.

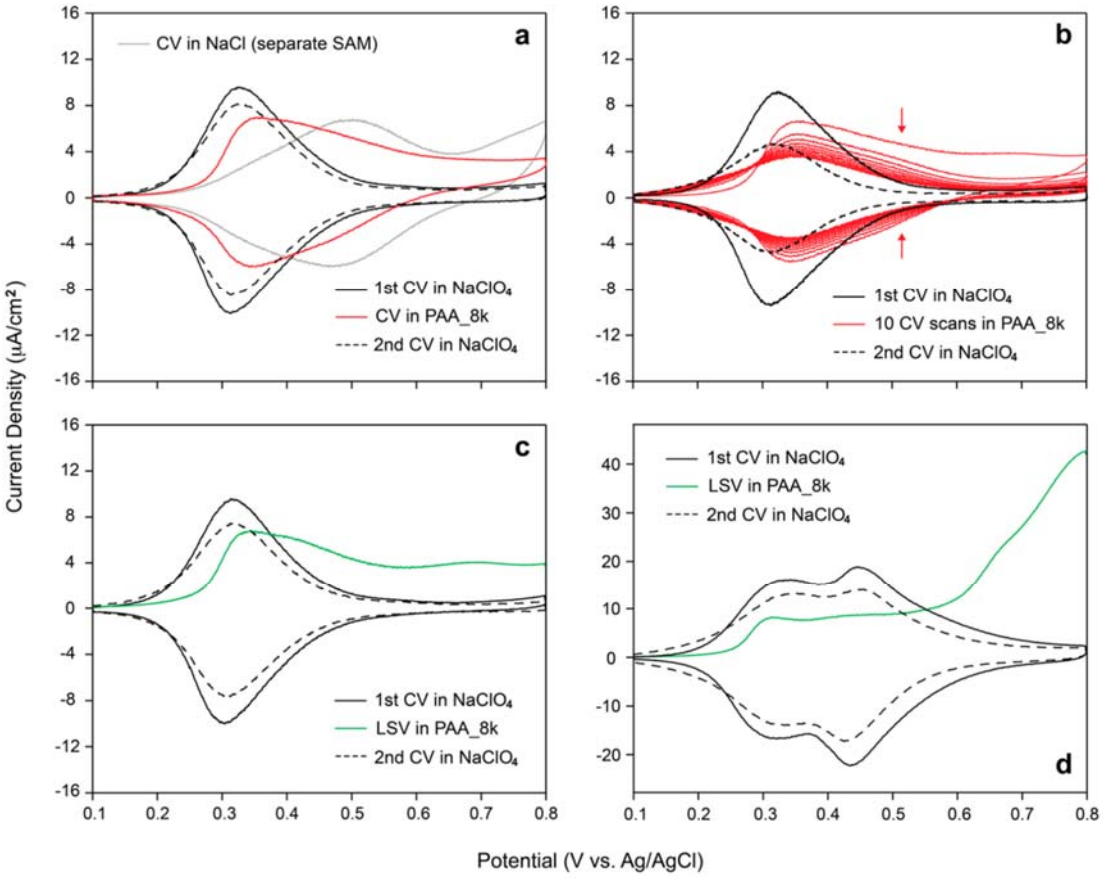


**Figure 2. 1** Voltammetric monitoring of Fc SAMs undergoing either linear or cyclic potential sweeps in 1.0 mM poly(acrylic acid sodium salt) (PAA, MW8000 Da) aqueous solutions. (a) Voltammetric monitoring of 1:1 Fc-C11SH/C12SH mixed SAMs treated by a cyclic potential sweep in 1.0 mM PAA. CVs shown in black were acquired in 0.1 M $NaClO_4$ aqueous solutions before (solid line) and after (dashed line) the CV scan in PAA. A control CV (in gray) obtained in 0.1 M NaCl is also included. (b) Voltammetric monitoring of 1:1 Fc-C11SH/C12SH mixed SAMs undergoing 10 consecutive cyclic potential scans in 1.0 mM PAA; the red arrows point to the direction of current decrease. (c) Voltammetric monitoring of 1:1 Fc- C11SH/C12SH mixed SAMs undergoing a linear potential sweep in 1.0 mM PAA. (d) Voltammetric monitoring of pure Fc-C11SH SAMs undergoing a linear potential sweep in 1.0 mM PAA. Potential scan rate: 100 mV/s.

On the other hand, PAA deposition may as well induce Fc activity decrease either by lowering the amount of Fc available for oxidation (due to $Fc^{+}PAA^{-}$ complexation) or by physically limiting perchlorate's access to the SAM surface (i.e., partial blocking) during the subsequent scan. Follow-up voltammetric measurements showed the first signs of this process. For example, when freshly prepared SAMs of the same composition were treated by a linear potential sweep (LSV) instead of CV in the presence of PAA, a larger decrease, ~20%, was obtained (Figure 2.1 c). This result argues against the material-loss mechanism-or, at least not as the sole mechanism in operation, because the Fc SAM was under longer potential bias in the CV treatment, which would have led to a greater loss and hence a larger decrease in electroactivity. Rather, this observation can be readily explained by the deposition scheme, in that the backward potential scan reduces most $Fc^{+}$ back to Fc, which lifts the electrostatic attraction and in turn causes some deposited PAA to desorb from the SAM. This was found to be indeed the case, for example, from fluorescence spectroscopic characterization (next section).

Additional voltammetric runs were also carried out using Fc SAMs of different compositions and on other polyanions. For example, when pure Fc SAMs were employed instead of Fc-C11SH/C12SH mixed SAMs, an LSV treatment in PAA led to a ~24% decrease of the ferrocene redox response (Figure 2.1 d), which is slightly larger than that obtained from the mixed Fc SAMs similarly treated. Provided that such a decrease is indeed indicative of polymer deposition, this result hints at the important possibility to control the amount of deposited polymer via Fc surface density in the SAM. On the other hand, we confirm the observation of similar trends when different polyanions or polyanions of different molecular weights were examined. One of such measurements, based on 7.5 kDa poly(L-glutamic acid, sodium salt) and

mixed Fc SAMs, is presented in Figure 2.2 a.

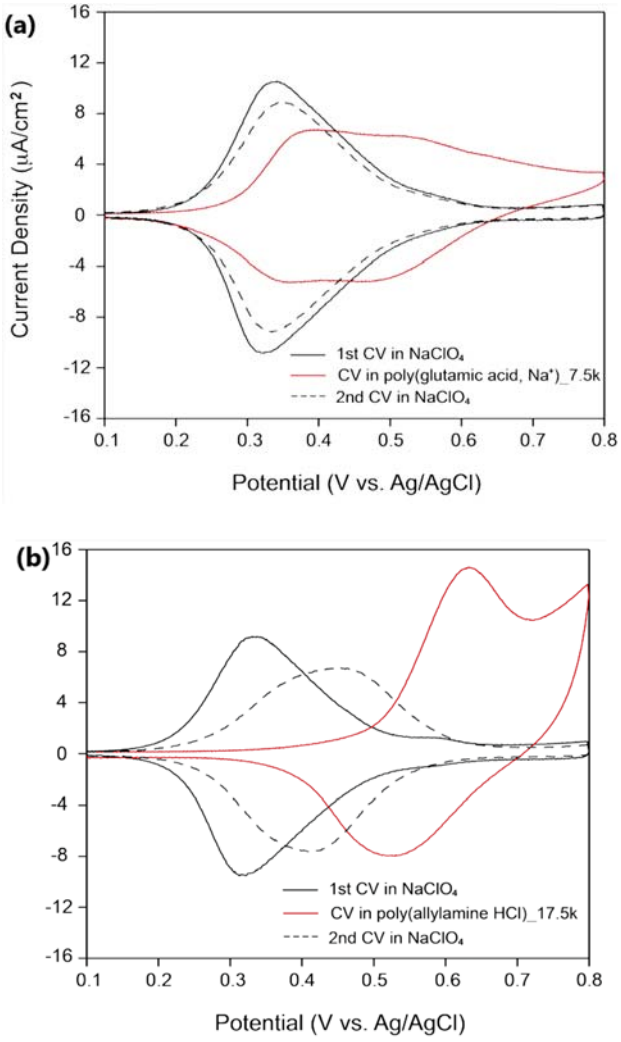


**Figure 2. 2** Voltammetric monitoring of 1:1 Fc-C11SH/C12SH mixed SAMs undergoing a cyclic potential scan in (a) 1.0 mM poly(L-glutamic acid sodium salt) (M.W. 7500 Da) (b) 1.0 mM poly(allylamine hydrochloride) (M.W. 17.5 kDa) aqueous solution. CVs shown in black were acquired in 0.1 M $NaClO_4$ aqueous solutions before (solid line) and after (dashed line) the CV scan in polyanion/polyanion. Potential scan rate: 100 mV/s.

Similar voltammetric treatments were also extended to cationic polymers, which, surprisingly, led to partial activity loss in Fc-SAMs as well. As shown in Figure 2.3 a, this amounts to a 16%

decrease after the 1:1 Fc-C11SH/C12SH mixed SAM is treated by a single LSV scan in a poly(L-lysine hydrochloride) (PL, MW 8200 Da) aqueous solution. This result is unexpected, as it stands to suggest deposition of polymers carrying the same (positive) charge as the surface. Compared to the case of anionic PAA, the LSV response obtained here displays significantly more sluggish ferrocene oxidation, whose peak lags the one obtained in $NaClO_4$ by >200 mV. When we treat the mixed SAMs with a single CV scan instead, a smaller (~9%) decrease in ferrocene activity results (Figure 2.3 b). Here, interestingly, the second CV in $NaClO_4$ consistently emerges a few tens of millivolts more positive than the first one. This shift is likely due to the deposited PLs, whose presence modifies the local charge environment around the Fc moieties and makes electron removal from the latter more costly. Potential shifts of similar nature have been previously observed, for example, on binary SAMs containing ferrocenes[23] as well as redox-active polyelectrolyte films.[24] Such a positive shift is also discernible from the LSV-treated SAMs but not as large, ~10 mV. In contrast, no shifts were found from the SAMs treated by either LSV or CV in the presence of PAA (Figure 2.1). This characteristic shift, therefore, once again suggests polycation deposition on Fc SAMs upon electrooxidation.

Another polycation, poly(allylamine HCl), produces even more pronounced sluggishness and shifts when similarly treated (Figure 2.2 b). To gain a better understanding of the involved deposition processes, we thus moved onto other techniques for characterization of these films.

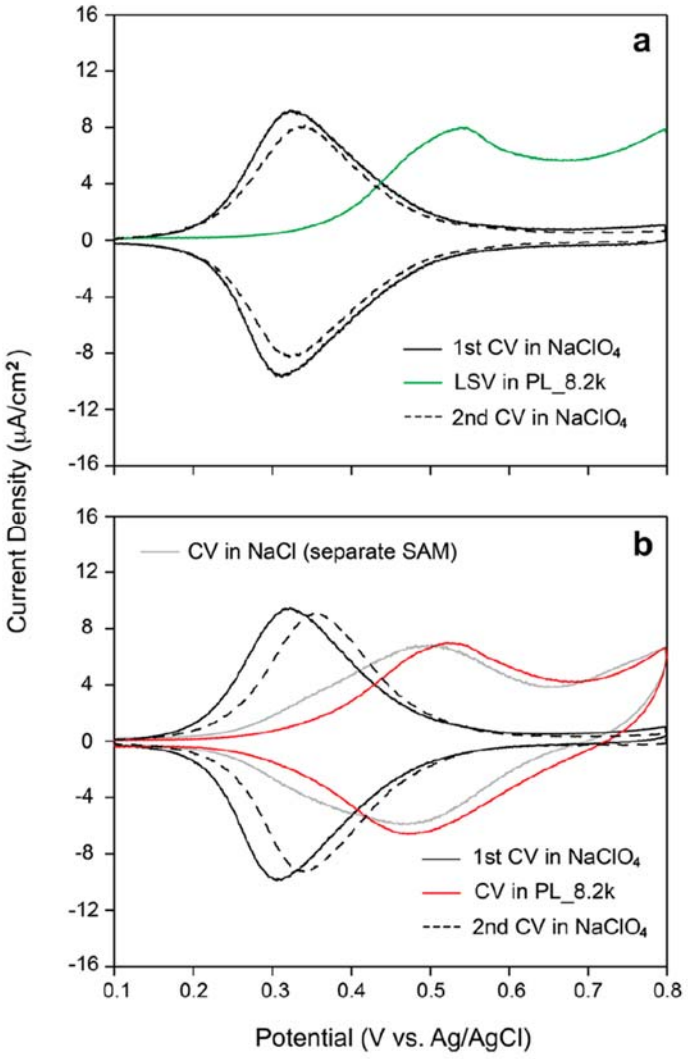


**Figure 2. 3** Voltammetric monitoring of 1:1 Fc-C11SH/C12SH mixed SAMs undergoing linear (a) and cyclic (b) potential sweeps in 1.0 mM poly(L-lysine hydrochloride) (PL, MW 8200 Da) aqueous solutions. All CVs shown in black were acquired in 0.1M $NaClO_4$ aqueous solutions, whereas voltammograms shown in green and red were recorded in 1.0 mM PL dissolved in water. A control CV (in gray) obtained in 0.1 M NaCl is also included in (b). Potential scan rate: 100 mV/s.

### 2.3.2 Fluorescence Spectroscopy

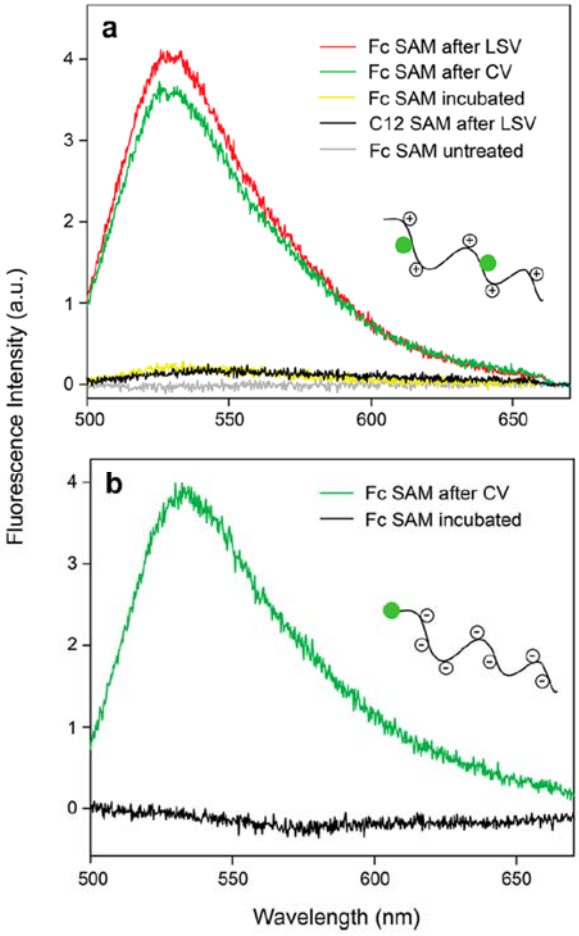


**Figure 2. 4** Fluorescence spectroscopic characterization of electrochemically triggered polyelectrolyte deposition processes. (a) Representative fluorescence emission spectra collected on 1:1 Fc-C11SH/C12SH mixed SAMs or pure C12SH SAMs undergoing various treatments. All treatments were carried out in 1.0 mM poly(fluorescein isothiocyanate allylamine hydrochloride) (MW 16200 Da) aqueous solutions. (b) Representative fluorescence emission spectra collected on 1:1 Fc- C11SH/C12SH mixed SAMs undergoing either CV deposition (green) or 30 min incubation (black) in 50.0 μM 5′-fluoresceinlabeled adenine 25-mer (MW ~ 8300 Da). The embedded cartoons depict the charge and skeleton of the fluorescent polyelectrolytes employed.

Shown in Figure 2.4 (a) are fluorescence emission spectra acquired directly on 1:1 Fc-C11SH/C12SH mixed SAM surfaces that have undergone various treatments with polyelectrolytes. The fluorophore probed here is fluorescein, which appears in the tested polycation in the form of poly(fluorescein isothiocyanate allylamine hydrochloride) and the polyanion, 5′-labeled adenine 25-mer. Due to existence of multiple complicating factors, such as fluorescence quenching (by gold[25] as well as ferrocene[26]) and variations in polymer conformation and placement, we focus here on identifying the trend in the signals. As evident from Figure 2.4 (a), both single LSV and CV treatments lead to successful polycation deposition, with the former displaying slightly but consistently higher fluorescence intensity. By contrast, very little deposition resulted from the following controls: (1) 30 min incubation of the SAM in the polymer solution (i.e., no electrochemical treatment) or (2) a single LSV scan of pure C12 SAM in polymer (i.e., no ferrocene). These negative controls thus confirm the necessity of electrochemically modifying the surface charge of these SAMs in order to achieve polymer deposition. A similar trend is also observed in the case of polyanions (Figure 2.4 b). In accordance with the voltammetric evidence presented earlier, these results show a very minor polymer desorption upon the returning potential scan. Such irreversibility is generally observed in electrostatic polyelectrolyte deposition and points to the existence of other intermolecular forces, such as van der Waals and hydrophobic interactions, besides electrostatic attraction, in facilitating polymer surface binding.

### 2.3.3 Water Contact Angle Measurements

Water contact angles measurements were also conducted on these Fc containing SAMs subjected to similar electrochemical treatments (Table 2.2 and Figure 2.5). As expected, the untreated 1:1 Fc-C11SH/C12SH mixed SAM displays a relatively hydrophobic surface with a

water contact angle of about 91°, which decreases only slightly after the SAM undergoes an LSV scan in water alone, 88°. By contrast, the SAM similarly treated in PAA gives a water contact angle of about 71°, indicating a more hydrophilic surface as a result of PAA deposition. If the SAM is treated by 10 consecutive CV scans instead, a very comparable angle, 72°, results, suggesting that deposition occurs mostly during the initial scan. On pure Fc SAMs, a lower angle, ~64°, is observed upon the same LSV treatment, which is suggestive of a higher PAA surface coverage due to higher Fc density.

**Table 2. 2** Water Contact Angle (in Degree) Measurements.[a] All SAMs Are Treated by an LSV Scan Unless Otherwise Specified.

| **Polymer** | **1:1 Mixed Fc-C11SH/C12SH** | **100% Fc-C11SH** |
|---|---|---|
| SAM alone | $90.7 \pm 0.4^{b}$<br>$88.1 \pm 0.5^{c}$ | $82.8 \pm 0.5^{b}$ |
| Poly(acrylic acid sodium salt) | $71.4 \pm 0.6^{c}$<br>$72.1 \pm 6.4^{d}$ | $63.5 \pm 1.5^{c}$ |
| Poly(L-lysine HCl)<br>Poly(allylamine HCl) | $87.3 \pm 0.2^{c}$<br>$82.6 \pm 4.3^{c}$ | $81.7 \pm 3.6^{c}$<br>$86.9 \pm 1.7^{c}$ |

[a]A sample of water contact angle images is presented in Figure 2.5; [b]Fresh SAM with no treatment; [c]LSV from 0.1 to 0.8 V vs. Ag/AgCl in water; [d]Ten consecutive CVs from 0.1 to 0.8 V in water; Standard deviation values are based on at least three parallel measurements obtained from either one or two samples.

In marked contrast, SAMs similarly treated in the presence of polycations only yield negligible (in the case of polylysine) to minor (in the case of polyallylamine) changes in water contact

angles. These results thus point to the distinctive surface characteristics between deposited polyanions and polycations, which in turn suggest different deposition mechanisms involved.

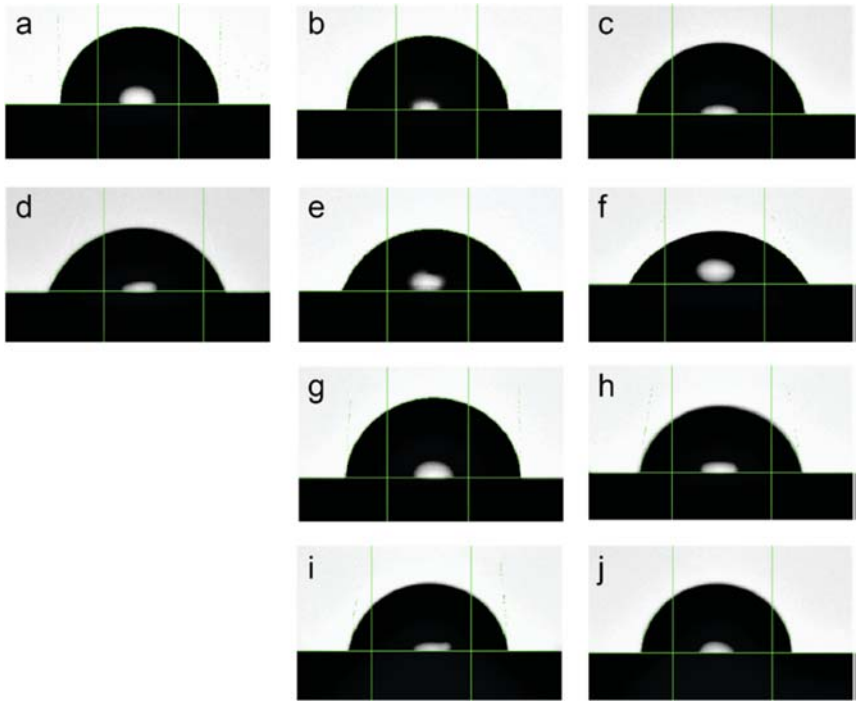


**Figure 2. 5** Photographs of water droplets formed on various Fc SAM surfaces as obtained from water contact angle measurement. Volume of water droplets ~ 4.0 μL. The numerical version of these results is given in Table 2.2 of the main text. Surface/Treatment conditions: a) 1:1 mixed Fc-C11SH/C12SH SAM/no treatment, b) 1:1 mixed Fc-C11SH/C12SH SAM/LSV in water, c) pure Fc-C11SH SAM/no treatment, d) 1:1 mixed Fc-C11SH/C12SH SAM/10 consecutive CVs in 1.0 mM PAA, e) 1:1 mixed Fc-C11SH/C12SH SAM/LSV in 1.0 mM PAA, f) pure Fc-C11SH SAM/LSV in 1.0 mM PAA, g) 1:1 mixed Fc-C11SH/C12SH SAM/LSV in 1.0 mM PL, h) pure Fc-C11SH SAM/LSV in 1.0 mM PL, i) 1:1 mixed Fc-C11SH/C12SH SAM/LSV in 1.0 mM poly(allylamine HCl), and j) pure Fc-C11SH SAM /LSV in 1.0 mM poly(allylamine HCl). See Experimental Section for more details.

### 2.3.4 Electrochemical Quartz Crystal Microbalance (EQCM)

We next followed the deposition of PAA and PL, each in three molecular weights, using electrochemical quartz crystal microbalance.

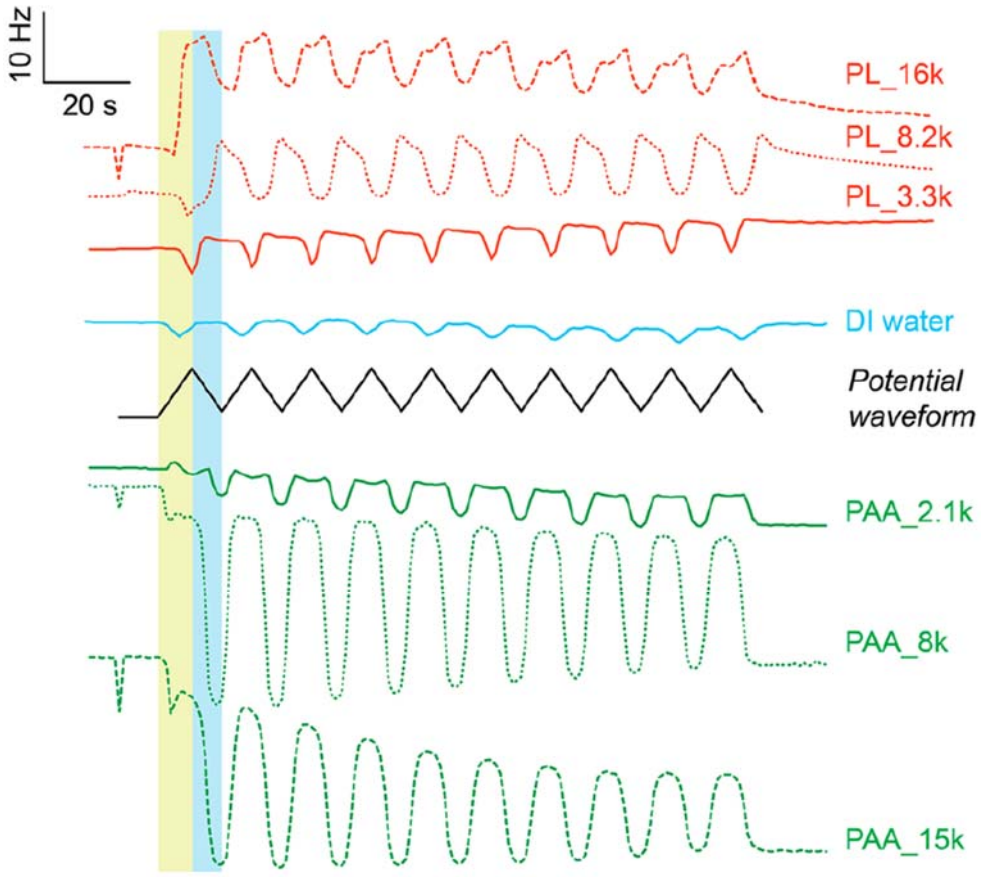


**Figure 2. 6** Electrochemical QCM monitoring of polyelectrolyte deposition on 1:1 Fc-C11SH/C12SH mixed SAMs. Responses of crystal oscillation frequency shift vs time obtained from 1.0 mM PAA (anionic) and PL (cationic) in water are shown in green and red, respectively. In each case, the solution-facing gold electrode on the crystal is biased between 0.1 and 0.8 V vs Ag/AgCl with a scan rate of 100 mV/s (waveform shown in solid black). A control response (in blue) recorded in water only is also included. The first complete CV scan is highlighted by light yellow/blue stripes.

For the anionic PAA of 8 and 15 kDa, the crystal oscillation frequencies start to drop almost immediately after the potential sweep commences (dotted and dashed traces in green, Figure 2.6), indicating mass gain at the SAM surface as a result of polymer deposition. In both cases, the drop is quickly replaced by a new frequency rise that reaches a local maximum at around 0.3 V vs Ag/AgCl, thereby registering a frequency decrease of 4 Hz (8 kDa) and 5Hz (15 kDa), respectively. Past the maximum, the frequency drops back down slowly toward the end of the forward potential scan at 0.8 V. Immediately following the start of the backward scan, a much larger frequency drop kicks in, producing a frequency decrease of 27 Hz (8 kDa) and 25 Hz (15 kDa) at the completion of the backward scan (regions highlighted in light blue, Figure 2.6). On subsequent CV scans, the frequency profiles track the applied potential closely, but not exactly. On a closer look, it can be discerned that the frequency maxima/minima consistently precede the potential maxima/ minima (0.8 and 0.1 V, respectively). These frequency maxima/ minima are not constant from scan to scan, moreover. As the potential scan proceeds, the maxima decrease progressively, while the minima increase, thus narrowing the frequency swing in between. This tendency is more pronounced in the case of 15 kDa PAA, measuring 11 vs 18 Hz for the 8 kDa PAA, at the end of the final CV scan. In both cases, a stable baseline follows the potential switch-off. In comparison to these two cases, the 2.1 kDa PAA similarly probed displays much smaller frequency shifts as well as a different shift profile (solid trace in green, Figure 2.6). Starting off, the crystal oscillation frequency shifts downward only slightly, which is then superseded by a similar but more powerful frequency increase that produces a local maximum at around 0.25 V. From that point on, the frequency continues to drop until the forward scan completes, which, upon potential reversal, starts to rise again. This produces a new frequency maximum, beyond which the frequency drops sharply and reaches a minimum at

the end of the backward scan. Consecutive CV scans afterward produce a profile that generally resembles the other two cases, except that each frequency maximum now contains edges and between them a local minimum. On the other hand, control measurements conducted in water alone only yield a low-magnitude, despite potential responding, profile, which reestablishes the initial frequency baseline at the end of each forward scan as well as at the completion of the consecutive CV treatment (solid trace in blue, Figure 2.6).

Similar EQCM characterization of cationic PLs deposition reveals a number of distinctive features as compared to PAAs (traces in red, Figure 2.6). (1) During the initial potential scan: For PLs of 3.3 and 8.2 kDa, the first forward scan lead to a monotonous frequency downshift starting at ~0.3 V. The 16 kDa PL behaves quite differently, in that the frequency initially drops slightly and then rises abruptly at 0.4 V. (2) Subsequent potential cycles: Here, once again, PLs of 3.3 and 8.2 kDa share the same trend, in which the frequency increases/decreases are brought forth by the backward/forward potential scans, respectively; matching frequency/potential highs and lows are instead observed from the 16 kDa PL. (3) Extent of frequency fluctuation: In all three cases, the magnitude of frequency shifts becomes relatively stable after the first potential cycle. (4) Net frequency shifts: For all three PLs, a positive frequency shift in the range of 4−6 Hz results at the completion of the potential cycle. By contrast, all PAAs produce negative net frequency shifts: −9 Hz for the 2.1 kDa and about −28 Hz for the other two. (5) The smallest PL (3.3 kDa) displays relatively flat frequency maxima as opposed to peaks from the other two in the series, which in a way is consistent with the PAA series.

EQCM provides highly convoluted information about the deposition processes because the deposited polymers simultaneously change the surface mass, viscoelasticity, and SAM/water

interfacial slippage condition, each modifying the crystal oscillation frequency in its own fashion.[27] Complicating the matter further are secondary processes caused by the applied potential bias, such as the swelling/shrinking of deposited polymers and accompanying ingress/egress of counterions and water. Fortunately, these secondary processes cannot take effect prior to polymer deposition. This thus points to the initial potential scan as the only window to observe the deposition alone, where the correspondence between frequency drops and polymer deposition suggests itself (yellow-highlighted region, Figure 2.6). Once deposited, both polyanions and polycations will electrostatically respond to the applied potential, which continues to drive the $Fc/Fc^+$ redox cycles. In the case of PAA, the reduction of $Fc^+$ back to Fc on the returning scan (blue-highlighted region, Figure 2.6) lifts the electrostatic attraction between $Fc^+$ and PAA, producing a mechanically more relaxed and elastic structure. An influx of sodium ions, accompanied by their water shells, is also expected, so that the newly liberated negative charges on PAA can be neutralized.

Collectively, these structural/compositional/mechanical changes register a large and abrupt frequency decrease on the oscillating crystal. The next forward potential sweep reverses the processes, whereupon a more adherent and rigid PAA layer enables the crystal to oscillate at a higher frequency. As the potential cycle continues, these processes repeat accordingly. Similar potential-modulated QCM responses have been observed previously, for example, from ferricyanide-doped polyelectrolyte films.[14] Evaluating these PAA profiles together, we may reach two additional conclusions. First, the polyanion deposition is largely an irreversible process. This is evident from the similarity in QCM responses between the initial and subsequent scans, both operating on the same population of polymers deposited in the first scan. Such irreversibility is commonly found in LbL polyelectrolyte deposition[28] and can be

generally attributed to (1) the large energy penalty associated with dissociating/rehydrating the surface and polymers, (2) the vanishingly small translational entropy[29] of polymers as compared to small solutes, and (3) the presence of other binding mechanisms, such as van der Waals interactions. Second, beyond the initial scan, the applied potential acts to "anneal" the deposited polyanions, as manifested by the progressively decreasing magnitude of frequency shifts. Such annealing effect is most visible in the 15 kDa PAA, whose long polymer chain affords the highest number of loose segments that are mostly responsive to the electric field among the three. The other interpretation of the observed trend would be a gradual loss of PAA deposits from the surface, which is considered less likely because of its absence from the case of 2.1 kDa PAA. With its short chain carrying the same charge density, such loss would have been at least comparable to the other two PAAs, if not more.

On the polycation side, PL deposition on Fc SAMs can be unequivocally identified from their highly characteristic QCM profiles. Similar to PAAs, their deposition is electrochemically triggered and takes place during the initial scan. But unlike their anionic counterparts, which are electrostatically drawn to the oxidized Fc SAM, these polycations experience repulsion as they move toward and subsequently land on the similarly charged surface. To overcome this repulsion, therefore, their counterions, $Cl^-$, have to be directly involved. A detailed discussion on this mechanism will be presented in a separate section below. As the potential shifts toward more negative (reducing) values on the returning scan, the deposited PLs are pulled further in, which leads to an overall more compact structure and hence the observed frequency up shift. The next forward potential scan sets everything on reverse: a relaxed film displaying a frequency downshift. As the potential scan continues, such shrinkage/expansion processes take turns to dominate the resulting frequency response. These features are shared by the 3.3 and 8.2

kDa PLs, with their frequency maxima/minima completely "out of phase" with the applied potential. Between these two, the 3.3 kDa PL clearly responds to the applied potential faster than the other, likely due to its smaller size. In comparison, the frequency shift observed in the 16 kDa PL not only kicks in early but also is in phase with the applied potential. The latter feature, which notably resembles PAA's frequency profiles past the initial potential cycle, is not well understood at this moment.

### 2.3.5 Atomic Force Microscopy (AFM)

To gain detailed information on the morphology of thus deposited polyelectrolytes, we also carried out AFM measurements. We started with imaging the untreated cleaned gold surface (a-c), and Fc-C11SH/C12SH 1:1 SAMs treated in deionized water by LSV scan (d-f) presented in Figure 2.7. From the comparison of their height vs distance profile, it seems the features on SAMs surface is ~2-3 nm higher than the features observed for bare gold surface. This observation is consistent with thickness of Fc-C11SH SAMs reported as 2.91 nm measured by ellipsometry and 1.84 ± 0.12 nm measured by AFM in air.[30,31] It is important to note that, presented in Figure 2.7 (d-f) is the surface of a Fc-C11SH/C12SH 1:1 SAMs treated in deionized water only. The 15 kDa PAA (a-c) and 16 kDa PL (d-f), LSV-deposited on the Fc mixed SAMs are presented in Figure 2.8. Since both 15 kDa PAA and 16 kDa PL are too small to be individually resolved with our current AFM setup, we cannot conclude from those images whether or not polyelectrolyte deposition has occurred.

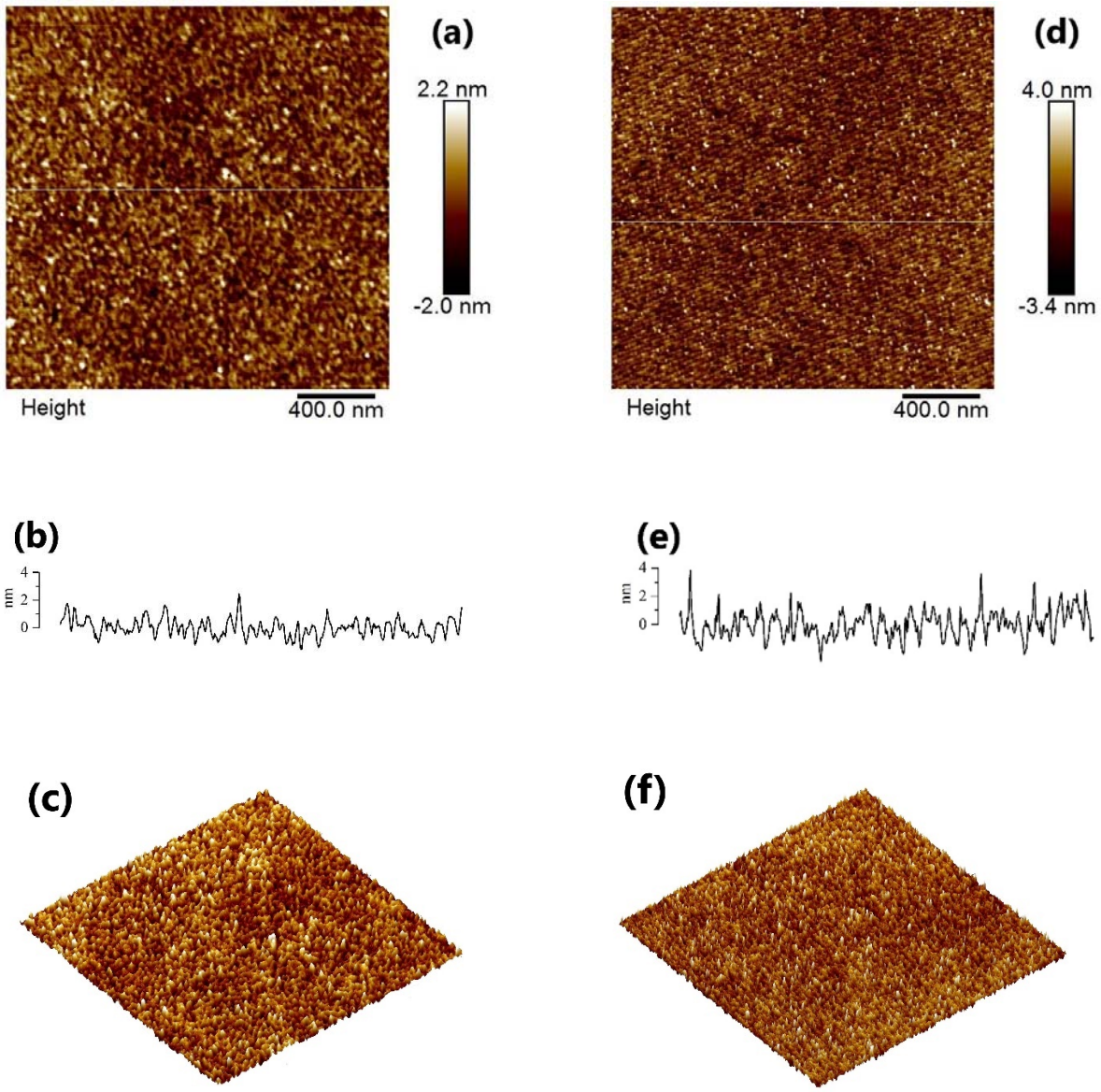


**Figure 2. 7** AFM characterization of untreated cleaned gold surface (a-c), and Fc-C11SH/C12SH 1:1 SAMs treated in deionized water by a linear potential sweep from 0.1 to 0.8 V vs Ag/AgCl (d-f). (a) & (d) are topographic images, (b) & (e) represents the height vs distance profiles of selected sections in images (a) & (d) respectively, (c) & (d) are the 3D representation of surfaces shown in images (a) & (d) respectively. Scan size: 2 × 2 μm.

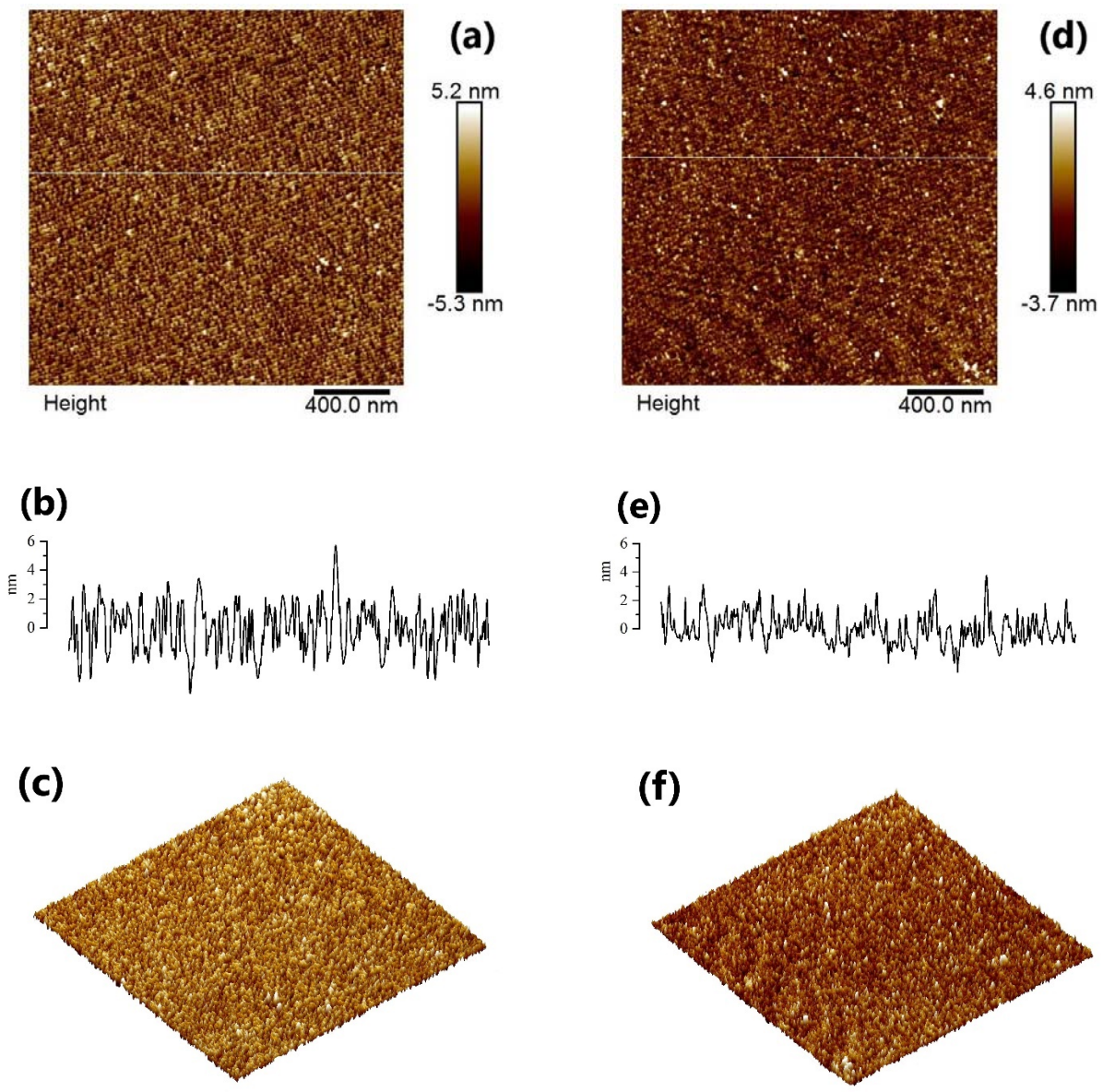


**Figure 2. 8** AFM characterization of polyelectrolyte deposition on Fc-C11SH/C12SH 1:1 SAMs triggered by a linear potential sweep from 0.1 to 0.8 V vs Ag/AgCl in 1.0 mM PAA (M.W. 15000 Da) solution (a-c) and 1.0 mM PL (M.W. 16000 Da) solution (d-f). (a) & (d) are topographic images, (b) & (e) represents the height vs distance profiles of selected sections in images (a) & (d) respectively, (c) & (d) are the 3D representation of surfaces shown in images (a) & (d) respectively. Scan size: 2 × 2 μm.

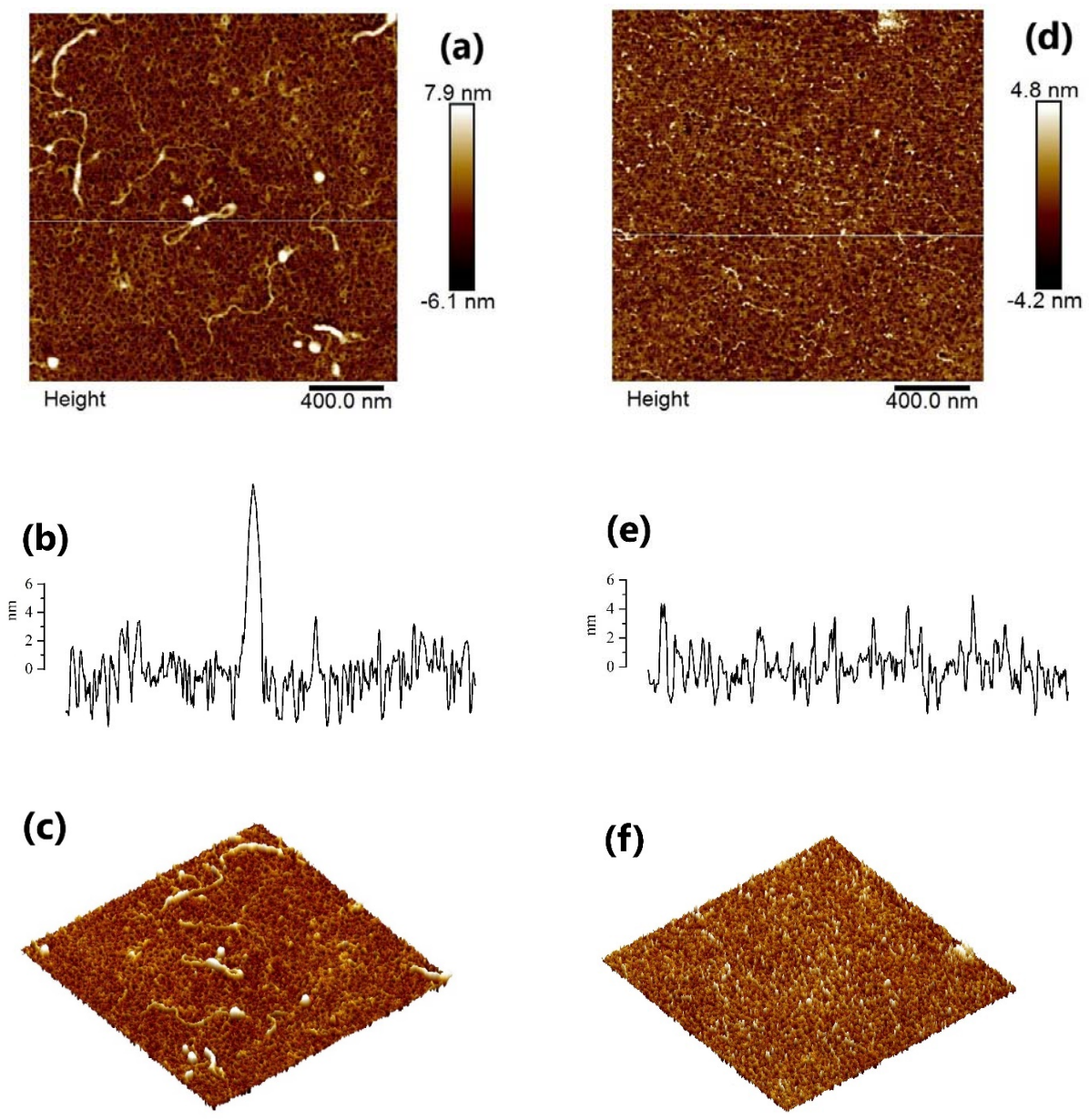


**Figure 2. 9** AFM characterization of DNA deposition triggered by a linear potential sweep from 0.1 to 0.8 V vs Ag/AgCl in DNA from calf thymus (MW ~ 10-15×$10^6$ Da) on a 1:1 Fc-C11SH/C12SH mixed SAMs (a-c) and on a pure Fc-C11SH SAMs (d-f). (a) & (d) are topographic images, (b) & (e) represents the height vs distance profiles of selected sections in images (a) & (d) respectively, (c) & (d) are the 3D representation of surfaces shown in images (a) & (d) respectively. Scan size: 2 × 2 μm. See the experimental section for details.

To circumvent this limitation, we then replaced PAA with DNA from calf thymus, a much larger polyanion with a MW of 10-15 million Da. This time, AFM imaging clearly identifies twisted, threadlike features spanning several hundred nanometers (Figure 2.9 a), which can be attributed to deposited DNAs with reasonable certainty. From their large sizes, i.e., tens of nanometers in width and >10 nm maximal height, we can further conclude that these threads represent bundles of DNA strands, whose formation may result from DNA minimizing hydrophobic contact. Beneath these DNA bundles, interestingly, another mesh like feature is also clearly visible. These meshes are relatively evenly distributed across the entire surface, and their sizes fall within a narrow range of 15-20 nm. Since this formation is exclusively observed for DNA, i.e., absent from SAMs similarly treated in PAA, PL, or water alone, we tentatively assign it to be the second main feature of DNA deposition besides the threads. To further verify this assignment, we also imaged DNA deposits formed on pure Fc-C11SH SAMs, which, once again, display a mesh like morphology (Figure 2.9 d). Here, a noticeable difference is that the DNAs deposited atop appear not only thinner but also shorter, which appear to resemble individual DNAs more than their bundles. This morphological difference may be due to the fact that, absent of hydrophobic C12 thiols, pure Fc SAMs produce a primarily charged surface upon oxidization, which can better accommodate binding of individual DNAs. By contrast, oxidation of the Fc-C11SH/C12SH mixed SAM yields a partially charged surface blended with hydrophobic components. From these images, we can further conclude that such electrochemically triggered polymer deposition proceeds evenly across the entire SAM surface.

### 2.3.6 Deposition Mechanisms

All the experimental evidence presented above suggests that the “trigger-and-trade” scheme describes the polyanion deposition reasonably well. Among these, the results of fluorescence,

contact angles, and AFM uniformly confirm the occurrence of such deposition, whereas the CV and EQCM data further shed light on the involved mechanism and dynamics. Of the latter, the well-defined Fc oxidation waves obtained in PAA (Figure 2.1) and poly(glutamic acid, sodium salt) (Figure 2.2 a) manifest their direct involvement and efficacy in charge compensation, despite their relatively low concentration and large size (e.g., vs 0.1 M NaCl). The EQCM responses of PAA (Figure 2.6) during the initial potential scan, on the other hand, identify a trend in which the mass gain on the electrode closely tracks the Fc oxidation. These results help establish a general sequence of events involved in the deposition: ferrocene oxidation→ charge compensation → polyanion deposition (Figure 2.10). Though not directly related, it should be pointed out that a similar scheme has been conceived by Badia and co-workers to attract anionic surfactants onto Fc SAMs.[32]

The characteristically distinctive responses observed in polycations signify a different deposition mechanism all together. This becomes evident first from voltammetry, in which Fc oxidation in the presence of polycations is found to significantly lag behind that obtained in polyanion solutions. Of these, the CV obtained in PL closely resembles that in NaCl (Figure 2.3 b), suggesting that chloride, the common anion of the two electrolytes, is responsible for compensating $Fc^+$. Nevertheless, these two voltammograms are not exactly identical: Fc oxidation in NaCl not only appears slightly more dragged out but also peaks earlier than the other. The latter shift is not caused by conductivity difference between the two solutions (i.e., the iR drop), which remains observable in 1 mM as well as 1.0 M NaCl solutions (data not shown). A similar but even more pronounced trend was found in the case of poly(allylamine HCl) (Figure 2.2 b). These distinctive features thus lead us to an important conclusion: *the movement of small counterions in polyelectrolyte aqueous solutions is not completely*

*independent of the polymer*. For this to be true, therefore, a certain level of association must exist between polyelectrolytes and their counterions when dispersed in water.

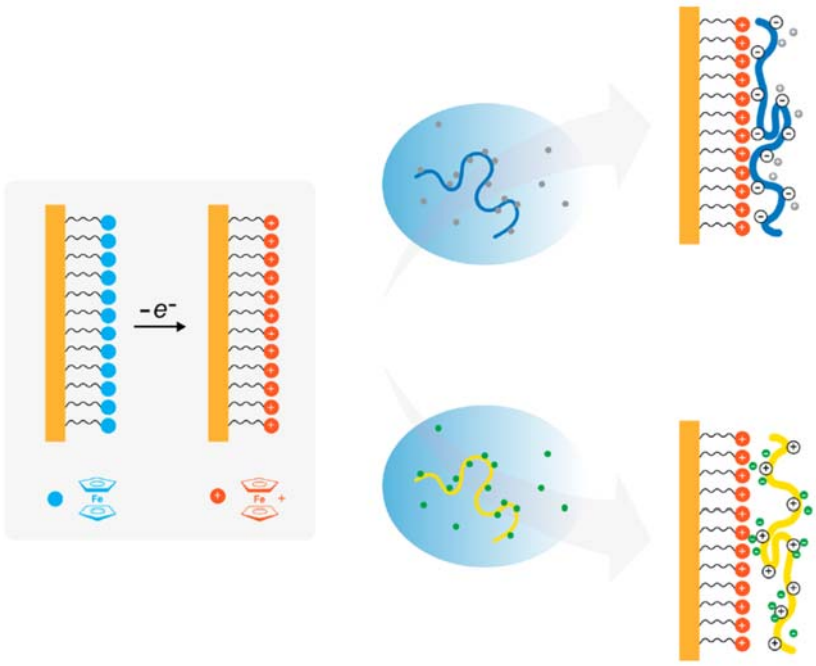


**Figure 2. 10** Schematic illustration of mechanisms involved in the electrochemically triggered deposition of polyelectrolytes. Polyanions and polycations are depicted by thick curves in blue and yellow, respectively, whereas their counterions are presented by small dots (gray for cations and green for anions). Intrinsic charges on polyelectrolytes are shown by circles.

Understandably, the strength and extent of such association is polymer dependent. In the case of PL, the pendant positive charge is located on the ε-position distant from the polymer backbone, which gives rise to a relatively "delocalized" charge distribution along the polymer. This in effect lowers the density of intrinsic charge carried by the polyanion and thus undermines its ability to electrostatically attract its counterion, $Cl^-$. As a result, a significant portion of chloride ions in the system can move about nearly as freely as in NaCl. By contrast, charges are more locally distributed along the polymer in the case of poly(allylamine HCl), thanks to the close

placement of its ammonium group to the polymer backbone. This results in a higher level of association between polymers and their counterions at any given time, due to stronger electrostatic attraction and an elevated need to screen the monomer-monomer charge repulsion within the polymer. Consequently, to call these polymer-associated counterions to participate in charge compensation, a higher energy input is required, as manifested by its positive-shifted Fc oxidation potential (Figure 2.2 b). Once these chloride ions start to move toward the electrode, critically, they drag the associated polymers along with them. To see the feasibility of this potential-induced co-movement, we may first invoke an analogy with another electrokinetic phenomenon-electroosmosis (EO). In the latter process, counterions accumulated in the double layer of a charged surface can carry water molecules to produce bulk solution movement under an external electric field.[33] With their stronger (charge-charge vs charge-dipole interaction in EO) and multiple binding with $Cl^-$, polycations in the current case are expected to be even more susceptible to such induced motion. Accepting this possibility for the time being, we immediately arrive at another important conclusion: *electrochemically triggered polycation deposition involves like-charge attraction*. This has to be true because the polymer plus associated counterions are net positively charged-the same as the oxidized Fc SAM.

Additional insights emerge when these electrochemically triggered processes are evaluated in light of established polyelectrolyte theories. In the classical Oosawa−Manning (OM) ion condensation theory,[34,35,36] small counterions are postulated to distribute between two states in aqueous polyelectrolyte solutions: freely mobile vs territorially bound with polymers. Underlying this distribution is the thermodynamic balance between electrostatic attraction, which pulls the counterions within close proximity to the polymer, and the entropic gain associated with the release of counterions into the bulk. A key parameter formulated in the OM

theory is Manning linear charge density of the polyelectrolyte, ξ, which can be calculated from the following equation: $\xi = e^2/\varepsilon k_B T b$, where e is the elementary charge, ε the dielectric constant of the solvent, $k_B T$ the thermal energy term, and b the average axial charge spacing of the polymer. Theoretically, counterion condensation sets in whenever ξ becomes greater than 1.[35,36] From this dimensionless quantity, one can also estimate the fraction of condensed ions, f, which takes the value of $1- (Z\xi)^{-1}$, where Z is the valence charge of the counterion. Approximating b to be 0.3 nm for poly(allylamine HCl),[37] we thus obtain $\xi = 2.3$ and $f = 0.6$ (in water and at 25 °C), which suggest substantial ion condensation. In comparison, such condensation is considerably less in the case of PL due to its larger charge spacing, e.g., in the range of 0.5-0.7 nm, depending on its secondary structure.[38] These numerical estimates thus corroborate well with our qualitative analysis above.

An important implication of ion condensation theory is attraction between polyelectrolytes carrying similar charges. This counterintuitive phenomenon arises because (1) the polyelectrolyte plus its counterions is a highly polarizable entity; as such, (2) thermal fluctuation causes temporary, but constant, uneven charge distribution along the polymer; and (3) correlated polarization between polyelectrolytes in close proximity lowers the total energy of the system. The latter, as Oosawa put forth first in his celebrated monograph, Polyelectrolytes, "...results in an attractive force between macroions, just as in the case of van der Waals interaction between atoms and molecules".[34] This thus leads to a peculiar scenario in which mobile ion clouds are shared by interacting polymers.[39] While this phenomenon is prevalent and relatively well understood in cases where polyvalent counterions are directly involved, e.g., in DNA/dication binding,[40,41] recent theoretical and experimental evidence[39,42] strongly suggests that like-charge attraction can be also mediated by monovalent ions. Besides

polyelectrolytes, similar theoretical treatments[43] can also be extended to explain attraction between like-charged surfaces. In this regard, therefore, our results on polycation deposition provide experimental evidence that the hybrid scenario, i.e., attraction between similarly charged polyelectrolytes and surfaces, also occurs (Figure 2.10).

Still, such attraction would not proceed without the electrochemical trigger. Electrooxidation not only puts charge on the Fc-SAM surface but, in doing so, also provides the driving force for polyelectrolytes (i.e., polymers plus counterions) to migrate toward the surface. In between the two binding parties, importantly, the applied potential also tips the thermodynamic and mechanical balances at the Fc-SAM/water interface. Prior to oxidation, both mixed and pure Fc SAMs are moderately hydrophobic (Table 2.2). To cope with such hydrophobicity and at the same time maximally maintain their H-bonding network, water molecules in direct contact with the surface collectively will have to adopt a certain nonrandom orientation. As oxidation brings charges onto the hydrophobic SAM, many interfacial water molecules find themselves in wrong orientation so a major restructuring is due. Similar processes can also be expected of the incoming polyelectrolytes. In the case of polyanions, these may involve shedding of counterions and reorganization of polymer segments, presumably guided by the local surface charge distribution, so that Fc+ moieties can be neutralized fully and effectively. Such restructuring should be less for polycations because their binding to $Fc^+$ is led by small counterions (no shedding is necessary, therefore), whose nimble movement allows quick adjustment of charge distribution around the polymers. This important distinction between polyanions and polycations is expected to cause further divergences after their landing, i.e., conformation/packing of deposited polyelectrolytes as well as the associated interfacial water structure. Such microscopic characteristics, in turn, lead to experimentally observable

differences, e.g., the constantly smaller signal fluctuations and deviations in EQCM (Figure 2.6) and water contact angles (Table 2.2) obtained from polycations. While the mechanisms discussed above are clearly plausible, it must be stressed that other parameters and scenarios, either operating alone or alongside electrostatic interactions, may also exist. For example, we have not explicitly considered the influence of lateral surface heterogeneity, which can be particularly relevant in the case of mixed Fc SAMs. In the case of polycations, moreover, deposition may as well result from their decreased solubility as the $Cl^-$ exodus (upon Fc oxidation) causes the deprotonation, and hence neutralization, of these polymers. All these potential contributors attest the complexity of involved processes, which we hope to continue to explore in the near future.

### 2.3.7 Layer-by-Layer Deposition

Finally, as a preliminary effort to explore the potential applications of this deposition strategy, we examined the formation of conventional layer-by-layer (LbL) polyelectrolyte films starting with an electrochemically deposited first polyelectrolyte layer. This, if successful, should promise a general formation strategy for electroactive LbL films, whose ferrocene adlayer can be exploited for both diagnosis and electroactuation purposes. As shown in Figure 2.11, PAA films LSV-deposited on pure Fc-C11SH SAMs can indeed serve as the starting surface to sustain the growth of LbL polyelectrolyte films. For the 10-layer PAA/poly(fluorescein isothiocyanate allylamine) films investigated here, moreover, we observed a nonlinear layer-by-layer growth profile. More detailed studies along this direction are currently ongoing in our laboratory to establish the structure and general properties of these electroactive polyelectrolyte films.

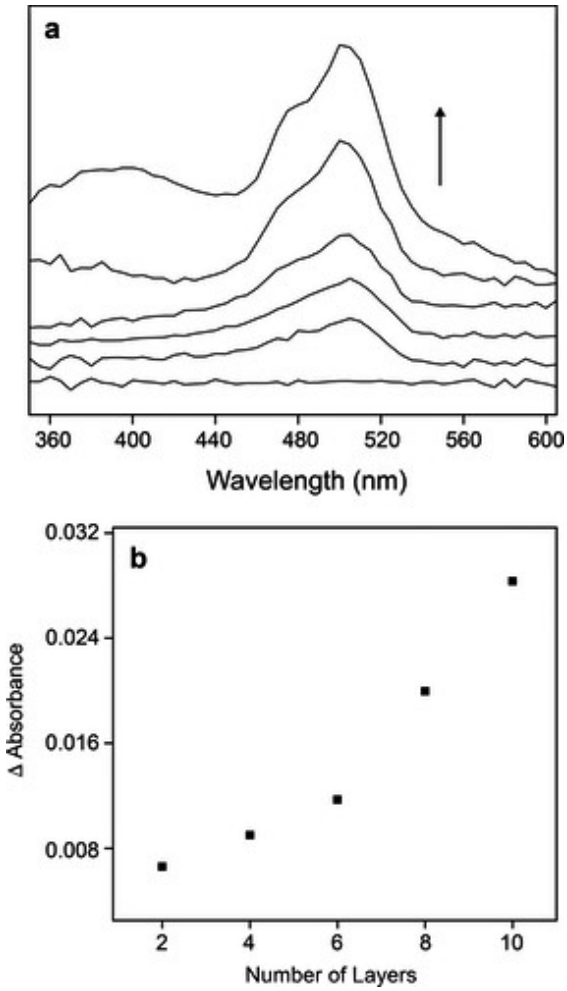


**Figure 2. 11** Layer-by-layer polyelectrolyte deposition starting from a PAA layer deposited by the reported method. (a) Ten-layer film growth monitored by UV−vis absorption responses of poly(fluorescein isothiocyanate allylamine hydrochloride), which is deposited at evennumbered rounds. (b) Net UV−vis absorbance of poly(fluorescein isothiocyanate allylamine hydrochloride) monitored at ~505 nm vs number of layers, replotted from (a).

### 2.4 Summary and Conclusion

In this chapter, we have presented a new approach to polyelectrolyte surface deposition based on electrochemical triggering. Starting from the same basic structure, ferrocene-decorated self-assembled monolayers (Fc-SAMs), this approach enables quantitative deposition of both

polyanions and polycations with a wide range of chemical identities (synthetic polymers, peptides, and DNA) and molecular weights ($10^3$-$10^7$ Da).

Such generality, combined with its ready access to conventional layer-by-layer film formation and electrochemical detection, should make this approach useful in a number of areas, for example, in polyelectrolyte-based diagnosis and electroactuation. Conceivably, the methodology detailed here may also be of some value in probing aqueous polyelectrolyte systems, in particular, their organization and mass transfer. To this end, for example, Osteryoung and co-workers demonstrated previously that quantitative information about counterion diffusion (in polyelectrolyte solutions[44] and their colloidal suspensions[45]) could be extracted from steady-state voltammetry of proton reduction on microelectrodes. Compared to their approach, our Fc-SAM-based methodology imposes little restriction on experimental conditions under which the polyelectrolytes can be examined, such as pH or the type of ions. As such, it enables counterions in polyelectrolytes to be directly compared to their simple ion counterparts. While a fair amount of information can already be obtained from $Fc/Fc^+$ voltammetry alone, such as shape, shift, and onset, additional information is possible when it is further coupled with a secondary technique, e.g., QCM. Some of these possibilities are currently being tested in our laboratory.

**References**

(1) Love, J. C.; Estroff, L. A.; Kriebel, J. K.; Nuzzo, R. G.; Whitesides, G. M. Self-Assembled Monolayers of Thiolates on Metals as a Form of Nanotechnology. *Chem. Rev.* **2005**, *105* (4), 1103-1170. https://doi.org/10.1021/cr0300789.

(2) Chidsey, C. E. D. Free Energy and Temperature Dependence of Electron Transfer at the

Metal-Electrolyte Interface. *Science* **1991**, *251* (4996), 919-922. https://doi.org/10.1126/science.251.4996.919.

(3) Smalley, J. F.; Finklea, H. O.; Chidsey, C. E. D.; Linford, M. R.; Creager, S. E.; Ferraris, J. P.; Chalfant, K.; Zawodzinsk, T.; Feldberg, S. W.; Newton, M. D. Heterogeneous Electron-Transfer Kinetics for Ruthenium and Ferrocene Redox Moieties through Alkanethiol Monolayers on Gold. *J. Am. Chem. Soc.* **2003**, *125* (7), 2004–2013. https://doi.org/10.1021/ja028458j.

(4) Eckermann, A. L.; Feld, D. J.; Shaw, J. A.; Meade, T. J. Electrochemistry of Redox-Active Self-Assembled Monolayers. *Coord. Chem. Rev.* **2010**, *254* (15–16), 1769–1802. https://doi.org/10.1016/j.ccr.2009.12.023.

(5) Umek, R. M.; Lin, S. W.; Vielmetter, J.; Terbrueggen, R. H.; Irvine, B.; Yu, C. J.; Kayyem, J. F.; Yowanto, H.; Blackburn, G. F.; Farkas, D. H.; et al. Electronic Detection of Nucleic Acids: A Versatile Platform for Molecular Diagnostics. *J. Mol. Diagnostics* **2001**, *3* (2), 74–84. https://doi.org/10.1016/S1525-1578(10)60655-1.

(6) Fan, C.; Plaxco, K. W.; Heeger, A. J. Electrochemical Interrogation of Conformational Changes as a Reagentless Method for the Sequence-Specific Detection of DNA. *Proc. Natl. Acad. Sci. U. S. A.* **2003**, *100* (16), 9134–9137. https://doi.org/10.1073/pnas.1633515100.

(7) Norman, L. L.; Badia, A. Redox Actuation of a Microcantilever Driven by a Self-Assembled Ferrocenylundecanethiolate Monolayer : An Investigation of the Origin of the Micromechanical Motion and Surface Stress. *J. Am. Chem. Soc.* **2009**, *131*, 2328−2337. https://doi.org/10.1021/ja808400s.

(8) Imahori, H.; Yamada, H.; Nishimura, Y.; Yamazaki, I.; Sakata, Y. Vectorial Multistep

Electron Transfer at the Gold Electrodes Modified with Self-Assembled Monolayers of Ferrocene - Porphyrin - Fullerene Triads. *J. Phys. Chem. B* **2000**, *104* (9), 2099–2108. https://doi.org/10.1021/jp993784f.

(9) Xie, H.; Jiang, K.; Zhan, W. A Modular Molecular Photovoltaic System Based on Phospholipid/Alkanethiol Hybrid Bilayers: Photocurrent Generation and Modulation. *Phys. Chem. Chem. Phys.* **2011**, *13* (39), 17712–17721. https://doi.org/10.1039/c1cp21701a.

(10) Clark, S. L.; Montague, M.; Hammond, P. T. Selective Deposition in Multilayer Assembly: SAMs as Molecular Templates. *Supramol. Sci.* **1997**, *4* (1–2), 141–146. https://doi.org/10.1016/S0968-5677(96)00055-7.

(11) Harris, J. J.; Bruening, M. L. Electrochemical and in Situ Ellipsometric Investigation of the Permeability and Stability of Layered Polyelectrolyte Films. *Langmuir* **2000**, *16* (4), 2006–2013. https://doi.org/10.1021/la990620h.

(12) Hodak, J.; Etchenique, R.; Calvo, E. J.; Singhal, K.; Bartlett, P. N. Layer-by-Layer Self-Assembly of Glucose Oxidase with a Poly(Allylamine)Ferrocene Redox Mediator. *Langmuir* **1997**, *13* (10), 2708–2716. https://doi.org/10.1021/la962014h.

(13) Lvov, Y. M.; Lu, Z.; Schenkman, J. B.; Zu, X.; Rusling, J. F. Direct Electrochemistry of Myoglobin and Cytochrome P450(Cam) in Alternate Layer-by-Layer Films with DNA and Other Polyions. *J. Am. Chem. Soc.* **1998**, *120* (17), 4073–4080. https://doi.org/10.1021/ja9737984.

(14) Grieshaber, D.; Vörös, J.; Zambelli, T.; Ball, V.; Schaaf, P.; Voegel, J. C.; Boulmedais, F. Swelling and Contraction of Ferrocyanide-Containing Polyelectrolyte Multilayers upon Application of an Electric Potential. *Langmuir* **2008**, *24* (23), 13668–13676.

https://doi.org/10.1021/la801875u.

(15) Schmidt, D. J.; C, F.; Kalcioglu, Z. I.; Wyman, S. G.; Ortiz, C. Electrochemically Controlled Swelling Nanocomposite. *ACS Nano* **2009**, *3* (8), 2207–2216.

(16) Rowe, G. K.; Creager, S. E. Redox and Ion-Pairing Thermodynamics in Self-Assembled Monolayers. *Langmuir* **1991**, *7* (10), 2307–2312. https://doi.org/10.1021/la00058a055.

(17) Ju, H.; Leech, D. Effect of Electrolytes on the Electrochemical Behaviour of 11-(Ferrocenylcarbonyloxy)Undecanethiol SAMs on Gold Disk Electrodes. *Phys. Chem. Chem. Phys.* **1999**, *1* (7), 1549–1554. https://doi.org/10.1039/a809754b.

(18) Valincius, G.; Niaura, G.; Kazakevičiene, B.; Talaikyte, Z.; Kažemekaite, M.; Butkus, E.; Razumas, V. Anion Effect on Mediated Electron Transfer through Ferrocene-Terminated Self-Assembled Monolayers. *Langmuir* **2004**, *20* (16), 6631–6638. https://doi.org/10.1021/la0364800.

(19) Popenoe, D. D.; Deinhammer, R. S.; Porter, M. D. Infrared Spectroelectrochemical Characterization of Ferrocene-Terminated Alkanethiolate Monolayers at Gold. *Langmuir* **1992**, *8* (10), 2521–2530. https://doi.org/10.1021/la00046a028.

(20) Abbott, N. L.; Whitesides, G. M. Potential-Dependent Wetting of Aqueous Solutions on Self-Assembled Monolayers Formed from 15-(Ferrocenylcarbonyl)Pentadecanethiol on Gold. *Langmuir* **1994**, *10* (5), 1493–1497. https://doi.org/10.1021/la00017a029.

(21) Jego-Evanno, P.; Hurvois, J. P.; Moinet, C. Electrooxidation of Substituted Ferrocenes: Indirect Oxidation of the Side Chain. *J. Electroanal. Chem.* **2001**, *507* (1–2), 270–274. https://doi.org/10.1016/S0022-0728(01)00455-7.

(22) Hurvois, J. P.; Moinet, C. Reactivity of Ferrocenium Cations with Molecular Oxygen in Polar Organic Solvents: Decomposition, Redox Reactions and Stabilization. *J.*

*Organomet. Chem.* **2005**, *690* (7), 1829–1839. https://doi.org/10.1016/j.jorganchem.2005.02.009.

(23) Lee, L. Y. S.; Sutherland, T. C.; Rucareanu, S.; Lennox, R. B. Ferrocenylalkylthiolates as a Probe of Heterogeneity in Binary Self-Assembled Monolayers on Gold. *Langmuir* **2006**, *22* (9), 4438–4444. https://doi.org/10.1021/la053317r.

(24) Tagliazucchi, M.; Calvo, E. J.; Szleifer, I. A Molecular Theory of Chemically Modified Electrodes with Self-Assembled Redox Polyelectrolye Thin Films: Reversible Cyclic Voltammetry. *Electrochim. Acta* **2008**, *53* (23), 6740–6752. https://doi.org/10.1016/j.electacta.2008.01.041.

(25) Kittredge, K. W.; Fox, M. A.; Whitesell, J. K. Effect of Alkyl Chain Length on the Fluorescence of 9-Alkylfluorenyl Thiols as Self-Assembled Monolayers on Gold. *J. Phys. Chem. B* **2001**, *105* (43), 10594–10599. https://doi.org/10.1021/jp004325d.

(26) Fery-Forgues, S.; Delavaux-Nicot, B. Ferrocene and Ferrocenyl Derivatives in Luminescent Systems. *J. Photochem. Photobiol. A Chem.* **2000**, *132* (3), 137–159. https://doi.org/10.1016/S1010-6030(00)00213-6.

(27) Buttry, D. A.; Ward, M. D. Measurement of Interfaclal Processes at Electrode Surfaces with the Electrochemical Quartz Crystal Microbalance. *Chem. Rev.* **1992**, *92* (6), 1355–1379. https://doi.org/10.1021/cr00014a006.

(28) Dubas, S. T.; Schlenoff, J. B. Factors Controlling the Growth of Polyelectrolyte Multilayers. *Macromolecules* **1999**, *32* (24), 8153–8160. https://doi.org/10.1021/ma981927a.

(29) Netz, R. R.; Andelman, D. Neutral and Charged Polymers at Interfaces. *Phys. Rep.* **2003**, *380* (1–2), 1–95. https://doi.org/10.1016/S0370-1573(03)00118-2.

(30) Ohtsuka, T.; Sato, Y.; Uosaki, K. Dynamic Ellipsometry of a Self-Assembled Monolayer of a Ferrocenylalkanethiol during Oxidation-Reduction Cycles. Langmuir 1994, 10 (10), 3658–3662. https://doi.org/10.1021/la00022a045.

(31) Norman, L. L.; Badia, A. Electrochemical Surface Plasmon Resonance Investigation of Dodecyl Sulfate Adsorption to Electroactive Self-Assembled Monolayers via Ion-Pairing Interactions. Langmuir 2007, 23 (20), 10198–10208. https://doi.org/10.1021/la7006028.

(32) Nguyen, K. L.; Dionne, E. R.; Badia, A. Redox-Controlled Ion-Pairing Association of Anionic Surfactant to Ferrocene-Terminated Self-Assembled Monolayers. *Langmuir* **2015**, *31* (23), 6393–6394. https://doi.org/10.1021/acs.langmuir.5b01196.

(33) Evans, D. F.; Wennerström, H. *The Colloidal Domain*, 2nd ed.; Wiley- VCH: New York, 1999.

(34) Oosawa, F. *Polyelectrolytes*; Marcel Dekker, Inc.: New York, 1971.

(35) Manning, G. S. Counterion Binding in Polyelectrolyte Theory. *Acc. Chem. Res.* **1979**, *12* (12), 443–449. https://doi.org/10.1021/ar50144a004.

(36) Manning, G. S.; Ray, J. Fluctuations of Counterions Condensed on Charged Polymers. *Langmuir* **1994**, *10* (3), 962–966. https://doi.org/10.1021/la00015a058.

(37) Donath, E.; Walther, D.; Shilov, V. N.; Knippel, E.; Budde, A.; Lowack, K.; Helm, C. A.; Möhwald, H. Nonlinear Hairy Layer Theory of Electrophoretic Fingerprinting Applied to Consecutive Layer by Layer Polyelectrolyte Adsorption onto Charged Polystyrene Latex Particles. *Langmuir* **1997**, *13* (20), 5294–5305. https://doi.org/10.1021/la970090u.

(38) Dos, A.; Schimming, V.; Tosoni, S.; Limbach, H. Acid-Base Interactions and Secondary Structures of Poly-L-Lysine Probed by 15 N and 13 C Solid State NMR And. **2008**, 15604–15615.

(39) Naji, A.; Jungblut, S.; Moreira, A. G.; Netz, R. R. Electrostatic Interactions in Strongly Coupled Soft Matter. *Phys. A Stat. Mech. its Appl.* **2005**, *352* (1), 131–170. https://doi.org/10.1016/j.physa.2004.12.029.

(40) Gelbart, W. M.; Bruinsma, R. F.; Pincus, P. A.; Parsegian, V. A. DNA-Inspired Electrostatics. *Phys. Today* **2000**, *53* (9), 38–44. https://doi.org/10.1063/1.1325230.

(41) Diehl, A.; Carmona, H. A.; Levin, Y. Counterion Correlations and Attraction between Like-Charged Macromolecules. *Phys. Rev. E - Stat. Physics, Plasmas, Fluids, Relat. Interdiscip. Top.* **2001**, *64* (1), 6. https://doi.org/10.1103/PhysRevE.64.011804.

(42) Manning, G. S. Counterion Condensation Theory of Attraction between like Charges in the Absence of Multivalent Counterions. *Eur. Phys. J. E* **2011**, *34* (12). https://doi.org/10.1140/epje/i2011-11132-6.

(43) Guldbrand, L.; Jönsson, B.; Wennerström, H.; Linse, P. Electrical Double Layer Forces. A Monte Carlo Study. *J. Chem. Phys.* **1984**, *80* (5), 2221–2228. https://doi.org/10.1063/1.446912.

(44) Ciszkowska, M.; Osteryoung, J. G. Voltammetric Studies of Counterion Transport in Polyelectrolyte Solutions. *J. Phys. Chem.* **1994**, *98* (12), 3194–3201. https://doi.org/10.1021/j100063a024.

(45) Roberts, J. M.; Linse, P.; Osteryoung, J. G. Voltammetric Studies of Counterion Diffusion in the Monodisperse Sulfonated Polystyrene Latex. *Langmuir* **1998**, *14* (1), 204–213. https://doi.org/10.1021/la9705726.

# CHAPTER 3. ELECTROCHEMICALLY TRIGGERED INTERFACIAL DEPOSITION/ASSEMBLY OF AQUEOUS-SUSPENDED COLLOIDS*

## 3.1 Introduction

We report herein a new electrochemical method for facile deposition/assembly of aqueous-suspended colloids on electrode surfaces. Key to the high efficiency of this method are ferrocene (Fc) moieties, which are introduced into the system via self-assembled alkanethiol monolayers (SAMs), and serve as an electrochemical trigger to initiate and control such deposition/assembly processes. With this method, high-fidelity colloid micropatterns can be formed in seconds. This work expands the utility of ferrocene-based redox-controlled surfaces, which was pioneered by the Whitesides group[1] and has since then seen quite exciting new development in the field of metallopolymers.[2,3]

Of particular relevance to this work is the research on electrically driven colloidal assembly on planar electrodes.[4,5,6] Ordered colloidal assemblies often display interesting photonic, spectroscopic and catalytic properties,[7,8,9] which, when interfaced directly with electrodes, can yield novel devices with improved functionality and controllability. In practice, both d.c. and a.c. electric fields have been commonly employed. Of the former, which is more related to this work, colloidal particles are driven toward the electrodes by one or a combination of the following mechanisms:[7,10,11,12] electrophoresis, electroosmosis, and electrohydrodynamic motion. While the experimental setup is usually simple, containing primarily two parallel electrodes with controlled spacing, sorting out these mechanisms can be quite complex. Such complexity arises first of all from the four components typically involved in the assembly process: the colloids, the working



*This chapter is copied from a published paper (*ChemElectroChem* **2020**, *7*, 1097–1106) with minor modification.

electrode (to some extent, the counter electrode as well), the aqueous medium and supporting electrolytes, which together give rise to at least two interfaces (i.e., electrode/water and colloid/water) with distinctive double-layer structure and charge distribution. Since any perturbation of charge distribution at these interfaces could potentially modify the electrohydrodynamics experienced by the colloids, their movement and assembly are subjected to the influence of not only the electrodes, but also each other. The latter effect is exemplified by the interesting observation of entrainment of colloidal particles,[13,14] yielding well-ordered 2D colloidal crystals on electrodes.

In the majority of existing work on electrically-driven formation of colloidal assemblies, faradaic electrode processes are not explicitly considered.[15,16] This is not an oversight in practice, of course, considering the largely physical nature of the involved mechanisms driving such formations. Of the few studies[17,18] in which the impact of faradaic reactions is specifically examined, the discussion has been primarily focused on the background redox processes, i. e., water hydrolysis. Nonetheless, it is clear that faradaic reactions can have a deciding influence on the electrokinetic and electrohydrodynamic behaviors[15,16,19] of aqueous systems. Understanding these behaviors, accordingly, will uncover new ways of controlling and improving colloidal deposition under such settings.

In this work, we studied the deposition/assembly behavior of negatively-charged colloidal particles on planar gold working electrodes grafted with ferrocene-terminated alkanethiol SAMs. This work follows our recent discovery[20] that polyelectrolytes can be deposited onto these SAMs upon Fc oxidation, which switches the SAM from a hydrophobic surface to positively charged surface. We demonstrate that this drastic change of surface characteristics can be quite generally applied to initiate and control interfacial deposition and assembly of aqueous suspended colloidal

particles. Key factors involved, including the starting electrode surfaces, colloid size, range/duration of the applied potential, and small supporting electrolytes, are examined in detail, using voltammetry, confocal fluorescence microscopy and quartz crystal microbalance. A particularly interesting finding among these is the superior efficiency of the electrochemically triggered assembly compared to the electrically driven process, which we utilize to form high-fidelity colloid micropatterns on electrodes. A detailed discussion on the deposition mechanisms is also provided.

## 3.2 Experimental Details

### 3.2.1 Chemicals

11-Ferrocenyl-1-undecanethiol (Fc-C11SH), 1-dodecanethiol (C12SH), sodium perchlorate hydrate (99.99% trace metal basis), sodium chloride (≥99.5 %), TWEEN 20 were products of Sigma- Aldrich (St. Louis, MO). Fluorescent carboxylate-modified polystyrene nanospheres/microspheres were obtained from Bangs Laboratories, Inc. (Fishers, IN). Deionized water of 18.2 MΩ·cm (Millipore) was used in preparing all aqueous colloid suspensions as well as in all rinsing and dilution steps.

### 3.2.2 Formation of Self-Assembled Monolayers

Self-assembled monolayers (SAMs) containing Fc-C11SH/C12SH binary mixtures formed on semi-transparent gold-coated microscope slides (Au thickness: 10 nm, Sigma-Aldrich) were used throughout this work. These SAMs were prepared in two fashions as follows:

*1) Solution Incubation*

Prior to the SAM formation, gold-coated substrates were immersed in a piranha solution (3 :1 v/v mixture of concentrated $H_2SO_4$ and $H_2O_2$ 30 wt% aqueous solution) for 3 min, thoroughly rinsed

with deionized water, ethanol, and then dried under $N_2$. Thus cleaned dry substrates were immediately immersed in an ethanol solution containing 0.5 mM Fc-C11SH and C12SH each; the incubation was allowed to proceed for 16-18 h in the dark. Upon completion, the substrates were rinsed first with methanol to remove excess thiols on surface, then DI water, and finally dried under $N_2$. These SAM covered gold slides were normally used within the same day of their preparation.

*2) Microcontact Printing*

Silicone rubber stamps, containing either circular pillar arrays or custom micropatterns, were obtained from Research Micro Stamps (Clemson, SC). Of the latter, hand-drawn features were first converted to digital files with a digital camera and shrunk to desired sizes in Adobe Illustrator (version: CS6); the resulting miniaturized patterns were saved in .svg format and subsequently passed to the manufacturer for stamp production. Before use, the stamps were first cleaned by sonicating in ethanol for 5 min, and gently dried under a stream of $N_2$. To ink, thus cleaned stamps were soaked in an ethanol solution of 0.5 mM Fc-C11SH and C12SH each for 10 min and then gently dried under $N_2$. Immediately afterwards, these inked stamps were placed conformally onto precleaned gold coated glass slides; the printing was allowed to proceed for 10 min, during which a small weight block was placed on top of the stamp to ensure a gentle and even press. Upon completion, the stamps were removed, and the substrates were thoroughly rinsed with methanol, then DI water, and dried under $N_2$. These SAM-patterned gold slides were normally used within the same day of their preparation.

### 3.2.3 Electrochemical Treatments and Characterization

Linear sweep voltammetry (LSV) operated by a PC-controlled potentiostat (CHI 910B, CH Instruments, Austin, TX) was used in this work to initiate colloidal deposition and assembly on

electrodes. A three-electrode setup was used throughout this work, consisting SAM-covered gold substrates as the working electrode, a platinum wire (diameter: 1 mm) as the counter electrode and Ag/AgCl in saturated KCl solution as the reference electrode, housed in homemade Teflon cells (Figure 3.1 a). To initiate the deposition, a given SAM was typically biased with an LSV scan in an intended colloid suspension in 0.05% (w/v) aqueous solution of TWEEN 20. After LSV scan, the initial suspension was thoroughly exchanged out with deionized water, and the gold electrode thus treated was taken out and dried under a gentle stream of ultrapure $N_2$. Deposits can also be formed from colloids suspended in DI water without adding TWEEN 20 but with a slightly inferior reproducibility.

### 3.2.4 Zeta Potential Measurements

Zeta potential values of polystyrene nanobeads and microbeads suspended in DI water were obtained from a Malvern Zetasizer (Nano-ZS, Malvern Instruments, Worcestershire, UK) using capillary cells (DTS1070) operated under a 150 V bias at 25°C. Typically three parallel readings were taken for each sample.

### 3.2.5 Electrochemical Quartz Crystal Microbalance (EQCM)

EQCM measurements were carried out at room temperature using a QCM analyzer with a 5 MHz crystal oscillator (Model: QCM25) from Stanford Research Systems (Sunnyvale, CA). The quartz crystals used are polished quartz wafers of 1-inch diameter with circular gold electrodes coated on both sides. Before use, these golf-coated quartz crystals were cleaned and grafted with a 1:1 Fc-C11SH/C12SH mixed SAM as described above. The SAM-coated crystal was subsequently mounted on the QCM crystal holder, and its solution facing electrode was used as the working electrode in a three electrode configuration together with a Pt-wire counter electrode

and a Ag/AgCl reference electrode (in saturated KCl). To do so, a PC controlled potentiostat (CHI 910B, CH Instruments) was connected to the QCM crystal holder via the crystal face bias connector of the QCM25 crystal controller. This setup enables simultaneous monitoring of the QCM frequency shift and current on the working electrode (crystal) as a function of the applied potential; the latter is furnished by the potentiostat in the form of LSV between 0.1 and 0.9 V at 10 mV/s.

### 3.2.6 Fluorescence Microscopy

Fluorescence images were acquired on a Nikon A1+/MP confocal scanning laser microscope (Nikon Instruments, Inc., Melville, NY) with 4x and 10x objectives. Laser beams at 488 and 561 nm were used to excite green- and red-emitting colloidal bead assemblies formed on semi-transparent gold-coated glass slides, and the corresponding emission signals were filtered at 525±25 and 595±25 nm, respectively.

## 3.3 Results and Discussion

### 3.3.1. Experimental Setup and Background Electrode Responses

Figure 1a depicts schematically the experimental setup employed in this work. At the top is a Teflon cell, which contains a cylindrical through-hole as the solution reservoir at the center and two smaller slant side holes housing a Ag/AgCl reference electrode and a Pt wire counter electrode. The ring-shaped Pt wire is positioned roughly in parallel with the bottom gold-film working electrode, 0.3 cm above. As colloidal samples, carboxylate polystyrene (PS-COOH) beads of six different sizes suspended in DI water, with/without additional supporting electrolytes, were employed. These beads are fluorescently labeled so their deposition/assembly at the semi-transparent gold film electrodes can be fully followed with fluorescence microscopy.

Besides size, these beads also differ each other in surface –COOH density, which is reflected by their various zeta potentials that range from –20 to –70 mV (Table 3.1).

**Table 3. 1** General properties of carboxylate polystyrene (PS-COOH) beads studied.

| Size (μm) | Parking Area[a] | Zeta Potential (mV) | Bead Concentration[c] |
|---|---|---|---|
| 0.06 | 57.2 | -20.9 ± 2.2[b] | 9.58 x $10^{10}$ |
| 0.22 | 30.2 | -36.3 ± 0.7[b] | 2.39 x $10^{10}$ |
| 0.51 | 9.4 | -35.6 ± 0.5[b] | 9.58 x $10^{9}$ |
| 1.0 | 21.8 | -49.4 ± 0.4[b] | 4.78 x $10^{9}$ |
| 2.19 | 186.2 | -51.0 ± 2.1[b] | 4.28 x $10^{8}$ |
| 4.95 | 23.8 | -69.1 ± 0.7[b] | 1.40 x $10^{7}$ |

[a] Average surface area ($Å^2$) corresponding to each -COOH group, manufacturer's data.

[b] Standard deviation, n=3. [c] Count of beads per mL of samples employed in Figure 3.8.

To identify the background electrochemical responses, we first ran linear sweep voltammetry (LSV) with this setup filled with DI water alone. With bare Au films as the working electrode, this yielded an i-V curve containing three main redox features (Figure 3.1 b, voltammogram in black). The first two broad peaks between 0.4 and 0.8 V appear to correspond to the monolayer and multilayer gold oxide formation,[21,22] whereas the rise in current past 0.9 V is associated with oxygen evolution. The latter process apparently overloads the 10-nm thick Au films, causing their complete strip-off from the glass slides evident to the naked eye (not shown). With the film gone, the cell loses its electrical contact past 1.3 V. For Au films covered with 1:1 Fc-C11SH/C12SH mixed SAMs, on the other hand, a quite distinctive LSV profile results (Figure 3.1b, voltammogram in red). Here, the first pair of redox features are shifted to more positive potentials by about 0.2 V, likely a result of the SAM shielding the Au surface from water and thus hindering gold oxide formation.

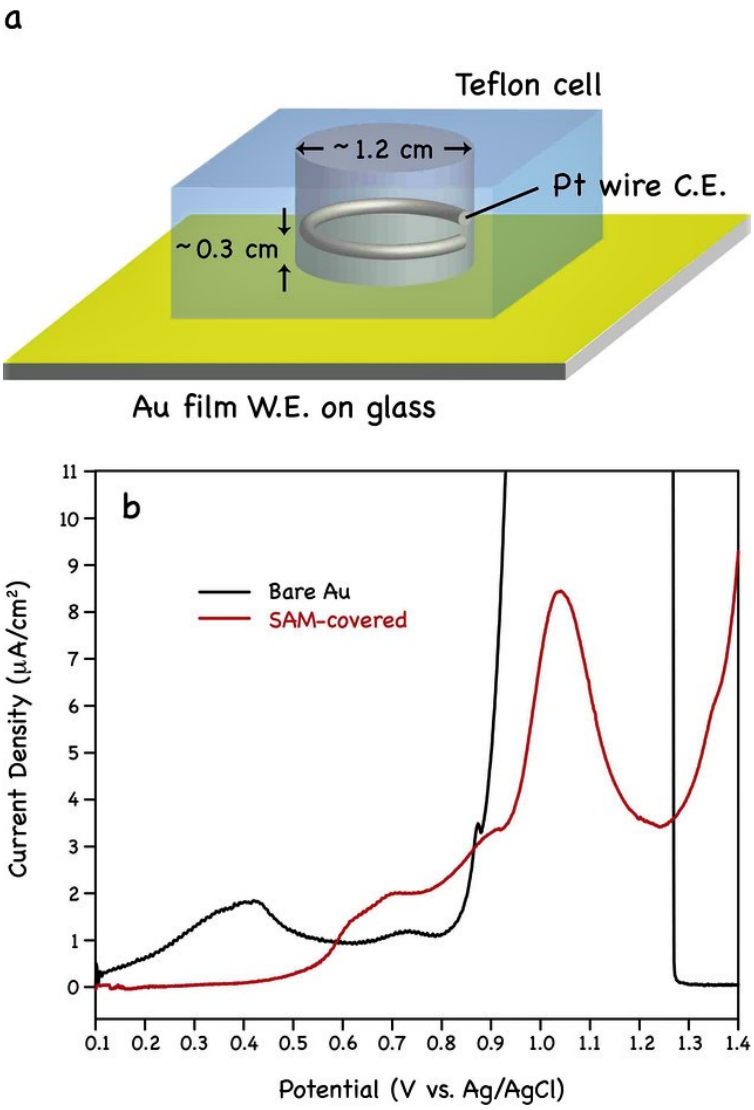


**Figure 3. 1** a) Schematic of the three-electrode experimental setup. For clarity, the Ag/AgCl reference electrode and assembly sockets are not included in the drawing. b) Background electrochemical processes probed in DI water using either bare or 1:1 Fc-C11SH/C12SH mixed SAM-covered gold films as working electrode.

Following this pair is a prominent, symmetrical wave between 0.9 and 1.2 V, which can be attributed to the delayed Fc oxidation. Comparing the magnitude of this wave with that obtained in $NaClO_4$ (see below), it appears that this feature contains in addition some other background

processes, perhaps e. g., continual oxide formation. After 1.2 V, the oxygen evolution sets in once again.

### 3.3.2. Fluorescence Microscopy Confirmation of Colloidal Deposition

With the background processes established, we next examined the deposition behavior of 0.5-μm-diameter PS-COOH beads using bare Au films as the working electrode. As evident from Figure 3.2 a, a sub-monolayer deposition of randomly distributed beads occurred readily when the electrode was biased by a linear potential sweep from 0.1 to 0.4 V vs. Ag/AgCl. The main redox feature within this potential window roughly coincides with that observed from bare Au probed in water alone (Figure 3.1 b), but with an intensified current output.

A similar deposition results when the bias is extended to 0.7 V, within which a small but discernable wave appears at about 0.6 V. Immediately following this wave, the current rises significantly, which, after a brief plateau, is substituted by the oxygen evolution reaction at about 0.9 V. Because this feature is absent from the background responses and prior to it microbead deposition has already occurred, we tentatively assign it as expedited Au oxide formation facilitated by the PS-COOH microbeads on-electrode. Since the oxygen evolution causes the Au film to dissolve, the majority of the deposited microbeads are removed from the surface at the end of the 0.1–1 V scan.

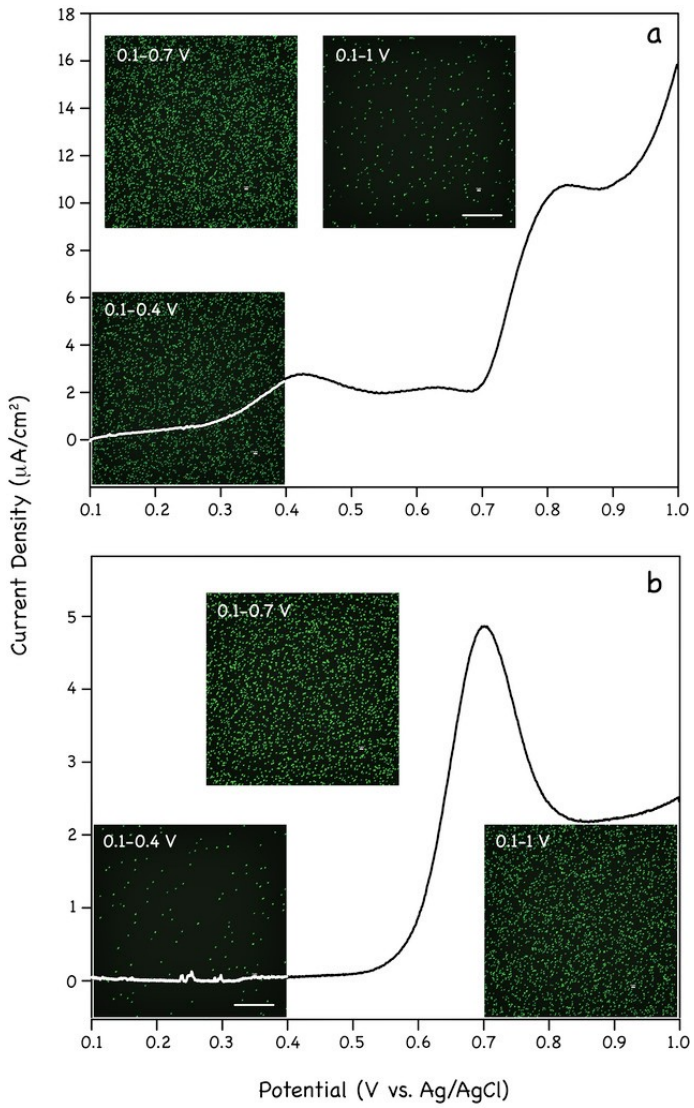


**Figure 3. 2** Linear sweep voltammograms (LSV) recorded on either bare gold films (a) or gold films covered with 1:1 Fc-C11SH/C12SH mixed SAMs (b) in aqueous suspensions of 0.5-μm PS-COOH beads (concentration: ca. $1x10^9$ per mL). The suspensions in addition contain 0.05% (w/v) TWEEN 20; scan rate: 10 mV/s. The embedded fluorescence images in each case are obtained from three separate potential scans covering 0.1-0.4 V, 0.1-0.7 V, and 0.1-1 V, respectively. Only the LSVs of 0.1-1 V are shown here; the two short scans overlap with the corresponding segments of the former and are omitted for clarity. The scale bar represents 50 μm and applies to all images.

Similar tests were then run on Au films covered with 1:1 Fc-C11SH/C12SH mixed SAMs. The SAM modification of the working electrode completely alters the redox processes in operation and hence the course of colloid deposition. Starting off, the relatively quiet electrochemical process within 0.1–0.4 V only led to low-level colloid deposition, whereas sub-monolayer colloid depositions with coverage comparable to that seen on bare gold were obtained in the next two potential windows (Figure 3.2 b).

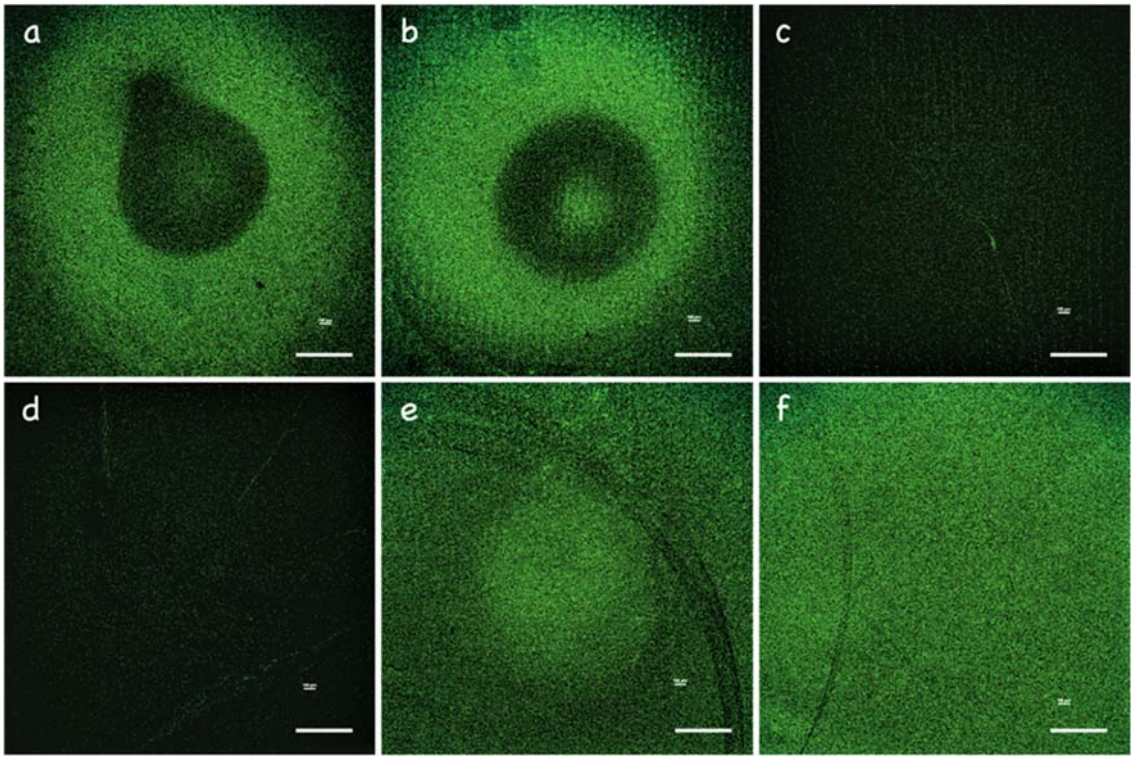


**Figure 3. 3** Large-area fluorescence images of 0.5-μm PS-COOH beads electrochemically deposited. Images a) to c) are obtained on bare gold electrodes from three separate potential scans covering 0.1-0.4 V, 0.1-0.7 V and 0.1-1 V, respectively. Images d) to f) are obtained from gold electrodes grafted with 1:1 Fc-C11SH/C12SH mixed SAMs undergone similar treatments. Bead concentration: ~1x$10^8$ per mL; scale bar: 500 μm.

The stable deposition obtained from 0.1–1 V scan apparently benefited from the shielding/protection of Au films by the SAM. In the entire scan, there exists only one main electrochemical wave, which starts to rise past 0.5 V and subsequently peaks at 0.7 V. This feature results from the superimposition of at least two redox processes: Au oxide formation (Figure 3.1b) and Fc SAM oxidation. The latter process, as will be elaborated in more detail later, is compensated mostly by chloride ions leaked into the solution from the Ag/ AgCl reference electrode.

While the fluorescence images in Figure 3.2 (as well as elsewhere in the main text) are taken using a 10x objective lens focused near the center of Au electrodes, low-magnification (4x) imaging was also performed on above samples to cover larger areas of colloidal deposits (Figure 3.3). These images display radially distributed microbead patterns, clearly due to the ring-shaped Pt wire C.E. that causes distortion of the electric field. The patterns formed on bare electrodes are very distinguishable from those on SAM-covered electrodes; the uniform coverage achieved on the latter after 0.1–1 V LSV scan is also evident.

### 3.3.3. Electrochemical QCM Characterization of Deposition

To further characterize these colloid deposition processes, we also carried out electrochemical quartz crystal microbalance (EQCM) analysis. By employing Au films directly coated on crystal disks as the working electrode, this technique reveals the mass change on the electrode in real time as the associated electrochemical process takes place.[23] For the bare Au electrode probed in water alone (Figure 3.4, black trace), the crystal oscillation frequency tips downward shortly after the inauguration of the LSV scan, indicating a mass gain on the electrode that is likely due to the oxide formation on the gold film. The frequency decrease continues at a slow pace before reaching a plateau after 0.7 V vs. Ag/AgCl.

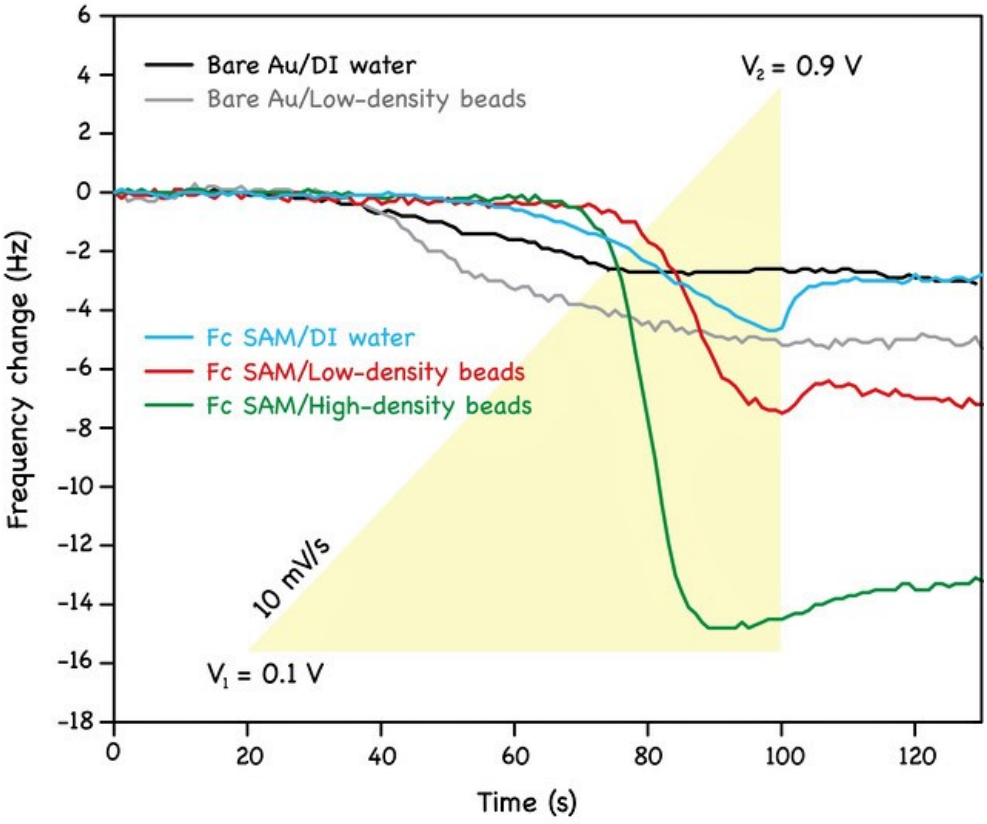


**Figure 3. 4** Electrochemical QCM monitoring of deposition of 0.5 μm PS-COOH beads (low-density: ca. $1\times10^7$ per mL vs. high density: ca. $1\times10^9$ per mL) on either bare gold electrodes or gold electrodes covered with 1:1 Fc-C11SH/C12SH mixed SAMs. The samples in addition contain 0.05% (w/v) TWEEN 20. In each case, the gold electrodes were biased by a liner potential scan from 0.1 to 0.9 V at 10 mV/s, as marked by the yellow triangle.

When the system is in addition suspended with 0.5 μm PS-COOH beads, the same LSV scan produces a frequency profile with greater downward shift, which can be assigned to the accompanying colloid deposition on the electrode (Figure 3.4, gray trace). The concurrency of frequency change shown by the two profiles, moreover, indicates a likely connection between Au oxide formation and bead deposition. To be consistent with the conventional nomenclature

and distinguish it from the Fc-SAM based process, however, we describe colloidal assemblies formed on bare Au as electrical deposition throughout this work.

Similar tests once again were carried out on Au films covered with 1:1 Fc-C11SH/C12SH mixed SAMs. Here, several deviations are apparent. 1) Onset potential for frequency downshift. Due to suppression of gold oxidation by the SAM, the crystal oscillation frequencies do not shift downward appreciably until 0.4 V (in water alone) or past 0.5 V (in colloid aqueous suspensions), matching well with the LSV results (Figures 3.1 b and 3.2 b); 2) Correspondence between the colloid deposition and Fc oxidation. The steepest frequency decreases coincide with the voltammetric peak of Fc oxidation, which strongly suggests the latter process is responsible for the observed deposition; 3) Magnitude/speed of frequency shifts. For the same concentration of suspended PS-COOH microbeads, the frequency shift takes place more steeply on SAM covered electrode than on the bare electrode. A >60% higher downshift was also observed on SAM-covered electrode (Figure 3.4, red vs. gray traces) at the end of the LSV scan; 4) Dependence of deposition on colloid concentration. When the bead density was increased from $1\times10^7$ to $1\times10^9$ per mL, an approximate doubling of frequency downshift was registered. In the latter case, a frequency minimum was reached before the end of the scan (~ 0.8 V), suggesting faster bead deposition and saturation on the SAM.

### 3.3.4. Simultaneous Electrochemical and Electrical Deposition

With the results presented above establishing colloidal deposition on both SAM-covered electrodes and bare electrodes, an interesting question emerges: Are they the same or different processes? To answer this question, we next employed Au films partially covered with SAMs so that the two formats of deposition can be run side-by-side on the same electrode.

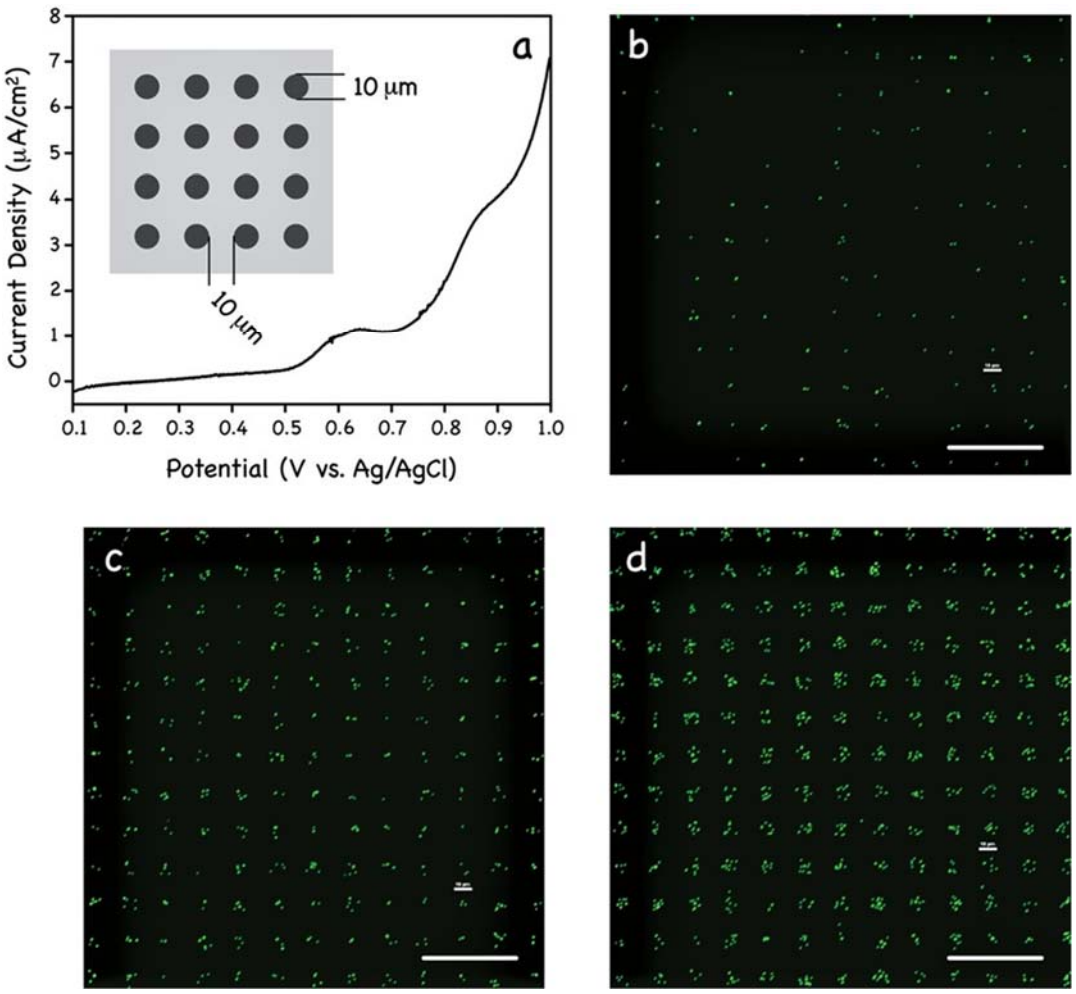


**Figure 3. 5** a) Linear sweep voltammogram of patterned 1:1 Fc-C11SH/C12SH mixed SAMs probed in 0.5 µm PS-COOH microbead aqueous suspensions (concentration: ~1x10$^9$ per mL, with 0.05% (w/v) TWEEN 20). Inset: schematic depiction of the layout and dimensions of the microarray employed in microcontact printing of thiols. See the Experimental section for more details. b) to d) Fluorescence images of gold film electrodes covered with 1 :1 Fc-C11SH/C12SH mixed SAM micropatterns after a single LSV scan from 0.1 to 0.4 V (b), 0.1 to 0.7 V (c), and 0.1 to 1 V (d), in 0.5 µm microbead aqueous suspensions. Potential scan rate: 10 mV/s; scale bar: 50 µm.

To achieve such partial coverage, we chose to graft the thiols onto the bare Au electrodes via a pre-patterned silicone rubber stamp, using the microcontact printing (μCP)[24] technique initially developed by the Whitesides group. As shown schematically in Figure 3.5 a, the stamp carries positive features of a 10-μm-diameter micropillar array with 10 μm spacing, which, upon printing, will yield SAM patterns with the same shape/dimension on the electrodes.

As before, we ran LSV scans on these thiol-patterned Au film electrodes in three potential windows in 0.5 μm-diameter PS-COOH bead aqueous suspensions. Upon the initial 0.1-0.4 V sweep, strikingly, a microbead array that reproduces the original pattern on the stamp results (Figure 3.5 b). Despite their low coverage, the fact that the beads only land on spots where the thiols are put down via μCP is unmistakable. Such exclusive deposition becomes more evident as a result of more extended potential scans (Figure 3.5 c, d), yielding on average 3–5 beads per SAM micropatch after the 0.1–0.7 V run and 7–10 beads after the 0.1–1 V run. Since deposition occurs more efficiently on bare Au alone than on SAM-covered electrodes in the potential window of 0.1–0.4 V (Figure 3.2), it follows that the thiol anchorage on gold completely disables the remaining open Au surface from recruiting microbeads. We will defer a detailed discussion of involved mechanisms till a later section.

### 3.3.5. Effect of Supporting Electrolyte

To better understand the electrohydrodynamic characteristics of these colloidal particles during Fc SAM oxidation, we then chose to examine a series of parameters critically involved in the deposition process. This started with small supporting electrolyte, in which we examined how the presence of either $NaClO_4$ or NaCl in the system would influence the deposition. Of the two, perchlorate stands clearly as the electrolyte of choice for probing Fc SAM electrochemistry, owing to its low hydration that leads to strong ion-pairing with ferrocenium.[25,26] In comparison,

the highly solvated chloride ions[26] are less effective in accommodating the $Fc/Fc^+$ transition, giving rise to a higher Fc oxidation potential.

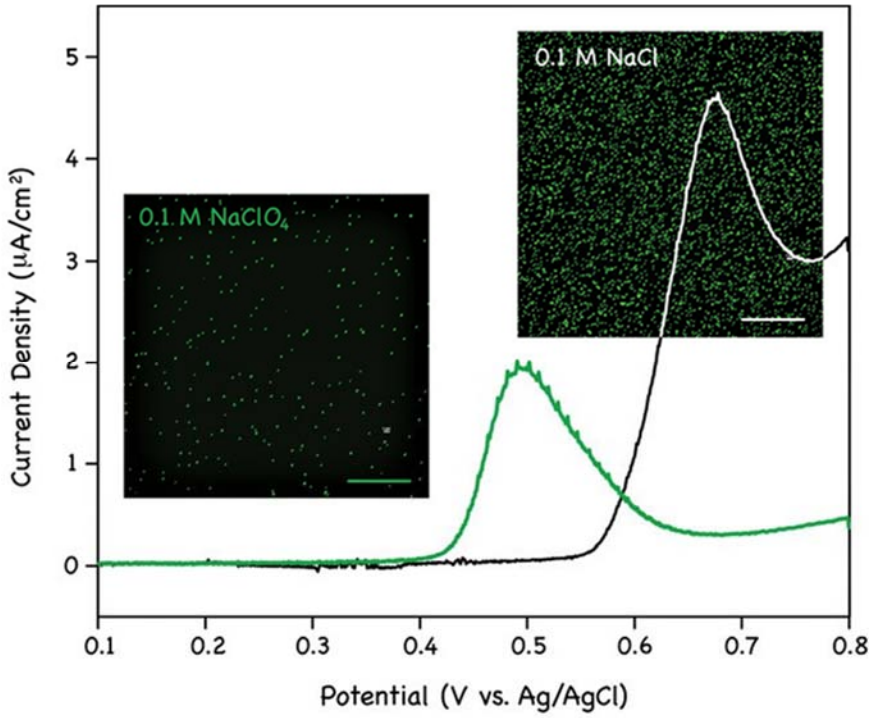


**Figure 3. 6** Linear sweep voltammograms of 1:1 Fc-C11SH/C12SH mixed SAMs probed in 0.5 μm PS-COOH microbead aqueous suspensions (bead concentration: ca. $1\times10^9$ per mL, 0.05% (w/v) TWEEN 20) in the presence of either 0.1 M $NaClO_4$ (green) or 0.1 M NaCl (black and white). Inset: fluorescence images of the SAM-covered gold surfaces following the LSV treatments. Potential scan rate: 10 mV/s; scale bar: 50 μm.

When the SAM-modified Au film electrodes were probed in 0.1 M $NaClO_4$ (together with 0.5-μm-diameter PS-COOH beads), a typical bell-shaped Fc SAM oxidation voltammogram was obtained[27] (Figure 3.6). Remarkably, a >80% decrease in the bead coverage was detected on the electrode compared to that obtained in DI water after the 0.1–0.7 V scan (Figure 3.2b), which indicates $NaClO_4$ can effectively suppress colloid deposition. In contrast, colloidal deposition

proceeds largely undisturbed in the presence of 0.1 M NaCl (Figure 3.6), which remains the case even when the NaCl concentration is raised to 2 M (Figure 3.7). Taken together, these results strongly suggest the direct involvement of ferrocenium in driving colloidal deposition, whose neutralization by perchlorate (but not chloride) effectively abolishes the deposition process.

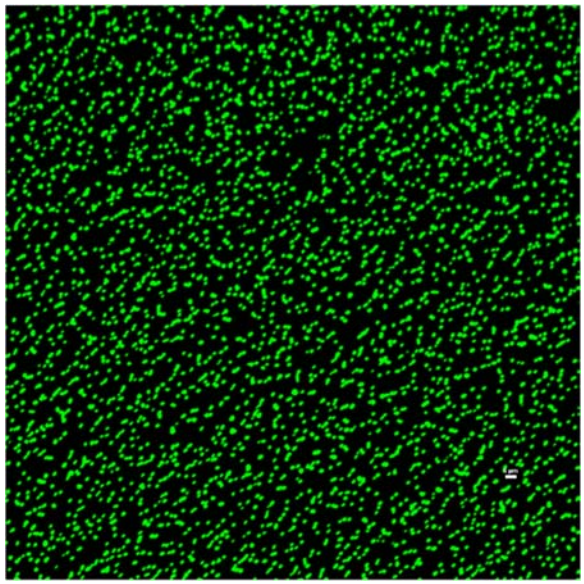

**Figure 3. 7** Fluorescence image of 0.5-μm PS-COOH beads electrochemically deposited on a 1:1 Fc-C11SH/C12SH mixed SAM. The beads were suspended in water at ~$1x10^8$ per mL additionally mixed with 0.05% (w/v) TWEEN 20 and 2 M NaCl. The deposit was prepared from a single LSV scan in the suspension from 0.1 to 0.8 V at 10 mV/s. The scale bar (at the lower right corner) corresponds to 5 μm.

On the other hand, the voltammogram obtained in 0.1 M NaCl matches the one shown in Figure 3.2 b closely in shape and peak position, confirming that chloride ions are also responsible for charge compensation in the earlier case.

### 3.3.6. Effect of Colloid Size

To further shed light on the deposition mechanisms, we also extended the above characterization procedure to 5 other PS-COOH bead samples, which together cover two orders of colloid size. The fluorescence imaging results of the deposited PS-COOH beads are shown in Figure 3.8. Among these, the 60 nm beads are not individually resolved due to their small size, resulting in a relatively weak, continuous fluorescent image. As will become evident later, their deposition has successfully occurred nevertheless.

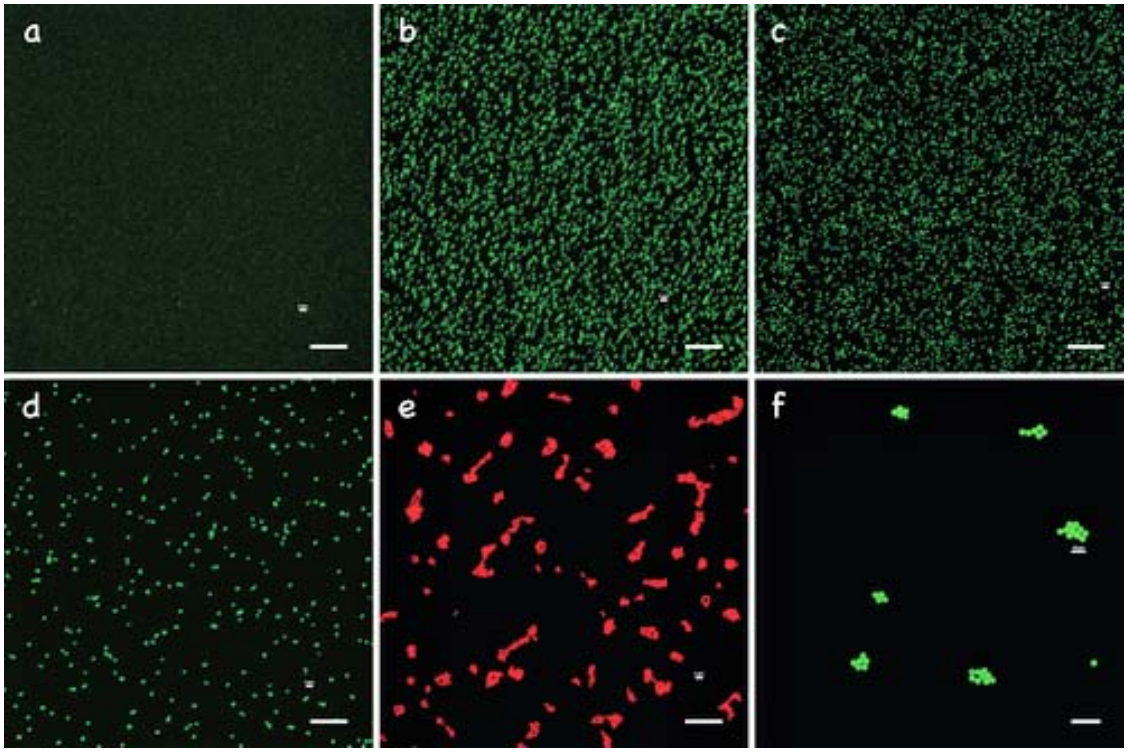


**Figure 3. 8** Fluorescence images of electrochemically triggered deposition of PS-COOH beads of various sizes on 1 :1 Fc-C11SH/C12SH mixed SAMs. Bead size: a) 0.06 μm, b) 0.22 μm, c) 0.51 μm, d) 1.0 μm, e) 2.19 μm and f) 4.95 μm; their concentrations are specified in Table 3.1. All samples were treated by a single LSV scan from 0.1 to 0.8 V at 10 mV/s. The scale bars correspond to 50 μm.

In general, as the size of colloids increases, their distribution becomes less even. This trend is most evident for the 2-μm and 5-μm samples, in which cases most deposited particles actually exist in clusters. The coverage of these two microbeads on electrodes is also noticeably lower than other samples. Factors that may cause such characteristic formations will be discussed in a later section.

**Table 3. 2** Scan rate dependence of electrochemically triggered deposition of 0.5-μm-diameter PS-COOH beads.

| Scan rate (mV/s)[a] | Particle coverage (%) | Particle count |
|---|---|---|
| 10 | 8.9 ± 0.7[b] | 3127 ± 138[b] |
| 100 | 9.4 ± 0.3[b] | 2955 ± 114[b] |
| 250 | 6.8 ± 0.5[b] | 1896 ± 97[b] |
| 500 | 3.7 ± 0.2[b] | 847 ± 48[b] |
| 1000 | 2.2 ± 0.5[b] | 559 ± 147[b] |

[a] Results obtained from a single LSV scan from 0.1 to 0.8 V; bead concentration: $9.58 \times 10^9$ per mL. [b] Standard deviation, n=3 or 4.

### 3.3.7. Effect of Scan Rate

Finally, we examined the effect of LSV scan rate on the colloid deposition. As summarized in Table 3.2, comparable deposition was obtained at relatively slow scan rates, i. e., between 10 mV/s and 100 mV/s, for 0.5-μm PS-COOH beads; as the scan rate increases further, a steady decrease of colloid surface coverage results. At the highest scan rate tested, 1 V/s, for example, the count of deposited particles drops by >80% compared to that obtained at 10 mV/s and 100

mV/s. Using the latter rate as the threshold at which the colloid mass transfer limit (by diffusion) sets in, we can roughly estimate a timescale of a few seconds, i.e., the minimum time needed for a full-extent deposition of 0.5 μm PS-COOH beads on 1 :1 Fc-C11SH/C12SH mixed SAMs.

### 3.3.8. Deposition Mechanisms

With all the characterization results presented above, we now attempt a preliminary and qualitative analysis of the involved deposition mechanisms in this section.

*1) Magnitude and Distribution of the Electric Field*

In order to assess the relative contribution of each possible mode of motion, it is helpful to first establish the size/distribution of electric field (E) present in our system. For that, we need to know the potential drop on both working and counter electrodes. For the latter, we take the value of -0.6 V vs. Ag/AgCl, assuming $2H^+ + 2e^- = H_2$ under neutral pH as the redox process occurring on the Pt wire.[28] Taking the peak potentials on working electrodes to be 0.4 V (bare Au, Figure 3.2 a) and 0.7 V (SAM-covered Au, Figure 3.2 b), respectively, and the distance between W.E. and C.E. to be 0.3 cm (Figure 3.1 a), we can roughly estimate their corresponding apparent electric field: 3.3 and 4.3 V/cm. It is important to note once again that the electric field is not uniform in either case (Figure 3.3).

As discussed above, significant concentrations of KCl were expected to be present in the colloidal suspensions due to its leakage from the reference electrode. This condition gives rises to a thin double-layer surrounding the PS-COOH beads, *i.e.* with their Debye length expected to be on the order of nm.[29] By contrast, the double-layer structure associated with the electrode prior to the potential sweep is less well-defined due mainly to the hydrophobicity of the SAM surface.

*2) Classical/Linear Electrophoretic Motion of Colloidal Particles*

As the linear potential sweep is switched on, an electric field starts to develop between the W.E. and C.E., to which the negatively charged colloidal particles have to respond with electrophoretic motion. The resultant electrophoretic mobility (μ) can be estimated from the zeta potential of the colloid according to the Helmholtz-Smoluchowski equation:[30] $\mu = \varepsilon_o \varepsilon \zeta / \eta$, in which ζ is the zeta potential of the particle, $\varepsilon_o$ the vacuum permittivity, ε and η are respectively the relative dielectric permittivity and viscosity of the medium. From the zeta potential measured for the 0.5 μm PS-COOH beads, -35.6 mV (Table 3.1), we then obtain μ at $-2.5\times10^{-4}$ $cm^2V^{-1}s^{-1}$, which, under the pertinent electric field, corresponds to a scenario where a microbead migrates at most 10 μm a second. On the other hand, if the bead movement is driven by such electrophoresis alone, longer runs should always result in more extensive deposition. The fact that this is not the case, e.g. in 10 mV/s vs. 100 mV/s depositions, therefore, points to the likely presence of other driving mechanism(s) in the current system.

*3) Faradaic-Charge-Induced Electrophoresis and Electroosmosis*

Upon Fc oxidation, a positively charged layer starts to emerge at the SAM/water interface. This instantaneously triggers an influx of anions toward the SAM-covered electrode, which in turn creates a region near the surface where surface cations (*i.e.* ferrocenium) and the incoming anions are separated in space. As the oxidative current continues to develop, this zone of charge imbalance expands further into the bulk, producing a double-layer that is considerably thicker than normal. The physical significance of this dipolar zone lies in that 1) it imposes a second electric field on top of the external electric field and 2) the electrostatic interactions between the two fields create a whole new series of electrokinetic flows in the system. To begin with, a

secondary electrophoretic motion arises because this bulk charge region directly modifies the charge distribution on the surface of colloidal particles dispersed within (Figure 3.9). Similarly, any tangential field component existing in the system can cause the incoming counter anions to slip at the SAM surface, i. e., electroosmotic flow (EOF), which in turn triggers circulating fluid movement capable of carrying the suspended colloids toward the electrode surface (Figure 3.9).

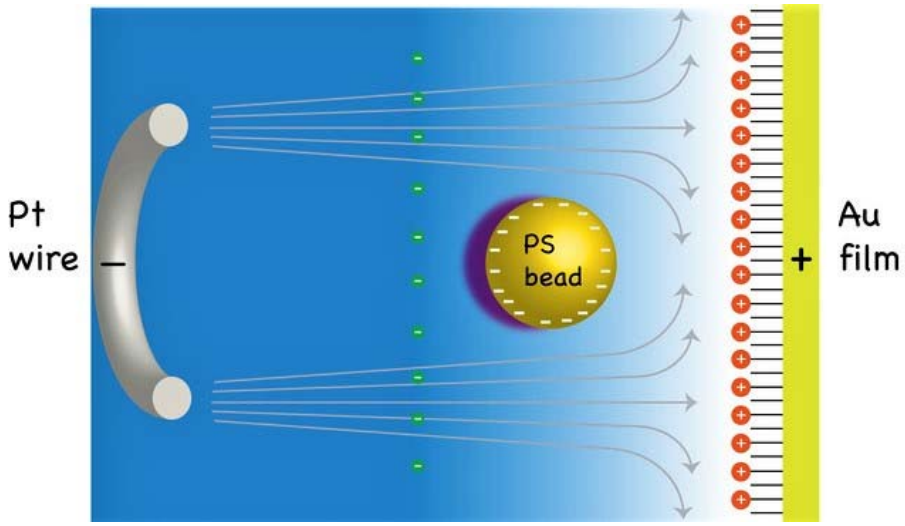


**Figure 3. 9** Schematic illustration of some key mechanistic features of the electrochemically triggered deposition. Following Figure 3.1a (with 90° rotation), the primary electric field is established between Au film W.E. and Pt wire C.E. Upon Fc-SAM oxidation, a secondary field also develops between the $Fc^{+}$ layer (orange circles with embedded plus signs) and the front of the counterion influx (green circles with embedded minus signs). Colloidal particles (one shown in gold) situated within this zone are subjected to the influence of both fields, whose interactions generate secondary electrokinetic flows. The drop shadow in purple depicts the distorted diffuse layer of the bead particularly caused by the local secondary electric field; arrowed lines in gray are idealized streamlines of the flow pattern.

According to the existing theoretical models on induced charge electroosmosis[15,16] as well as the 'electrokinetic phenomena of the second kind',[31,32] the velocity (u) of such induced electrokinetic flows generally takes the nonlinear Smoluchowski form, $u \propto \varepsilon_o \varepsilon E E_i a/\eta$, where E and $E_i$ are the primary and induced electric field components, respectively, and a the particle radius. In comparison to the linear Smoluchowski formula,[30] here $E_i$ appears in place of $\zeta$, whereas the new term, a, marks the size-dependent nature of such flows. Of the former, it is precisely because $E_i$ can be substantially larger than $\zeta$ that these secondary electrokinetic flows sometimes exceed the classical motions in velocity by several orders of magnitude.[31,32] On the other hand, it is tempting to attribute the observed clustering of large microbeads (2 μm and 5 μm, Figure 3.8) to the size dependence predicted of these nonlinear induced electrokinetic flows. Their low surface coverage, on the other hand, is likely due to a combination of the following two factors: their lower starting concentrations (Table 3.1) and slower diffusion. The latter process scales with 1/a and is expected to pose a more severe mass-transfer limit on these larger beads once they are depleted near the electrode by the secondary electrokinetic flows. This attribution is also in line with the different impacts on the colloidal deposition observed between $ClO^{4-}$ and $Cl^-$ (Figure 3.6): due to its strong ion-pairing with $Fc^+$, $ClO^{4-}$ does not effectively sustain EOF. Without EOF carrying the microbeads toward the electrode, accordingly, the resulting deposition is greatly suppressed.

Extrapolating from the observations above, we can see easily the likely importance of many other factors associated with the Faradaic processes, such as type/kinetics of the involved electrochemical reaction(s), in the colloidal deposition. For instance, although gold oxidation itself is sufficient to trigger deposition on bare Au electrodes (Figure 3.2a), it is sluggish and does not produce nearly as much charge as the competing reaction, $Fc - e^- = Fc+$. These enable

the latter reaction to sustain secondary electrokinetic flows much more strongly, which in turn lead to faster colloid deposition (Figure 3.4) and a complete dominance over the gold oxidation based process (Figure 3.5).

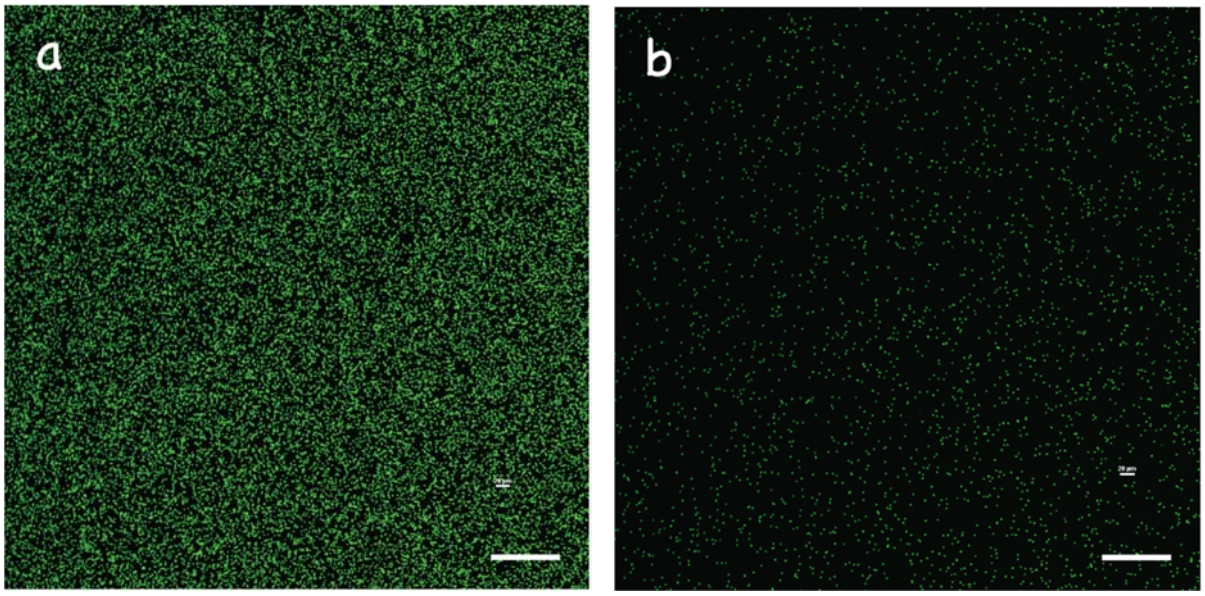


**Figure 3. 10** Removal of deposited microbeads by thiol desorption. a) Fluorescence image of 0.5- μm PS-COOH beads deposited on 1:1 Fc-C11SH/C12SH by a single LSV from 0.1 to 0.8 V vs. Ag/AgCl at 10 mV/s. b) Fluorescence image of the deposit shown in a) after 5 consecutive cyclic voltammetry scans in DI water from 0 to – 2 V vs. Ag/AgCl at 0.1 V/s. Scale bar: 100 μm.

*4) The Actual Deposition and Post-deposition Stability*

Another conclusion we may draw from the discussion so far is that Faradaic reactions can accelerate the arrival of colloidal particles at the electrode. Mechanically, this fast motion may lead to a 'hard landing' scenario, in which the momentum due to colloid stoppage at the surface may afford the particle a closer contact with the SAM and hence more intimate electrostatic and van der Waal interactions than otherwise possible. Of course, with the colloid's fixed surface charge releasing small ions and water into the bulk, the deposition process also leads to an

entropy gain of the system. These considerations help explain the observation of irreversible surface adhesion of microbeads following electrochemically triggered deposition. For example, the deposited beads can withstand typical washing steps well and do not come off the electrode until we electrochemically desorb the SAM underneath at -2.0 V vs. Ag/AgCl (Figure 3.10). By contrast, colloidal formations driven by electrophoretic deposition are often reversible assemblies.[7] Once the electric field is switched off, a random distribution of the colloidal particles often resumes as a result of Brownian motion; alternatively, the initially deposited colloids can be lifted off from the electrode by reversing the field polarity.

### 3.3.9. Electrochemically Triggered Colloid Micropattern Formation on Electrodes: An Application

Taking advantage of the superior efficiency of the electrochemically triggered assembly compared to the electrically driven process, we conclude this investigation with a demonstration of fast, high-fidelity colloid micropattern formation on electrodes. Shown in Figure 3.11a is a ~200×300 μm portrait of Einstein formed by 60 nm fluorescent PS-COOH beads electrochemically assembled on a Au film electrode. Fine lines down to just a few microns are satisfactorily resolved. Obtained under similar conditions, a cartoon rendering of the historical 'Moon Landing' with similar resolution is also shown in Figure 3.11b. Separately, we also attempted similar patterning/assembly using C12SH alone as the ink followed by electrical deposition, which fails to produce any recognizable microbead patterns on the electrode (not shown). This negative control once again illustrates the critical role played by Fc in achieving successful micropattern formation. Using better-resolved stamps and colloids of smaller size, it should be possible construct still finer features in a similar fashion.

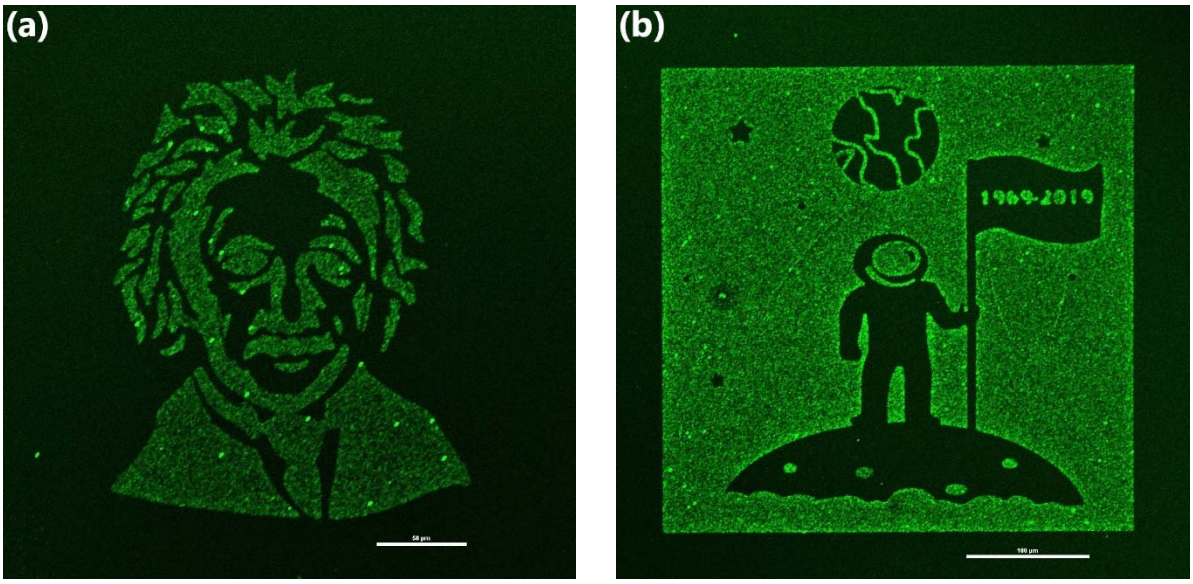


**Figure 3. 11** (a) Head portrait of Einstein (b) cartoon rendering of the historical 'Moon Landing', formed by 0.06 μm green-fluorescent PSCOOH beads assembled on a gold film electrode using our electrochemically triggered approach. Prior to the assembly step, the portrait patterns were first microcontact-printed onto the gold electrode in form of 1:1 Fc-C11SH/ C12SH mixed SAMs via a silicone rubber stamp. A linear potential sweep from 0.1 to 0.8 V was then applied at 10 mV/s; scale bar: 50 μm (a) and 100 μm (b).

### 3.4 Conclusion

Above we have presented a new electrochemical method for efficient and straightforward deposition/assembly of aqueous suspended colloids on electrode surfaces. Using carboxylic terminated polystyrene nano-/microbeads as a model colloid, we characterized this electrochemically triggered process in detail; by comparing its performance with conventional, electrically driven processes, we demonstrated superior deposition efficiency achievable with this new method. A qualitative discussion of the involved deposition mechanisms is also given, featuring secondary, induced electrokinetic flows carrying the microbeads toward the electrode

surface. To showcase the potential utility of this method, we also demonstrated fast and high-fidelity colloid micropattern formation on electrodes.

The approach described here offers several exciting new possibilities. Fundamentally, adding well-defined faradaic reactions into the deposition process offers a new and largely independent mechanism to induce secondary electric field components. With their great design flexibility, SAMs brings a new dimension into controlling/tuning various physicochemical parameters involved the deposition process. Through control of Fc density in the SAMs, for instance, one can easily access a range of surface potentials following the same preparation procedure. Since all redox-active materials are surface-bound, importantly, such gains in control and efficiency are achieved without complicating/compromising the solution phase. On the other hand, the low-voltage and fast operation characteristic of this approach should make it an appealing alternative for applications involving colloidal assemblies.[7,8,9] Auxiliary techniques amenable to the SAM formation, such as microcontact printing we employed here, will certainly extend the level of control and sophistication of these practices further. Work is ongoing in our laboratory to explore some of these possibilities.

**References**


(1) Abbott, N. L.; Whitesides, G. M. Potential-Dependent Wetting of Aqueous Solutions on Self-Assembled Monolayers Formed from 15-(Ferrocenylcarbonyl)Pentadecanethiol on Gold. *Langmuir* **1994**, *10* (5), 1493–1497. https://doi.org/10.1021/la00017a029.

(2) Whittell, G. R.; Manners, I. Metallopolymers: New Multifunctional Materials. *Adv. Mater.* **2007**, *19* (21), 3439–3468. https://doi.org/10.1002/adma.200702876.

(3) Gallei, M.; Rüttiger, C. Recent Trends in Metallopolymer Design: Redox-Controlled

Surfaces, Porous Membranes, and Switchable Optical Materials Using Ferrocene-Containing Polymers. *Chem. - A Eur. J.* **2018**, *24* (40), 10006–10021. https://doi.org/10.1002/chem.201800412.

(4) Giersig, M.; Mulvaney, P. Preparation of Ordered Colloid Monolayers by Electrophoretic Deposition. *Langmuir* **1993**, *9* (12), 3408–3413. https://doi.org/10.1021/la00036a014.

(5) Trau, M.; Saville, D. A.; Aksay, I. A. Field-Induced Layering of Colloidal Crystals. *Science (80-. ).* **1996**, *272* (5262), 706 LP – 709. https://doi.org/10.1126/science.272.5262.706.

(6) Seulst, M.; Shraimang, B. I. Assembly of Ordered Colloidal Aggregrates by Electric-Field Induced Fluid Flow. **1997**, *386* (March), 57–59.

(7) Prieve, D. C.; Sides, P. J.; Wirth, C. L. 2-D Assembly of Colloidal Particles on a Planar Electrode. *Curr. Opin. Colloid Interface Sci.* **2010**, *15* (3), 160–174. https://doi.org/10.1016/j.cocis.2010.01.005.

(8) Lu, Z.; Yin, Y. Colloidal Nanoparticle Clusters: Functional Materials by Design. *Chem. Soc. Rev.* **2012**, *41* (21), 6874–6887. https://doi.org/10.1039/c2cs35197h.

(9) Boles, M. A.; Engel, M.; Talapin, D. V. Self-Assembly of Colloidal Nanocrystals: From Intricate Structures to Functional Materials. *Chem. Rev.* **2016**, *116* (18), 11220–11289. https://doi.org/10.1021/acs.chemrev.6b00196.

(10) O'Brien, R. W.; White, L. R. Electrophoretic Mobility of a Spherical Colloidal Particle. *J. Chem. Soc. Faraday Trans. 2 Mol. Chem. Phys.* **1978**, *74*, 1607–1626. https://doi.org/10.1039/F29787401607.

(11) Anderson, J. Colloid Transport By Interfacial Forces. *Annu. Rev. Fluid Mech.* **1989**, *21* (1), 61–99. https://doi.org/10.1146/annurev.fluid.21.1.61.

(12) Solomentsev, Y.; Böhmer, M.; Anderson, J. L. Particle Clustering and Pattern Formation during Electrophoretic Deposition: A Hydrodynamic Model. *Langmuir* **1997**, *13* (23), 6058–6061. https://doi.org/10.1021/la970294a.

(13) Böhmer, M. In Situ Observation of 2-Dimensional Clustering during Electrophoretic Deposition. *Langmuir* **1996**, *12* (24), 1994–1997. https://doi.org/10.1021/la960183w.

(14) Trau, M.; Saville, D. A.; Aksay, I. A. Assembly of Colloidal Crystals at Electrode Interfaces. *Langmuir* **1997**, *13* (24), 6375–6381. https://doi.org/10.1021/la970568u.

(15) Squires, T. M.; Bazant, M. Z. Induced-Charge Electro-Osmosis. *J. Fluid Mech.* **2004**, *509* (509), 217–252. https://doi.org/10.1017/S0022112004009309.

(16) Bazant, M. Z.; Squires, T. M. Induced-Charge Electrokinetic Phenomena. *Curr. Opin. Colloid Interface Sci.* **2010**, *15* (3), 203–213. https://doi.org/10.1016/j.cocis.2010.01.003.

(17) Kershner, R. J.; Bullard, J. W.; Cima, M. J. The Role of Electrochemical Reactions during Electrophoretic Particle Deposition. *J. Colloid Interface Sci.* **2004**, *278* (1), 146–154. https://doi.org/10.1016/j.jcis.2004.05.017.

(18) Ristenpart, W. D.; Aksay, I. A.; Saville, D. A. Electrically Driven Flow near a Colloidal Particle Close to an Electrode with a Faradaic Current. *Langmuir* **2007**, *23* (7), 4071–4080. https://doi.org/10.1021/la062870l.

(19) Duval, J. F. L.; Huijs, G. K.; Threels, W. F.; Lyklema, J.; Van Leeuwen, H. P. Faradaic Depolarization in the Electrokinetics of the Metal-Electrolyte Solution Interface. *J. Colloid Interface Sci.* **2003**, *260* (1), 95–106. https://doi.org/10.1016/S0021-9797(02)00134-0.

(20) Iqbal, M. S.; Zhan, W. Electrochemically Triggered Surface Deposition of Polyelectrolytes. *Langmuir* **2018**, *34* (43), 12776–12786. https://doi.org/10.1021/acs.langmuir.8b02671.

(21) Jaksic, M. M.; Johansen, B.; Tunold, R. Electrochemical Behaviour of Iridium in Alkaline and Acidic Solutions of Heavy and Regular Water. *Int. J. Hydrogen Energy* **1994**, *19* (4), 321–335. https://doi.org/10.1016/0360-3199(94)90064-7.

(22) Xia, S. J.; Birss, V. I. A Multi-Technique Study of Compact and Hydrous Au Oxide Growth in 0.1 M Sulfuric Acid Solutions. *J. Electroanal. Chem.* **2001**, *500* (1–2), 562–573. https://doi.org/10.1016/S0022-0728(00)00415-0.

(23) Buttry, D. A.; Ward, M. D. Measurement of Interfaclal Processes at Electrode Surfaces with the Electrochemical Quartz Crystal Microbalance. *Chem. Rev.* **1992**, *92* (6), 1355–1379. https://doi.org/10.1021/cr00014a006.

(24) Kumar, A.; Biebuyck, H. A.; Whitesides, G. M. Patterning Self-Assembled Monolayers: Applications in Materials Science. *Langmuir* **1994**, *10* (5), 1498–1511. https://doi.org/10.1021/la00017a030.

(25) Rowe, G. K.; Creager, S. E. Interfacial Solvation and Double-Layer Effects on Redox Reactions in Organized Assemblies. *J. Phys. Chem.* **1994**, *98* (21), 5500–5507. https://doi.org/10.1021/j100072a017.

(26) Valincius, G.; Niaura, G.; Kazakevičiene, B.; Talaikyte, Z.; Kažemekaite, M.; Butkus, E.; Razumas, V. Anion Effect on Mediated Electron Transfer through Ferrocene-Terminated Self-Assembled Monolayers. *Langmuir* **2004**, *20* (16), 6631–6638. https://doi.org/10.1021/la0364800.

(27) *The Peak Potential, ~0.5 V vs. Ag/AgCl, Is Noticeably More Positive than the Values Typically Reported in Literature, e. g., 0.32 V in Our Earlier Report (Ref. 20), Which We Find Is Mostly Caused by the Different Electrode Configuration Employed in This W.*

(28) Pourbaix, M. J. N.; Van Muylder, J.; de Zoubov, N.; PROTECTION, C. Electrochemical Properties of the Platinum Metals. *Platin. Met. Rev.* **1959**, *3* (2), 47–53.

(29) Israelachvili, J. N. *Intermolecular and Surface Forces*, 3rd ed.; Elsevier Inc.: Amsterdam, The Netherlands, 2001.

(30) Hunter, R. J. *Zeta Potential in Colloid Science*; Academic Press Inc.: London, UK, 1981.

(31) Dukhin, S. S. Electrokinetic Phenomena of the Second Kind and Their Applications. *Adv. Colloid Interface Sci.* **1991**, *35* (C), 173–196. https://doi.org/10.1016/0001-8686(91)80022-C.

(32) Mishchuk, N. A.; Barany, S.; Tarovsky, A. A.; Madai, F. Superfast Electrophoresis of Electron-Type Conducting Particles. *Colloids Surfaces A Physicochem. Eng. Asp.* **1998**, *140* (1–3), 43–51. https://doi.org/10.1016/S0927-7757(97)00322-1

# CHAPTER 4. ELECTROCHEMICALLY TRIGGERED INTERFACIAL DEPOSITION OF NANOMATERIALS AND SOFT MATERIALS

## 4.1 Introduction

In previous two chapters, we have discussed about a general and facile electrochemical method for deposition/assembly of polyelectrolytes and aqueous suspended colloids. We have demonstrated in detail their deposition on electrode surfaces and some keys factors involving deposition processes. We have also discussed utilization of the newly developed method towards innovative applications using those materials. In this chapter, the utility of this new methodology is further extended to other types of materials such as metal and metal oxides nanoparticles, quantum dots, multi walled carbon nanotubes (MWCNTs), and soft materials such as liposomes. This should demonstrate the power and generality of this method for fabrication of surface with a different class of chemical entities with varying sizes and shapes using the same electroactive platform. Apart from that, using liposomes with well-defined surface charge, enabled us to demonstrate mechanistic differences utilizing this approach among deposition of materials with positive, negative and neutral surfaces respectively.

Modification of electrodes with nanomaterials[1,2], micromaterials[3] and biomaterials[4] are common practices, in an attempt to provide the electrode with new identity where numerous chemistries can be launched. One of the widely used strategies to deposit those materials on electrode is first modify the electrode surface with self-assembled monolayers (SAMs) of thiols which contain a functional group or redox species to its distal end, and then deposition of materials on SAMs surface. For example, many have used this strategy to deposit carbon nanotubes (CNTs) on electrode surface to allow the CNTs working as nanoelectrodes[5,6,7], and some demonstrated

deposition of metal nanoparticles on electrode for enhancement of electron transfer.[8,9] Moreover, assembly of the AuNPs-SAMs-gold substrate provides metal-metal junctions formed between nanoparticles and metal substrates where electron tunneling and nonlinear optical properties such as Raman scattering can occur.[10] Other attractive materials for photovoltaic applications are colloidal quantum dots (CQDs) upon adsorbed on SAMs; the resulting platforms are capable of providing proper band alignment at electrodes to confer efficient charge extraction.[11] Similarly, electrode surfaces modified with different materials have been employed in a wide range of applications including electroanalytical analysis[12], heterogeneous catalysis[12,13], corrosion protection[14], antireflective films[15], substrates for cell adhesion[16], bioelectronics[17,18], energy storage device, energy conversion[19], microelectronics[20], etc. Various types of materials are used for coating surfaces such as metal nanoparticles (Au, Ag, Pt, Cu)[9,21,22,23], metal oxides nanoparticles ($Fe_2O_3$, $SnO_2$)[24,25], fluorescent quantum dots (CdS, CdSe, ZnS)[26,27], polymeric (polystyrene)[28], carbon nanotubes[5,29], biomaterials (peptides, proteins, DNA, liposomes)[30,31], etc. However, deposition of nanomaterials in device structures requires precise control in size, their distribution on surface, and their ability to electronically connect them to microscopic structures. On the other hand, fabrication of biomaterials on surface often need to satisfy a more subtle set of requirements for life science applications.

In the majority of the existing works, deposition of different materials on SAMs are usually performed by simply soaking/incubating the SAMs surface in a solution or suspension of a desired material for hours.[7,8,32] This kind of depositions are often random and exhibit low stabilities on surface. Nano- and micro- particles can also be tethered onto surfaces by different chemical ligation methods[33,34], electrodeposition[35,36], sol-gel[37] techniques, etc. While we have already demonstrated the superiority of our electrochemical method[28] over conventional

electrodeposition, other methods generally require substrate-specific procedures. On the other hand, we have utilized well defined redox active SAMs to electrochemically deposit materials on surface which found to have higher stability compared to conventional methods.[28,30] Other than offering a well-defined surface with tunable surface properties (such as wetting, adhesion, corrosion resistance, etc.), redox active SAMs also offers utilization of redox species within the surface devoid of many complicating solution characteristics. Our method can be considered as a one-step electrofabrication of materials as the deposition can be achieved with a single liner voltammetric sweep within seconds. Distribution of particles/materials on surface can also be controlled with parameters such as scan rates, concentration, small ions, Fc-loading on SAMs, etc. This kind of platform is useful especially for biomaterials and soft materials deposition where materials need to retain their biological capabilities and functions after deposition. The redox active layer at the bottom of the deposited materials film also holds the potential to guide biological responses through electrical cues. We envision that this electrobiofabrication method will emerge as an important platform for organizing biomaterials and soft materials towards formation of dynamic material systems that are capable of mimicking complex biological structures and their versatile functionalities.

Here, we have shown the deposition of carboxyl functionalized gold nanoparticles, carboxyl functionalized iron-oxide ($Fe_3O_4$) nanoparticles, carboxyl functionalized multi-walled carbon nanotubes (MWCNTs), carboxyl functionalized CdSSe/ZnS based quantum dots, and charged liposomes on Fc-terminated alkanethiol SAMs on planner gold electrode. We employed atomic force microscope and confocal laser scanning microscope to characterize the electrode surface and deposited materials on them. In an attempt to demonstrate mechanistic differences among

the deposition of materials with positive, negative and neutral surfaces respectively, we have used liposomes with well-defined surface charges as our model material.

## 4.2 Experimental Details

### 4.2.1 Chemicals

11-Ferrocenyl-1-undecanethiol (Fc-C11SH), 1-dodecanethiol (C12SH), sodium perchlorate hydrate (99.99% trace metal basis), TWEEN 20 were products of Sigma- Aldrich (St. Louis, MO). Carboxyl functionalized gold nanoparticles (Au NPs) were obtained from NNCrystal US corp. (Fayetteville, AR). Carboxyl functionalized iron oxide ($Fe_3O_4$) nanoparticles, and carboxyl CdSSe/ZnS based quantum dots (QDs) were obtained from Ocean NanoTech (San Diego, CA). Carboxyl functionalized multi walled carbon nanotubes (MWCNT's) (>95%) were obtained from US Research Nanomaterials, Inc. (Houston, TX). 1-palmitoyl-2-oleoyl-glycero-3-phosphocholine (POPC), 1-palmitoyl-2-oleoyl-sn-glycero-3-phospho-(1'-rac-glycerol) (sodium salt) (POPG), 1,2-dioleoyl-3-trimethylammonium-propane (chloride salt) (DOTAP), 23-(dipyrromethene boron difluoride)-24-norcholesterol (Bodipy-Cholesterol) were obtained from Avanti Polar Lipids (Alabaster, Alabama). Deionized water of 18.2 MΩ·cm (Millipore) was used in preparing all aqueous colloid suspensions as well as in all rinsing and dilution steps.

### 4.2.2 Formation of Self-Assembled Monolayers

Self-assembled monolayers (SAMs) containing Fc-C11SH/C12SH binary mixtures formed on semi-transparent gold-coated microscope slides (Au thickness: 10 nm, Sigma-Aldrich) were used throughout this work. These SAMs were prepared in two fashions as follows:

*1) Solution Incubation*

Prior to the SAM formation, gold-coated substrates were immersed in a piranha solution (3 :1 v/v mixture of concentrated $H_2SO_4$ and $H_2O_2$ 30 wt% aqueous solution) for 3 min, thoroughly rinsed with deionized water, ethanol, and then dried under $N_2$. Thus cleaned dry substrates were immediately immersed in an ethanol solution containing 0.5 mM Fc-C11SH and C12SH each; the incubation was allowed to proceed for 16–18 h in the dark. Upon completion, the substrates were rinsed first with methanol to remove excess thiols on surface, then DI water, and finally dried under $N_2$. These SAM covered gold slides were normally used within the same day of their preparation.

*2) Microcontact Printing*

Silicone rubber stamps, containing either circular pillar arrays or custom micropatterns, were obtained from Research Micro Stamps (Clemson, SC). Of the latter, hand-drawn features were first converted to digital files with a digital camera and shrunk to desired sizes in Adobe Illustrator (version: CS6); the resulting miniaturized patterns were saved in .svg format and subsequently passed to the manufacturer for stamp production. Before use, the stamps were first cleaned by sonicating in ethanol for 5 min, and gently dried under a stream of $N_2$. To ink, thus cleaned stamps were soaked in an ethanol solution of 0.5 mM Fc-C11SH and C12SH each for 10 min and then gently dried under $N_2$. Immediately afterwards, these inked stamps were placed conformally onto precleaned gold coated glass slides; the printing was allowed to proceed for 10 min, during which a small weight block was placed on top of the stamp to ensure a gentle and even press. Upon completion, the stamps were removed, and the substrates were thoroughly rinsed with methanol, then DI water, and dried under $N_2$. These SAM-patterned gold slides were normally used within the same day of their preparation.

### 4.2.3 Electrochemical Treatments

Linear sweep voltammetry (LSV) operated by a PC-controlled potentiostat (CHI 910B, CH Instruments, Austin, TX) was used in this work to initiate colloidal deposition and assembly on electrodes. A three-electrode setup was used throughout this work, consisting SAM-covered gold substrates as the working electrode, a platinum wire (diameter: 1 mm) as the counter electrode and Ag/AgCl in saturated KCl solution as the reference electrode, housed in homemade Teflon cells. To initiate the deposition, a given SAM was typically biased with an LSV scan in an intended colloid materials suspension in aqueous solution. Particle/materials sizes, concentration and other specifications are provided in Table 1. After LSV scan, the initial suspension was thoroughly exchanged out with deionized water. The gold electrode thus treated was taken out and dried under a gentle stream of ultrapure $N_2$ in all cases except for liposomes in which case the gold electrode left immersed under water after deposition and exchange throughout the characterization process. Deposits can also be formed from colloids suspended in DI water without adding TWEEN 20 but with a slightly inferior reproducibility.

### 4.2.4 Preparation of Liposomes

The preparation of small unilamellar vesicles (SUVs) was carried out using an extrusion based method.[38] To start, appropriate quantities of lipids dissolved in chloroform were combined into a 50 mL round-bottom flask and thoroughly dried by rotary evaporation. The resulting thin lipid film on the flask wall was then rehydrated with deionized water by 1 h sonication at room temperature (25 °C) since transition temperatures for all lipids used are under the room temperature. Such lipid suspensions were then extruded consecutively through polycarbonate membranes with 800 and 200 nm pores (Nuclepore, Whatman). The final concentration of the

as-prepared liposomes is typically ~4.0 mM while the suspension was diluted to working concentration for electrochemically triggered deposition was ~1 mM.

### 4.2.5 Zeta Potential Measurements

Zeta potential values of liposomes suspended in deionized water were obtained from a Malvern Zetasizer (Nano-ZS90, Malvern Instruments, Worcestershire, UK) using capillary cells (DTS1060/DTS1061) operated under a 150 V bias at 25°C. The measurements were made on diluted samples of freshly prepared liposomes with a total lipid concentration of ~1 mM. Typically five parallel readings were taken for each sample.

### 4.2.6 Fluorescence Microscopy

Fluorescence images were acquired on a Nikon A1+/MP confocal scanning laser microscope (Nikon Instruments, Inc., Melville, NY) with 4x and 10x objectives. Laser beams at 488 and 561 nm were used to excite blue quantum dots and green fluorescent tagged liposomes deposited on semi-transparent gold-coated glass slides, and the corresponding emission signals were filtered at 450 ± 25 and 525 ± 25 nm, respectively.

### 4.2.7 Atomic Force Microscopy (AFM)

AFM characterization of materials-modified SAMs was carried out using a Bruker MultiMode 8 atomic force microscope (Bruker, USA) in air and at room temperature. Silicon nitride probes (Model: ScanAsyst AIR, Bruker) used in these measurements have a force constant of 0.4 N/m, a resonant frequency of 70 kHz, and a nominal tip radius of 2 nm and are operated in Scanasyst Air mode with a scan rate of 1 Hz and a resolution of 512 × 512 pixels. The substrates used are semitransparent gold-coated microscope slides, on which ferrocene SAMs were first formed as described above. For deposition of carboxyl functionalized materials, these SAMs were then

subjected to a linear potential sweep from 0.1 to 0.8 V vs Ag/AgCl at 10 mV/s in the following aqueous solutions: $2.61 \times 10^{10}$ particles/mL of carboxyl functionalized gold nanoparticles, 10.0 nM carboxyl functionalized iron oxide ($Fe_3O_4$) nanoparticles, and 0.015 wt% of carboxyl functionalized multi walled carbon nanotubes (MWCNT's) respectively. Thus, treated SAMs were thoroughly rinsed with deionized water and then dried under $N_2$ before AFM scanning. Right before probing the mixed Fc-SAMs with carboxyl functionalized multi walled carbon nanotubes (MWCNT's) suspension, 0.015 wt% aqueous suspension was centrifuged at 10,000 rpm for 5 minutes. Then the resulting supernatant suspension was used for probing or deposition purpose.

### 4.3 Results and Discussion

**Table 4. 1** Carboxyl functionalized nanoparticles (NPs) or nanomaterials, their size and working concentration/ particle counts in aqueous suspension employed in this study.

| **Nanomaterials** | **Size (nm)[a]** | **Concentration[b]** |
|---|---|---|
| Au NPs | 20 | $2.61 \times 10^{10}$ |
| $Fe_3O_4$ NPs | 25 | 10.0 nM |
| MWCNTs | 15 ± 5 | 0.015 wt% |
| CdSeS/ZnS based QDs | 13 ± 1 | 25.0 µM |

[a] According to manufacturer's data. Given is the outside diameter of MWCNTs while the length is 20 ± 10 µm, and QDs hydrodynamic size while inorganic core size is ~ 4 nm. [b] Particle count of Au NPs per mL of samples.

### 4.3.1 Atomic Force Microscopy (AFM) Characterization

We have carried out AFM measurement to characterize the deposited carboxyl functionalized gold nanoparticles, carboxyl functionalized iron oxide ($Fe_3O_4$) nanoparticles, carboxyl functionalized multi walled carbon nanotubes (MWCNTs), and thus resulted surface.

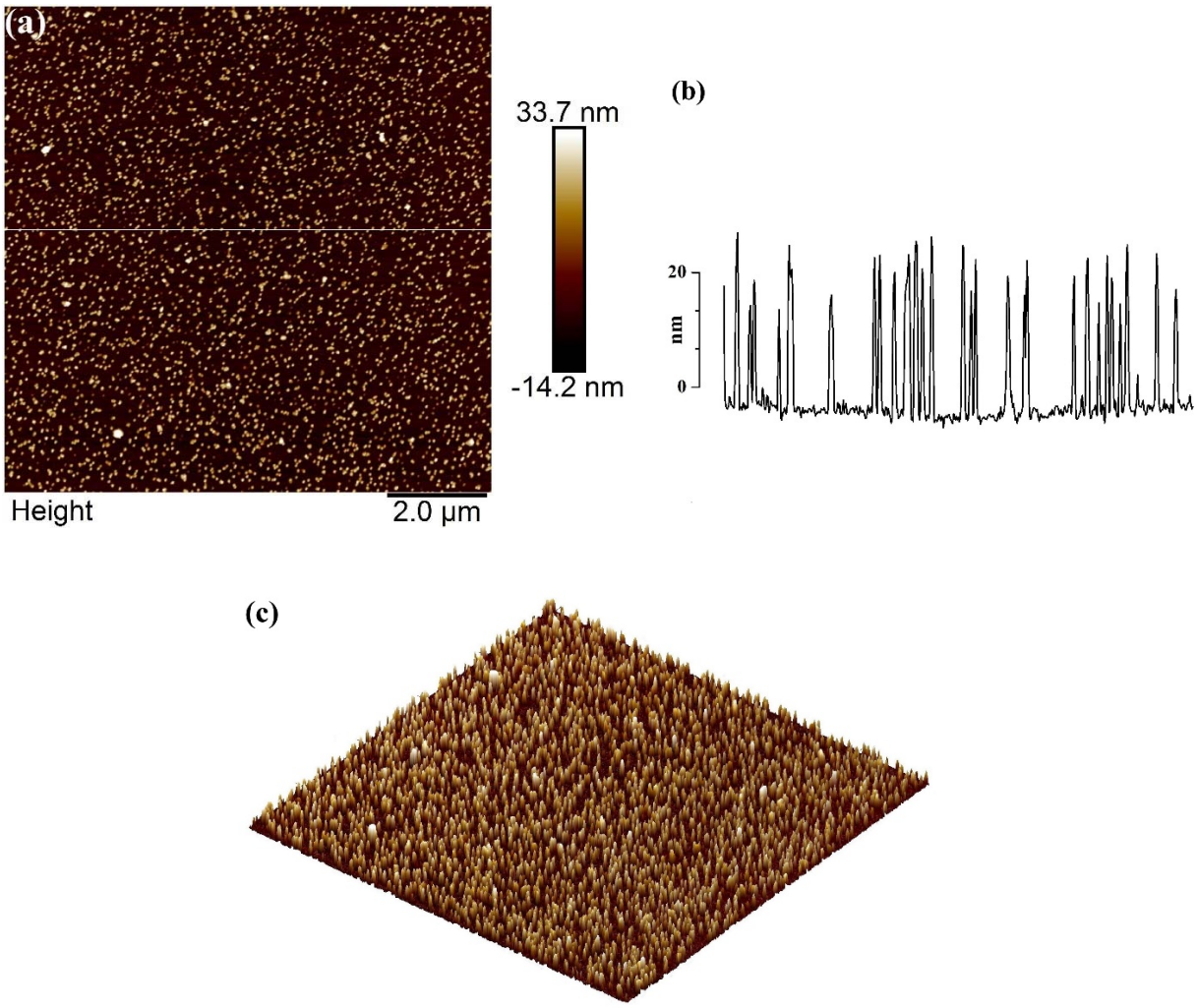


**Figure 4. 1** AFM characterization of carboxyl functionalized gold nanoparticles. (a) Topography image of resulted surface after deposition of carboxyl functionalized gold nanoparticles on mixed Fc-SAMs. (b) Height vs distance profile of the selected section (white line) in the image. (c) 3D image of the surface presented in (a).

In all cases, it also enabled us to gain some detailed information about the surface morphology upon materials deposition on surface. Images obtained with AFM for the deposition of these materials and thus obtained surfaces are shown in Figure 4.1- 4.3 respectively.

#### 4.3.1.1 Carboxyl functionalized gold nanoparticles (Au NPs)

Figure 4.1(a) represents the surface resulted from the deposition of carboxyl functionalized gold nanoparticles (Au NPs) on mixed Fc-SAMs (1:1 Fc-C11SH/C12SH) on gold. From 4.1(a), AFM image with a scan size of 10 × 10 μm, it can be said that the deposition of gold nanoparticles occurs almost homogeneously across the surface as AuNPs are found relatively evenly distributed. From this image, it is evident that Au NPs aggregates mostly in 2D clusters from two to several nanoparticles clustered together while there is some single particle deposition. There are also a few large clusters with minimal z-overlapping. Figure 4.1(b) represents height distance profile which supports the visual observation in Figure 4.1(a) while Figure 4.1(c) is the 3D image of the surface. These observations are also is agreement with Calvo & co-worker where they demonstrated electrostatic adsorption of negatively charged gold nanoparticles (-COOH functionalized) on $NH_2$- terminated SAMs surface.[9]

#### 4.3.1.2 Carboxyl Functionalized iron oxide ($Fe_3O_4$) nanoparticles

Figure 4.2(a) depicted resulted surface after deposition of carboxyl functionalized iron oxide ($Fe_3O_4$) nanoparticles on mixed Fc-SAMs. It is evident from Figure 4.2(a) that, deposited $Fe_3O_4$ NPs are distributed relatively even across the mixed Fc-SAMs surface. It is observable that $Fe_3O_4$ NPs aggregates mostly in 2D clusters from two to several nanoparticles clustered together. There is also some single particle deposition while very few large clusters with minimal z-overlapping can be spotted. $Fe_3O_4$ NPs are more densely populated in comparison to Au NPs in

Figure 4.1(a). Figure 4.2(b) represents height distance profile which supports the visual observation in Figure 4.1(a) while Figure 4.2(c) is the 3D image of the surface.

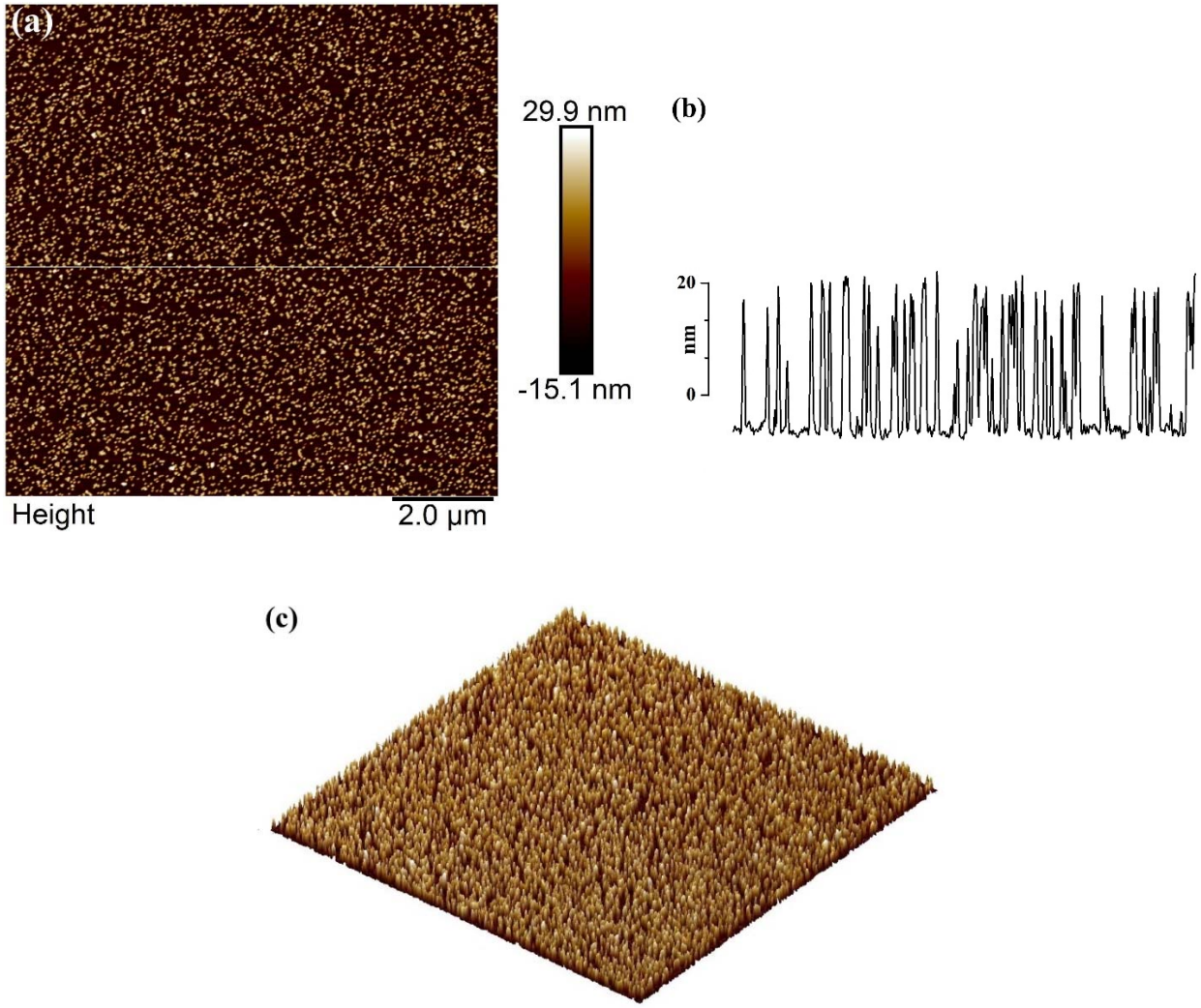


**Figure 4. 2** AFM characterization of carboxyl functionalized iron oxide ($Fe_3O_4$) nanoparticles. (a) Topography image of resulted surface after deposition of carboxyl functionalized iron oxide nanoparticles on mixed Fc-SAMs. (b) Height vs distance profile of the selected section (white line) in the image. (c) 3D image of the surface presented in (a).

These results are found in agreement with the observation by Pichon & co-workers who reported carboxyl functionalized $Fe_3O_4$ NPs deposition on thiol SAMs on gold through incubation of

SAMs in THF suspended $Fe_3O_4$ NPs.[39] Other groups also reported similar observations in case of distribution of NPs across the surface.[40]

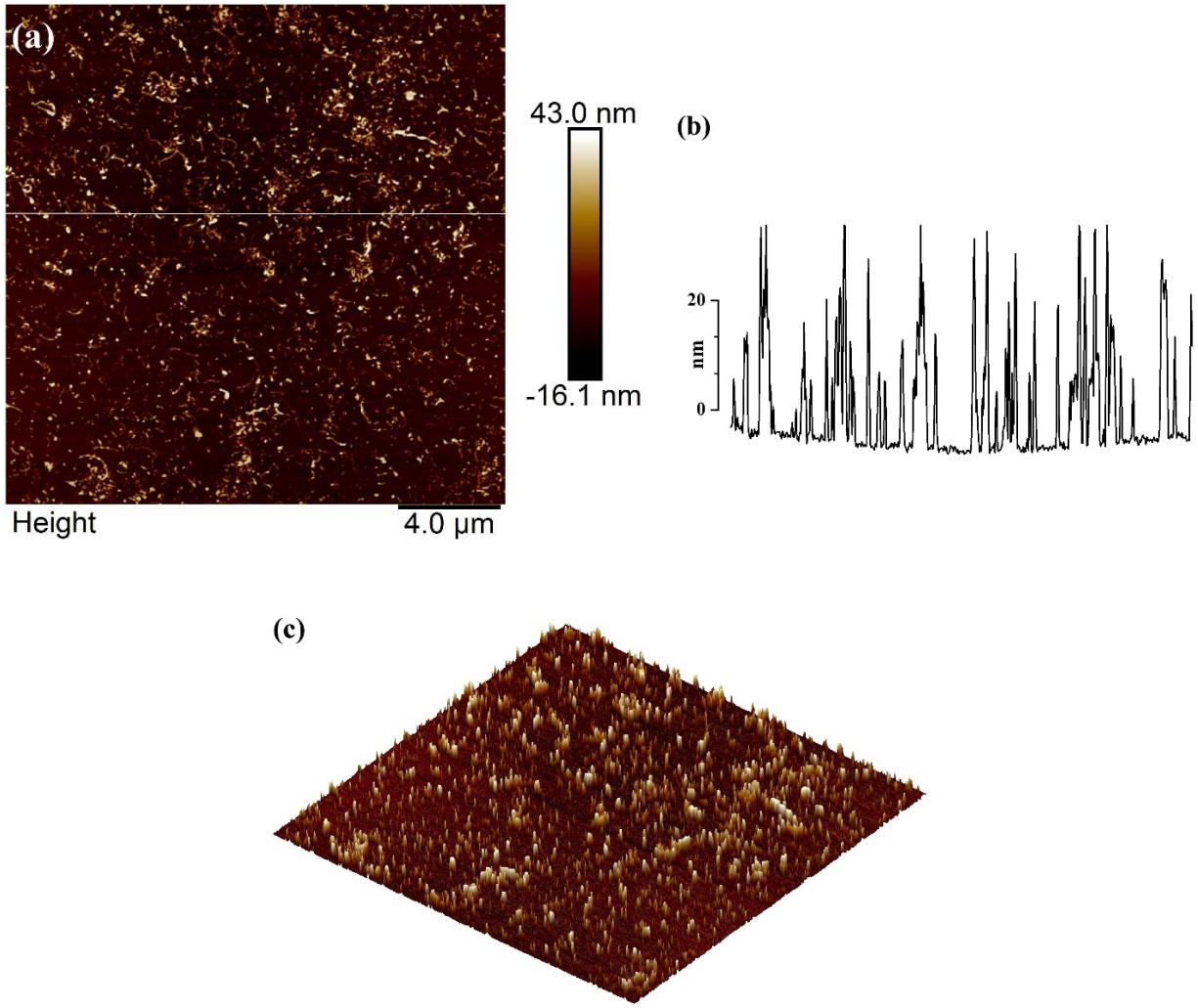


**Figure 4. 3** AFM characterization of carboxyl functionalized multi walled carbon nanotubes (MWCNTs). (a) Topography image of resulted surface after deposition of carboxyl functionalized multi walled carbon nanotubes (MWCNTs) on mixed Fc-SAMs. (b) Height vs distance profile of the selected section (white line) in the image. (c) 3D image of the surface presented in (a).

#### 4.3.1.3 Carboxyl Functionalized Multi Walled Carbon Nanotubes (MWCNT's)

Figure 4.3(a) portrayed resulted surface after deposition of carboxyl functionalized multi walled carbon nanotubes (MWCNTs) on mixed Fc-SAMs surface. From the image, it can be said that MWCNTs aren't evenly distributed across the surface rather they are found in 2D clusters mostly in various sizes. This cluster formation could be due to the presence of charge across the CNT's outer wall, and while in solution they would form conformation with minimal interaction between those functional groups containing charges. It is not clear though whether these structures are formed due to some kinds of rearrangement while CNTs are on the surface upon responding to Fc-oxidation i.e. electrochemical trigger. By analyzing height distance profile in Figure 4.3(b), it is evident though CNTs are distributed as 1D and 2D structures across the surface with an outer diameter ranging ~10-40 nm while according to manufacturer data the outer diameter of these MWCNTs are 15 ± 5 μm which are in agreement with our observation. The 3D image in Figure 4.3(c) is suggesting that, the CNTs deposited are a combination of single and cluster structures across the surface while validating previous observations. Deposition of CNTs on SAMs reported are almost exclusively through covalent coupling between -COOH functional group within CNTs and -$NH_2$ terminal of the thiol SAMs.[5,41,42] Our deposition method can provide an alternative and easier way to deposit CNTs on SAMs surface. Further investigations are necessary to explore the nature of the deposition, deposited CNTs, and their properties.

### 4.3.2. Fluorescence Microscopy Characterization

We then decided to test our electrochemical method with two more interesting materials- colloidal quantum dots, and liposomes. While quantum dots are fluorescent, liposomes during preparation can easily be labeled with fluorescent tagged lipids. While liposomes are very

interesting soft material and widely used in different applications, the charge on the surface can also be easily controlled and varied by using charged lipids in various compositions. Moreover, confocal microscopy is convenient and time efficient, we believed these materials on surface can be studied thoroughly in quick time using confocal laser scanning fluorescence microscope.

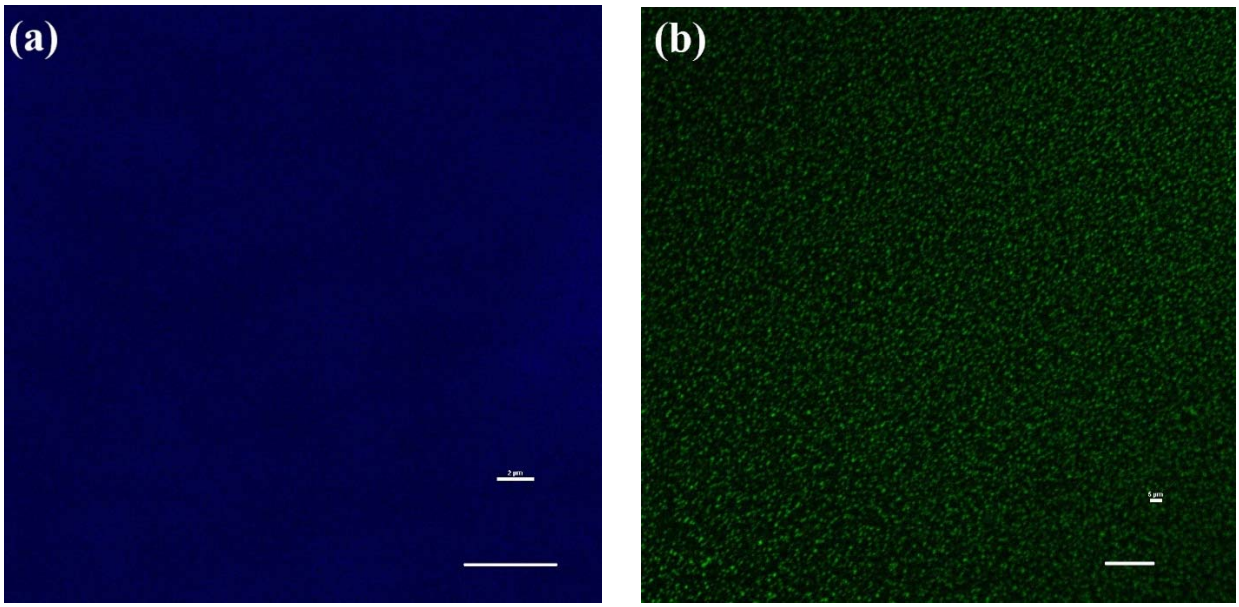


**Figure 4. 4** Fluorescence images of electrochemically triggered deposition of (a) carboxyl functionalized CdSSe/ZnS based quantum dots and (b) negatively charged liposomes (POPC/POPG/Bodipy-Chol 89:10:1 ratio) on mixed Fc-SAMs. The scale bars correspond to (a) 5 μm, and (b) 20 μm.

#### 4.3.2.1 Carboxyl Functionalized CdSSe/ZnS based colloidal quantum dots

Figure 4.4(a) depicting the surface resulting from deposition of carboxyl functionalized CdSSe/ZnS based colloidal quantum dots on mixed SAMs surface. Due to their tiny sizes (13 ± 1 nm; hydrodynamic size including the outer functionalized layer), quantum dots are not individually resolved by confocal microscope used. However, their deposition across the surface is evident, and in good agreement with observation made by Karim and co-workers who

investigated the deposition of CdSe/ZnS core-shell quantum dots on -$NH_2$ functionalized thiol SAMs surface.[27] This confirms the effectiveness of our method for deposition of quantum dots. Again, further investigations are required to fully characterize and reveal the properties of the resulted surface.

#### 4.3.2.2 Liposomes

To begin with we choose a ternary system, POPC/POPG/Bodipy-Cholesterol as our model liposome. We combined POPC (with no charge) with anionic lipid POPG to obtain liposome containing negative charges while Bodipy-Cholesterol was introduced as fluorescent labeled lipid for easy characterization under fluorescence microscope. Figure 4.4(b) represents the resulting surface obtained while mixed Fc-SAMs were probed with 1.0 mM suspension of POPC/POPG/Bodipy-cholesterol (89:10:01) liposomes in water, and usual LSV treatment. Liposome depositions are evident with mostly individual liposomes (~200 nm) depositions while brighter spot might indicate towards multidirectional depositions. This kind of deposition on SAMs surface are novel to the best of our knowledge. Drop coating deposition of liposome suspension on surfaces were reported by Procházka and co-workers where they demonstrated deposition of liposomes on solid surface upon evaporation of a drop of biomolecular solution on substrate surface.[31] In our case, the deposition was monitored while the surface was still covered with deionized water to help keeping the liposome structure intact on surface if there is so. Although further characterization is necessary to characterize the true structure of the deposited liposomes on surface and thus resulted surface, it is encouraging to see sustained deposition of those liposome on surface. This will provide us with an opportunity to explore the deposition of different charged system (negative, positive and neutral) utilizing our electrochemical method while controlling the charge on materials effectively and quantitatively. In an effort to do so, we

constructed two more liposome system along with our previous one, POPC/POPG/Bodipy-Cholesterol. Structures of all lipids used in this study is given in Table 4.2. All the liposome systems and their corresponding zeta potential values are given in Table 4.3. In all cases, working concentration of liposome used was ~ 1.0 mM.

**Table 4. 2** Lipids used in this study and their structures.

| Lipids | Structure |
|---|---|
| 1-palmitoyl-2-oleoyl-glycero-3-phosphocholine (**POPC**) | 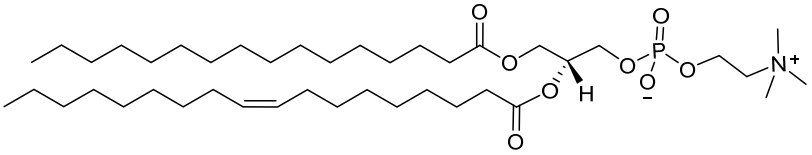 |
| 1-palmitoyl-2-oleoyl-sn-glycero-3-phospho-(1'-rac-glycerol) (sodium salt) (**POPG**) | 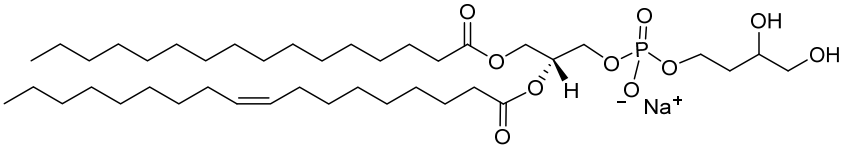 |
| 1,2-dioleoyl-3-trimethylammonium-propane (chloride salt) (**DOTAP**) | 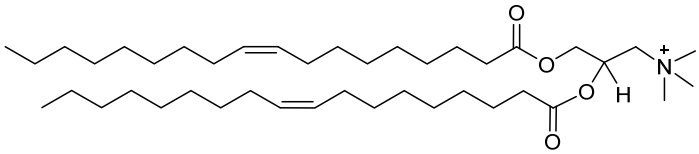 |
| 23-(dipyrromethene boron difluoride)-24-norcholesterol (**Bodipy-Cholesterol**) | 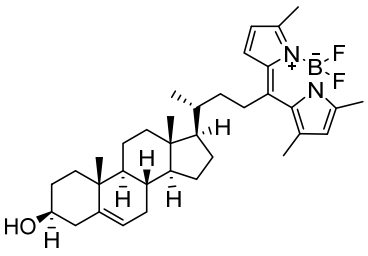 |

Figure 4.5 (a) represents the resulted surfaces after deposition of POPC/POPG/Bodipy-cholesterol (89:10:01) liposomes on mixed Fc-SAMs (a-top), and on patterned mixed Fc-SAMs on gold (a-bottom). We have already discussed about deposition on surface fully covered with mixed Fc-SAMs. For surface patterned with mixed SAMs on gold, it is notable that deposition of

liposomes occurred preferably on the round patches where the mixed Fc-SAMs are situated. This observation is consistent with liposomes zeta potential value of -31.8 ± 1.8 mV, indicating primary interaction between the liposomes and the electrode surface is electrostatic in nature. In contrast, the areas with bare gold surface is very fade in color indicating some sort of physical deposition might have occurred or it could be due to the presence of some fused lipids from liposome core on to gold the surface. But these probabilities are yet to be confirmed. As observed, these deposits are minor to negligible compared to the deposition on Fc-SAMs patches. Further investigation is required at this point to draw any definitive conclusion.

**Table 4. 3** Zeta potential of different liposomes systems in aqueous suspensions.

| **Lipid composition in liposomes** | **Zeta potential (mV)** |
|---|---|
| POPC/POPG/Bodipy-cholesterol (89:10:01) | - 31.8 ± 1.8 |
| POPC/Bodipy-cholesterol (99:01) | - 1.06 ± 1.12 |
| POPC/DOTAP/Bodipy-cholesterol (89:10:01) | 54.6 ± 2.6 |

Standard deviation, n = 5.

In Figure 4.5 (b), resulted surfaces after deposition of POPC/Bodipy-cholesterol (99:01) liposomes on mixed Fc-SAMs (b-top), and on patterned mixed Fc-SAMs on gold (b-bottom) are depicted. In case of surface fully covered with mixed Fc-SAMs, it has been noted that the deposition is much more uniform across the surface compared to the ternary system POPC/POPG/Bodipy-cholesterol. Again, in patterned Fc-SAMs deposition is found to be exclusive compared to bare gold surface. There are only a very few liposome depositions occurred across bare gold surface as observed, and those seems to be individual liposomes. As this binary liposome POPC/Bodipy-cholesterol are reasonably neutral with zeta potential of -1.06

± 1.12 mV, their response to Fc-oxidation and preferential deposition on Fc-SAMs are quite surprising.

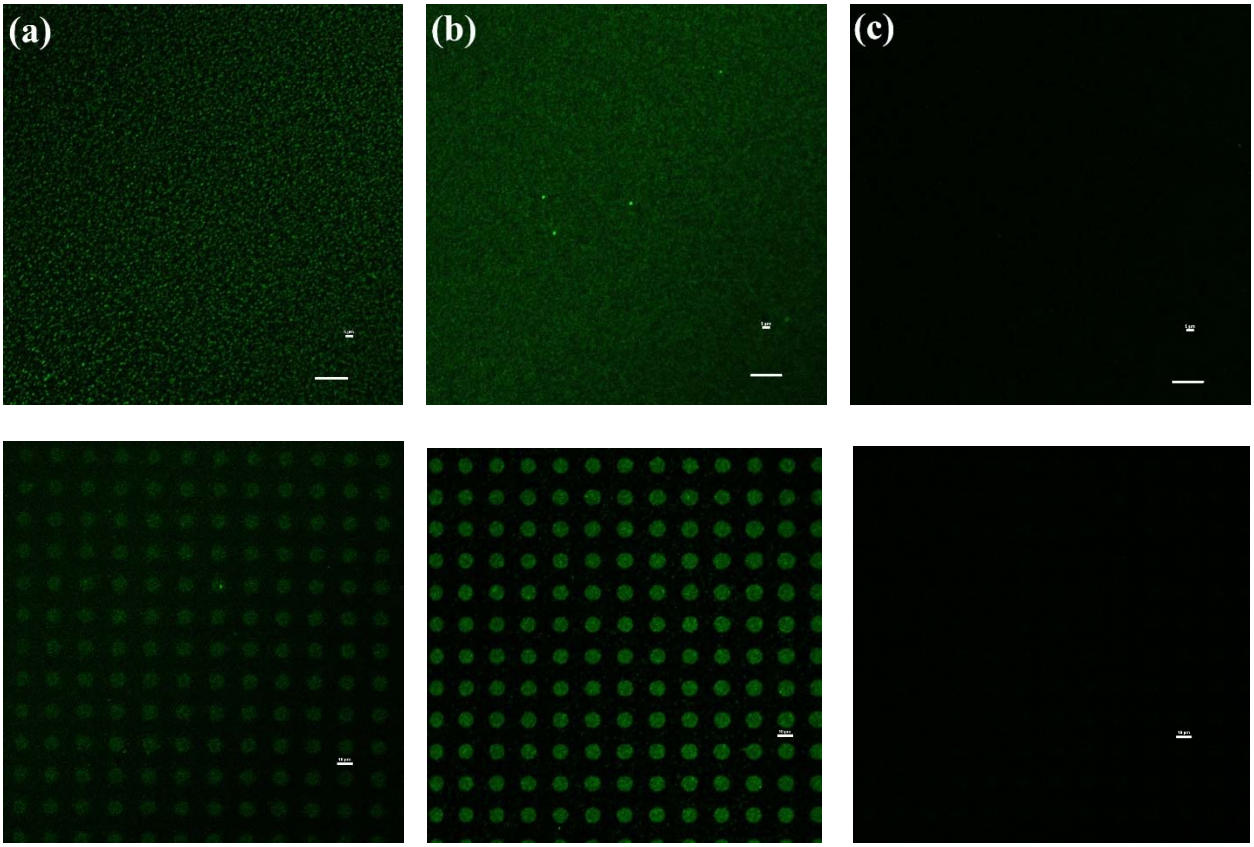


**Figure 4. 5** Fluorescence images of electrochemically triggered deposition of (a) POPC/POPG/Bodipy-Chol (89:10:01), (b) POPC/Bodipy-Chol (99:01), and (c) POPC/DOTAP/Bodipy-Chol (89:10:01) ratio on mixed Fc-SAMs (upper row) and patterned mixed Fc-SAMs co-existed with bare gold (bottom row).

Figure 4.5 (c) represents the resulted surfaces after deposition of POPC/DOTAP/Bodipy-cholesterol (89:10:01) liposomes on mixed Fc-SAMs (a-top), and on patterned mixed Fc-SAMs on gold (a-bottom). It is evident from both images that, there is almost no deposition occurred. If seen carefully, the patterns are found to be very faint. From these observations and considering liposomes zeta potential 54.6 ± 2.6 mV, it can be concluded that due to repulsion between the

like charges, depositions of liposomes are discouraged. This also indicates that, electrostatic interaction being the primary contributing factor for initiating the deposition.

In case of neutral liposome system POPC/Bodipy-Chol, we observed good deposition even if the electrostatic attraction was absent assuming the value of zeta potential of the liposomes (-1.06 ± 1.12 mV) is true. And, the deposition almost exclusively occurred on patches of Fc-SAMs while both SAMs and gold surface was offered as patterned Fc-SAMs on gold. These observations suggest, there might be some secondary factors contributing towards deposition despite there is no electrostatic attraction between liposomes and surface. Upon Fc-oxidation, the SAMs surface suddenly holding all these $Fc^{+}$, incurred a dramatic change in surface hydrophilicity while increased. The water molecule in the vicinity of the surface has to rearrange themselves to maintain dipole-dipole balance. At the same time, the solvated liposomes near the surface also has to respond to this sudden change. Polar headgroup of the lipids constitutes the outer surface of the liposomes, those polar headgroup can easily interact with the hydrophilic SAMs surface, and hence deposited on surface. Since rehydration of deposited liposomes and the SAMs-surface would burden the system with large entropic penalty, the deposited liposomes prefer to stay on the surface even after lifting the applied potential. In case of positively charged liposomes, the electrostatic repulsion is so strong that, it surpasses any secondary polar interactions that might have been in effect otherwise between liposomes and the SAMs surface. Although these assumptions are being made according to current observation, further study in detail is required to be able to establish a definitive mechanistic difference between the deposition processes of negative, charge neutral, and positively charged particles/materials. Studies are currently ongoing in our laboratory to serve the purpose.

## 4.4. Conclusion

Above we have demonstrated deposition of various materials including metal & metal oxide nanoparticles, carbon nanotubes, quantum dots, and especially a novel kind of deposition for liposomes using our previously developed electrochemical method.[28,28] We have characterized the depositions of metal nanoparticles, metal-oxide nanoparticles, and carbon nanotubes by using AFM. We also have characterized deposition for quantum dots and three different liposome systems with confocal fluorescence microscope. Although further characterization is required in each case, this study helps us to establish our electrochemical method as a truly general deposition method for a wide variety of chemical entities including charged polymers (negative & positive), aqueous suspended colloids, biomaterials, soft materials, and various nano- and micro- materials of technological interest. To showcase the true capability of our deposition method while demonstrated deposition of charge neutral materials in this study. We also have attempted to explore the mechanistic differences between the deposition processes of negative, charge neutral, and positively charged particles/materials.

The approaches described here offers exciting new possibilities. Deposition of all these materials on electrode surface would provide the electrode to gain new identities upon which numerous chemistries can be launched. On the other hand, the low-voltage, convenient and fast operation characteristic of this approach should make it an appealing alternative for materials deposition. Since its an electrochemical approach, this deposition in principle should work for planar, non-planer and substrate with any size as long as a uniform distribution of potential is maintained across the substrate surface. Therefore, it can be particularly interesting for large industrial applications also.

**References**


(1) Katz, E.; Willner, I.; Wang, J. Electroanalytical and Bioelectroanalytical Systems Based on Metal and Semiconductor Nanoparticles. *Electroanalysis* **2004**, *16* (1–2), 19–44. https://doi.org/10.1002/elan.200302930.

(2) Kang, M.; Mun, C. W.; Jung, H. S.; Ansah, I. B.; Kim, E.; Yang, H.; Payne, G. F.; Kim, D. H.; Park, S. G. Tethered Molecular Redox Capacitors for Nanoconfinement-Assisted Electrochemical Signal Amplification. *Nanoscale* **2020**, *12* (6), 3668–3676. https://doi.org/10.1039/c9nr08136d.

(3) Li, J.; Maniar, D.; Qu, X.; Liu, H.; Tsao, C. Y.; Kim, E.; Bentley, W. E.; Liu, C.; Payne, G. F. Coupling Self-Assembly Mechanisms to Fabricate Molecularly and Electrically Responsive Films. *Biomacromolecules* **2019**, *20* (2), 969–978. https://doi.org/10.1021/acs.biomac.8b01592.

(4) Li, J.; Wu, S.; Kim, E.; Yan, K.; Liu, H.; Liu, C.; Dong, H.; Qu, X.; Shi, X.; Shen, J.; et al. Electrobiofabrication: Electrically Based Fabrication with Biologically Derived Materials. *Biofabrication* **2019**, *11* (3). https://doi.org/10.1088/1758-5090/ab06ea.

(5) Gooding, J. J.; Wibowo, R.; Liu, J.; Yang, W.; Losic, D.; Orbons, S.; Mearns, F. J.; Shapter, J. G.; Hibbert, D. B. Protein Electrochemistry Using Aligned Carbon Nanotube Arrays. *J. Am. Chem. Soc.* **2003**, *125* (30), 9006–9007. https://doi.org/10.1021/ja035722f.

(6) Patolsky, F.; Weizmann, Y.; Willner, I. Long-Range Electrical Contacting of Redox Enzymes by SWCNT Connectors. *Angew. Chemie - Int. Ed.* **2004**, *43* (16), 2113–2117. https://doi.org/10.1002/anie.200353275.

(7) Chou, A.; Böcking, T.; Liu, R.; Singh, N. K.; Moran, G.; Gooding, J. J. Effect of Dialysis on the Electrochemical Properties of Acid-Oxidized Single-Walled Carbon Nanotubes. *J.*

*Phys. Chem. C* **2008**, *112* (36), 14131–14138. https://doi.org/10.1021/jp7113785.

(8) Shein, J. B.; Lai, L. M. H.; Eggers, P. K.; Paddon-Row, M. N.; Gooding, J. J. Formation of Efficient Electron Transfer Pathways by Adsorbing Gold Nanoparticles to Self-Assembled Monolayer Modified Electrodes. *Langmuir* **2009**, *25* (18), 11121–11128. https://doi.org/10.1021/la901421m.

(9) Herrera, S. E.; Davia, F. G.; Williams, F. J.; Calvo, E. J. Metal Nanoparticle Enhancement of Electron Transfer to Tethered Redox Centers through Self-Assembled Molecular Films. *Langmuir* **2019**, *35* (19), 6297–6303. https://doi.org/10.1021/acs.langmuir.9b00280.

(10) Lee, S.; Yoon, J. H.; Yoon, S. Adsorption Patterns of Gold Nanoparticles on Methyl-Terminated Self-Assembled Monolayers. *J. Phys. Chem. C* **2011**, *115* (25), 12501–12507. https://doi.org/10.1021/jp202013j.

(11) Kim, G. H.; García De Arquer, F. P.; Yoon, Y. J.; Lan, X.; Liu, M.; Voznyy, O.; Yang, Z.; Fan, F.; Ip, A. H.; Kanjanaboos, P.; et al. High-Efficiency Colloidal Quantum Dot Photovoltaics via Robust Self-Assembled Monolayers. *Nano Lett.* **2015**, *15* (11), 7691–7696. https://doi.org/10.1021/acs.nanolett.5b03677.

(12) Hu, X.; Dong, S. Metal Nanomaterials and Carbon Nanotubes - Synthesis, Functionalization and Potential Applications towards Electrochemistry. *J. Mater. Chem.* **2008**, *18* (12), 1279–1295. https://doi.org/10.1039/b713255g.

(13) Lee, S. W.; Drwiega, J.; Wu, C. Y.; Mazyck, D.; Sigmund, W. M. Anatase TiO2 Nanoparticle Coating on Barium Ferrite Using Titanium Bis-Ammonium Lactato Dihydroxide and Its Use as a Magnetic Photocatalyst. *Chem. Mater.* **2004**, *16* (6), 1160–1164. https://doi.org/10.1021/cm0351902.

(14) Shen, G. X.; Chen, Y. C.; Lin, C. J. Corrosion Protection of 316 L Stainless Steel by a TiO2 Nanoparticle Coating Prepared by Sol-Gel Method. *Thin Solid Films* **2005**, *489* (1–2), 130–136. https://doi.org/10.1016/j.tsf.2005.05.016.

(15) Prevo, B. G.; Hwang, Y.; Velev, O. D. Convective Assembly of Antireflective Silica Coatings with Controlled Thickness and Refractive Index. *Chem. Mater.* **2005**, *17* (14), 3642–3651. https://doi.org/10.1021/cm050416h.

(16) Kommireddy, D. S.; Sriram, S. M.; Lvov, Y. M.; Mills, D. K. Stem Cell Attachment to Layer-by-Layer Assembled TiO2 Nanoparticle Thin Films. *Biomaterials* **2006**, *27* (24), 4296–4303. https://doi.org/10.1016/j.biomaterials.2006.03.042.

(17) Chen, D.; Wang, G.; Li, J. Interfacial Bioelectrochemistry: Fabrication, Properties and Applications of Functional Nanostructured Biointerfaces. *J. Phys. Chem. C* **2007**, *111* (6), 2351–2367. https://doi.org/10.1021/jp065099w.

(18) Liu, Y.; Li, J.; Tschirhart, T.; Terrell, J. L.; Kim, E.; Tsao, C. Y.; Kelly, D. L.; Bentley, W. E.; Payne, G. F. Connecting Biology to Electronics: Molecular Communication via Redox Modality. *Adv. Healthc. Mater.* **2017**, *6* (24), 1–19. https://doi.org/10.1002/adhm.201700789.

(19) Lan, X.; Voznyy, O.; Kiani, A.; García De Arquer, F. P.; Abbas, A. S.; Kim, G. H.; Liu, M.; Yang, Z.; Walters, G.; Xu, J.; et al. Passivation Using Molecular Halides Increases Quantum Dot Solar Cell Performance. *Adv. Mater.* **2016**, *28* (2), 299–304. https://doi.org/10.1002/adma.201503657.

(20) Jin, D.; Yu, J.; Yuan, K.; Zhang, L. Mimicking the Structure and Function of Ant Bridges in a Reconfigurable Microswarm for Electronic Applications. *ACS Nano* **2019**, *13* (5), 5999–6007. https://doi.org/10.1021/acsnano.9b02139.

(21) Hu, X.; Wang, T.; Wang, L.; Dong, S. Surface-Enhanced Raman Scattering of 4-Aminothiophenol Self-Assembled Monolayers in Sandwich Structure with Nanoparticle Shape Dependence: Off-Surface Plasmon Resonance Condition. *J. Phys. Chem. C* **2007**, *111* (19), 6962–6969. https://doi.org/10.1021/jp0712194.

(22) Jiang, C.; Elliott, J. M.; Cardin, D. J.; Tsang, S. C. An Electrochemical Study of 4-Aminothiophenol/Pt Nanoparticle Multilayers on Gold Electrodes. *Langmuir* **2009**, *25* (1), 534–541. https://doi.org/10.1021/la802567a.

(23) Dong, T. Y.; Wu, H. H.; Lin, M. C. Superlattice of Octanethiol-Protected Copper Nanoparticles. *Langmuir* **2006**, *22* (16), 6754–6756. https://doi.org/10.1021/la053438r.

(24) Jun, Y. W.; Seo, J. W.; Cheon, J. Nanoscaling Laws of Magnetic Nanoparticles and Their Applicabilities in Biomedical Sciences. *Acc. Chem. Res.* **2008**, *41* (2), 179–189. https://doi.org/10.1021/ar700121f.

(25) Chavali, M. S.; Nikolova, M. P. Metal Oxide Nanoparticles and Their Applications in Nanotechnology. *SN Appl. Sci.* **2019**, *1* (6), 1–30. https://doi.org/10.1007/s42452-019-0592-3.

(26) Coe-Sullivan, S.; Steckel, J. S.; Woo, W. K.; Bawendi, M. G.; Bulovic, V. Large-Area Ordered Quantum-Dot Monolayers via Phase Separation during Spin-Casting. *Adv. Funct. Mater.* **2005**, *15* (7), 1117–1124. https://doi.org/10.1002/adfm.200400468.

(27) Park, J. J.; De Paoli Lacerda, S. H.; Stanley, S. K.; Vogel, B. M.; Kim, S.; Douglas, J. F.; Raghavan, D.; Karim, A. Langmuir Adsorption Study of the Interaction of CdSe/ZnS Quantum Dots with Model Substrates: Influence of Substrate Surface Chemistry and PH. *Langmuir* **2009**, *25* (1), 443–450. https://doi.org/10.1021/la802324c.

(28) Iqbal, M. S.; Zhan, W. Electrochemically Triggered Interfacial Deposition/Assembly of Aqueous-Suspended Colloids. *ChemElectroChem* **2020**, *7* (5), 1097–1106. https://doi.org/10.1002/celc.201902143.

(29) Tamrakar, S.; An, Q.; Thostenson, E. T.; Rider, A. N.; Haque, B. Z.; Gillespie, J. W. Tailoring Interfacial Properties by Controlling Carbon Nanotube Coating Thickness on Glass Fibers Using Electrophoretic Deposition. *ACS Appl. Mater. Interfaces* **2016**, *8* (2), 1501–1510. https://doi.org/10.1021/acsami.5b10903.

(30) Iqbal, M. S.; Zhan, W. Electrochemically Triggered Surface Deposition of Polyelectrolytes. *Langmuir* **2018**, *34* (43), 12776–12786. https://doi.org/10.1021/acs.langmuir.8b02671.

(31) Kočišová, E.; Petr, M.; Šípová, H.; Kylián, O.; Procházka, M. Drop Coating Deposition of a Liposome Suspension on Surfaces with Different Wettabilities: "Coffee Ring" Formation and Suspension Preconcentration. *Phys. Chem. Chem. Phys.* **2017**, *19* (1), 388–393. https://doi.org/10.1039/c6cp07606h.

(32) Smoukov, S. K.; Bishop, K. J. M.; Kowalczyk, B.; Kalsin, A. M.; Grzybowski, B. A. Electrostatically "Patchy" Coatings via Cooperative Adsorption of Charged Nanoparticles. *J. Am. Chem. Soc.* **2007**, *129* (50), 15623–15630. https://doi.org/10.1021/ja075456w.

(33) Chen, S. Langmuir-Blodgett Fabrication of Two-Dimensional Robust Cross-Linked Nanoparticle Assemblies. *Langmuir* **2001**, *17* (9), 2878–2884. https://doi.org/10.1021/la001728w.

(34) Niemeyer, C. M.; Ceyhan, B.; Noyong, M.; Simon, U. Bifunctional DNA-Gold Nanoparticle Conjugates as Building Blocks for the Self-Assembly of Cross-Linked

Particle Layers. *Biochem. Biophys. Res. Commun.* **2003**, *311* (4), 995–999. https://doi.org/10.1016/j.bbrc.2003.10.103.

(35) Quinn, B. M.; Dekker, C.; Lemay, S. G. Electrodeposition of Noble Metal Nanoparticles on Carbon Nanotubes. *J. Am. Chem. Soc.* **2005**, *127* (17), 6146–6147. https://doi.org/10.1021/ja0508828.

(36) López, I.; Vázquez, A.; Hernández-Padrón, G. H.; Gómez, I. Electrophoretic Deposition (EPD) of Silver Nanoparticles and Their Application as Surface-Enhanced Raman Scattering (SERS) Substrates. *Appl. Surf. Sci.* **2013**, *280*, 715–719. https://doi.org/10.1016/j.apsusc.2013.05.048.

(37) Fan, H.; Wright, A.; Gabaldon, J.; Rodriguez, A.; Brinker, C. J.; Jiang, Y. B. Three-Dimensionally Ordered Gold Nanocrystal/Silica Superlattice Thin Films Synthesized via Sol-Gel Self-Assembly. *Adv. Funct. Mater.* **2006**, *16* (7), 891–895. https://doi.org/10.1002/adfm.200500603.

(38) Xie, H.; Jiang, K.; Zhan, W. A Modular Molecular Photovoltaic System Based on Phospholipid/Alkanethiol Hybrid Bilayers: Photocurrent Generation and Modulation. *Phys. Chem. Chem. Phys.* **2011**, *13* (39), 17712–17721. https://doi.org/10.1039/c1cp21701a.

(39) Pichon, B. P.; Demortière, A.; Pauly, M.; Mougin, K.; Derory, A.; Beǵin-Colin, S. 2D Assembling of Magnetic Iron Oxide Nanoparticles Promoted by SAMs Used as Well-Addressed Surfaces. *J. Phys. Chem. C* **2010**, *114* (19), 9041–9048. https://doi.org/10.1021/jp101872u.

(40) Nakanishi, T.; Masuda, Y.; Koumoto, K. Deposition of γ-FeOOH, Fe3O4 and Fe on Pd-Catalyzed Substrates. *J. Cryst. Growth* **2005**, *284* (1–2), 176–183.

https://doi.org/10.1016/j.jcrysgro.2005.07.012.

(41) Diao, P.; Liu, Z. Electrochemistry at Chemically Assembled Single-Wall Carbon Nanotube Arrays. *J. Phys. Chem. B* **2005**, *109* (44), 20906–20913. https://doi.org/10.1021/jp052666r.

(42) Wayu, M. B.; Pannell, M. J.; Labban, N.; Case, W. S.; Pollock, J. A.; Leopold, M. C. Functionalized Carbon Nanotube Adsorption Interfaces for Electron Transfer Studies of Galactose Oxidase. *Bioelectrochemistry* **2019**, *125*, 116–126. https://doi.org/10.1016/j.bioelechem.2018.10.003.

# CHAPTER 5. CONCLUSION

In previous three chapters, we have discussed about a general and facile electrochemical method for deposition/assembly of various chemical entities including polyelectrolytes, aqueous suspended colloids, biomaterials, soft materials, and nano- & micro- materials of other kinds. We have demonstrated in detail deposition of those materials on electrode surface and some keys factors involving deposition processes.

We have started with a redox active surface i.e. ferrocene terminated self-assembled monolayers (SAMs) of thiol on gold. Surface confined redox assemblies in the form of SAMs are superior to solution based redox species because of several reasons: (i) they provide ordered and densely packed assemblies leading to stronger and specific interactions which ensures fast responses, (ii) these are compatible with different media, (iii) offer high sensitivity, and (iv) ensure reproducibility in responses/results. Ferrocene-terminated SAMs have been used in the system for studying fundamental electron transfer processes,[1,2] biosensing[3,4], electroactuation[5], and molecular photovoltaics[6,7], etc. We had envisioned to expand the utility of Fc-SAMs by integrating them with different materials via electrochemical deposition of materials on the surfaces utilizing their built-in redox capabilities. This kind of integration would provide the SAMs surface (electrode surface) a new identity with the materials deposited/assembled. Those surfaces with new properties offer the possibility of launching a variety of new chemistries. Moreover, the redox active layer beneath the deposited materials can be removed by electrochemical desorption of thiols. Electrode surfaces modified with different materials have been employed in a wide range of applications including electroanalytical analysis[8], heterogeneous catalysis[8,9], corrosion protection[10], antireflective films[11], substrates for cell adhesion[12], bioelectronics[13], energy storage device, energy conversion[14], microelectronics[15], etc.

In chapter 2, we have presented a new approach to polyelectrolyte surface deposition based on electrochemical triggering. Starting from the same basic structure, ferrocene-decorated self-assembled monolayers (Fc-SAMs), this approach enables quantitative deposition of both polyanions and polycations with a wide range of chemical identities (synthetic polymers, peptides, and DNA) and molecular weights ($10^3$–$10^7$ Da). Such generality, combined with its ready access to conventional layer-by-layer (LbL) film formation and electrochemical detection, should make this approach useful in a number of areas.

For example, these polyelectrolytes modified redox active surfaces are promising for electroactuation applications. Redox actuation of a microcantilever driven by a self-assembled ferrocenyl undecane thiolate monolayer has been reported earlier by Badia and co-workers. They reported, oxidation of the Fc-SAMs in a perchlorate electrolyte generating a cantilever deflections ranging from ~0.8 μm to ~60 nm for spring constants between ~0.01 and ~0.8 $Nm^{-1}$.[5] Although encouraging but these deflections are relatively small for a real life application. On the other hand, our integrated Fc-SAMs with polyelectrolytes on their surfaces might be a better candidate towards improvement in this regard. This kind of platform may respond to electric field upon potential sweep. The electrostatic attraction/repulsion between flexible polyelectrolytes with the charges on electroactive surface might be able to exert/release stress on electrode which may results in deflection at a certain direction. As we have ready access to deposition of both polyanion and polycation[16], the direction of the deflection may be better controlled. Further investigations are required to make our platform useful towards development of an actuator.

LbL films or polyelectrolytes (PE) films can be used as membranes for nanofiltration and water purification.[17,18] Now, even after deposition of polyelectrolytes, our Fc-SAMs was found to

remain active as a redox surface, and the polyelectrolyte films are porous.[16] Thus loading the resulting system with different kinds of materials to further enhance the films filtration property seems possible. Redox active Fc-SAMs may also act as a probe to monitor the ingress and egress of small ions through PE films to monitor the effectivity of the thick LbL film as a filter. Investigations can be done to test these capabilities. Moreover, this technology can also be used in polyelectrolyte-based diagnosis, drugs/biomaterials delivery, etc.[19]

Polyelectrolytes when deposited on surface, are capable of modifying the wettability of the surface. Since our method is suitable for deposition of both negative and positively charged polyelectrolytes with wide range of molecular weights, this can be useful towards attaining desired surface wettability. Surfaces with controlled wettability might find prospective biological applications as optimum surface conditions are often required for biomaterials.[20] On the other hand, surfaces modified with polyelectrolytes or LbL are well known for enhanced durability, corrosion prevention and flame retardation.[21,22] Further investigation on these direction can be launched using our electrochemical method for modifying surfaces with polyelectrolytes. The release of LbL film might be possible by electrochemical means by utilizing the redox active Fc-SAMs layer beneath the resulting film. All these possibilities can be tested.

In chapter 3, we have presented a new electrochemical method for efficient and straightforward deposition/assembly of aqueous suspended colloids on electrode surfaces. Using carboxylic terminated polystyrene nano-/microbeads as a model colloid, we characterized this electrochemically triggered process in detail; by comparing its performance with conventional, electrically driven processes, we demonstrated superior deposition efficiency achievable with this new method. To showcase the potential utility of this method, we also demonstrated fast and high-fidelity colloid micropattern formation on electrodes.[23]

In addition to SAMs great ability to control and tune various physicochemical parameters involved the deposition process, the addition of well-defined faradaic reactions offers a new and largely independent mechanism to induce secondary electric field components. By controlling the Fc-density across the SAMs, one can control the materials deposition. Moreover, we have demonstrated that, by varying the scan rate or adjusting potential window, it is also possible to control the amount of materials deposition on surface. These easy to maneuver controls provide this methodology a great flexibility. More importantly, such gains in control and efficiency can be achieved without complicating/compromising the solution phase.

Recently Zhang and co-workers demonstrated facile fabrication process for microswarm on electrode surface using conductive paramagnetic nanoparticles. Their microswarm system is capable of generating a conductive pathway for electrons across a gap far beyond the capabilities of the individual building blocks.[15] This kind on platform can be used as a switch in electrical circuits. Our developed technology has a similar potential with better control factors on board. Our electrochemical method is already capable of micropattern formation of materials on electrode surfaces. Since we have an electroactive layer underneath, we can possibly use that trigger to desorb material by electrochemical triggering and reabsorbing the materials with a reverse potential. Investigation towards this direction can be launched to explore these capabilities.

Colloidal semiconductor nanocrystals (SCNCs) have found recent attention for their potential application in display devices. Controlling size, shape and composition of these materials in devices is essential to benefit from their powerful properties in optoelectronic applications.[24] We have demonstrated not only the deposition of colloidal materials towards 2D crystal formation but also explored size dependent depositions. More importantly, with our electrochemical

method in combination with conventional microcontact printing, micropattern formation is possible. With control of size, shape and composition, application towards display devices can be explored. Moreover, colloidal crystals has found applications in photodetectors & solar cells[25], field-effect transistors (FETs)[26,27], memory devices[28], etc. All these possibilities can be tested with our developed techniques.

In chapter 4, we have demonstrated deposition of various materials including metal nanoparticles (Au NPs) metal oxide nanoparticles ($Fe_3O_4$ NPs), multi walled carbon nanotubes (MWCNTs), CdSSe/ZnS core-shell quantum dots (QDs), and especially a novel kind of deposition for liposomes using our previously developed electrochemical method. We have also explored mechanistic differences among the deposition processes of negative, charge neutral, and positively charged particles/materials using different liposomes system as models by effective charge control.

Colloidal nanocrystals formed from quantum dots have exciting applications in electronic devices. For example, colloidal nanocrystals (NCs) have been explored as emitters for thin film light emitting diodes (LEDs). CdSe/ZnS core–shell NCs and QDs are often used for this purpose.[29,30] We have demonstrated deposition of carboxyl functionalized CdSSe/ZnS core shell QDs on surface. Since our technique is capable of micropattern formation by a combination of top down and bottom up approaches, it is possible to have patterned structures with different compositions on electrode surfaces seems possible. This will enable controlled device fabrication for LED applications.

CNTs are often grafted on surface using bottom up chemical approaches in the form of amide bond formation between functional groups of CNTs and substrates, which are time consuming

and costly. And, physical deposition of CNTs are suffered with stability issue. Our method on the other hand is very strait forward, cost effective and time efficient. We also found better stability of materials on surface compared to conventional similar techniques.[23] CNTs modified electrodes are being used as nanoelectrode to enhance electrode efficiency.[31,32] Investigations on stability of CNTs on electrode surface produced by our techniques should be explored to claim its prospective superiority over conventional tethering methods.

Scientists have demonstrated deposition of metal nanoparticles on electrode for enhancement of electron transfer.[33,34] Assembly of the AuNPs-SAMs-gold substrate provides metal-metal junctions formed between nanoparticles and metal substrates where electron tunneling and nonlinear optical properties such as Raman scattering can occur.[35] There are numerus applications already demonstrated for metal and metal oxide modified surfaces. By utilizing our novel techniques, formation of different types of meta nanocrystals, and different pattern formation and their utility can be explored.

Another general application of this method can be integration of materials of interest onto electrode surface to generate chemically modified electrodes. Thus produced platform might be useful towards enhancing the electrocatalytic efficiency of oxidation or reduction processes commonly used in energy transfer reactions.

Last but not the least, we have demonstrated a novel electrochemical deposition technique for liposomes on surface. Surfaces modified with this deposition process can now be widely explored. Currently, in our lab we are exploring the impact of charge density on deposition and on the resulted surface using EQCM. This should provide us with a clearer picture about the mechanism involved. Liposomes has received attention over last couple of decades for drug

delivery applications.[36,37] As we demonstrated a novel deposition for liposomes, key factors such as their size, lipid composition, and other aspects involving their deposition can be explored.

Our developed electrochemical deposition technique can be regarded as one pot electrofabrication. This process offers convenient operations, cost effectiveness, robustness, and capability of handling many materials including polyelectrolytes (both negative & positive), colloidal materials, biomaterials (peptides, proteins, DNA), soft materials (lipids, liposomes), and many other nano- and micro- materials would make this technique truly useful and efficient for material deposition on surfaces. Its ready access to LbL film formation, and micropattern formation on electrode surface would open doors to many useful technological advances in different areas of scientific research.

**References**


(1) Smalley, J. F.; Finklea, H. O.; Chidsey, C. E. D.; Linford, M. R.; Creager, S. E.; Ferraris, J. P.; Chalfant, K.; Zawodzinsk, T.; Feldberg, S. W.; Newton, M. D. Heterogeneous Electron-Transfer Kinetics for Ruthenium and Ferrocene Redox Moieties through Alkanethiol Monolayers on Gold. *J. Am. Chem. Soc.* **2003**, *125* (7), 2004–2013. https://doi.org/10.1021/ja028458j.

(2) Eckermann, A. L.; Feld, D. J.; Shaw, J. A.; Meade, T. J. Electrochemistry of Redox-Active Self-Assembled Monolayers. *Coord. Chem. Rev.* **2010**, *254* (15–16), 1769–1802. https://doi.org/10.1016/j.ccr.2009.12.023.

(3) Umek, R. M.; Lin, S. W.; Vielmetter, J.; Terbrueggen, R. H.; Irvine, B.; Yu, C. J.; Kayyem, J. F.; Yowanto, H.; Blackburn, G. F.; Farkas, D. H.; et al. Electronic Detection of Nucleic Acids: A Versatile Platform for Molecular Diagnostics. *J. Mol. Diagnostics* **2001**, *3* (2), 74–84. https://doi.org/10.1016/S1525-1578(10)60655-1.

(4) Fan, C.; Plaxco, K. W.; Heeger, A. J. Electrochemical Interrogation of Conformational Changes as a Reagentless Method for the Sequence-Specific Detection of DNA. *Proc. Natl. Acad. Sci. U. S. A.* **2003**, *100* (16), 9134–9137. https://doi.org/10.1073/pnas.1633515100.

(5) Norman, L. L.; Badia, A. Redox Actuation of a Microcantilever Driven by a Self-Assembled Ferrocenylundecanethiolate Monolayer: An Investigation of the Origin of the Micromechanical Motion and Surface Stress. *J. Am. Chem. Soc.* **2009**, *131* (6), 2328–2337. https://doi.org/10.1021/ja808400s.

(6) Imahori, H.; Yamada, H.; Nishimura, Y.; Yamazaki, I.; Sakata, Y. Vectorial Multistep Electron Transfer at the Gold Electrodes Modified with Self-Assembled Monolayers of Ferrocene - Porphyrin - Fullerene Triads. *J. Phys. Chem. B* **2000**, *104* (9), 2099–2108. https://doi.org/10.1021/jp993784f.

(7) Xie, H.; Jiang, K.; Zhan, W. A Modular Molecular Photovoltaic System Based on Phospholipid/Alkanethiol Hybrid Bilayers: Photocurrent Generation and Modulation. *Phys. Chem. Chem. Phys.* **2011**, *13* (39), 17712–17721. https://doi.org/10.1039/c1cp21701a.

(8) Hu, X.; Dong, S. Metal Nanomaterials and Carbon Nanotubes - Synthesis, Functionalization and Potential Applications towards Electrochemistry. *J. Mater. Chem.* **2008**, *18* (12), 1279–1295. https://doi.org/10.1039/b713255g.

(9) Lee, S. W.; Drwiega, J.; Wu, C. Y.; Mazyck, D.; Sigmund, W. M. Anatase TiO2 Nanoparticle Coating on Barium Ferrite Using Titanium Bis-Ammonium Lactato Dihydroxide and Its Use as a Magnetic Photocatalyst. *Chem. Mater.* **2004**, *16* (6), 1160–1164. https://doi.org/10.1021/cm0351902.

(10) Shen, G. X.; Chen, Y. C.; Lin, C. J. Corrosion Protection of 316 L Stainless Steel by a TiO2 Nanoparticle Coating Prepared by Sol-Gel Method. *Thin Solid Films* **2005**, *489* (1–2), 130–136. https://doi.org/10.1016/j.tsf.2005.05.016.

(11) Prevo, B. G.; Hwang, Y.; Velev, O. D. Convective Assembly of Antireflective Silica Coatings with Controlled Thickness and Refractive Index. *Chem. Mater.* **2005**, *17* (14), 3642–3651. https://doi.org/10.1021/cm050416h.

(12) Kommireddy, D. S.; Sriram, S. M.; Lvov, Y. M.; Mills, D. K. Stem Cell Attachment to Layer-by-Layer Assembled TiO2 Nanoparticle Thin Films. *Biomaterials* **2006**, *27* (24), 4296–4303. https://doi.org/10.1016/j.biomaterials.2006.03.042.

(13) Chen, D.; Wang, G.; Li, J. Interfacial Bioelectrochemistry: Fabrication, Properties and Applications of Functional Nanostructured Biointerfaces. *J. Phys. Chem. C* **2007**, *111* (6), 2351–2367. https://doi.org/10.1021/jp065099w.

(14) Lan, X.; Voznyy, O.; Kiani, A.; García De Arquer, F. P.; Abbas, A. S.; Kim, G. H.; Liu, M.; Yang, Z.; Walters, G.; Xu, J.; et al. Passivation Using Molecular Halides Increases Quantum Dot Solar Cell Performance. *Adv. Mater.* **2016**, *28* (2), 299–304. https://doi.org/10.1002/adma.201503657.

(15) Jin, D.; Yu, J.; Yuan, K.; Zhang, L. Mimicking the Structure and Function of Ant Bridges in a Reconfigurable Microswarm for Electronic Applications. *ACS Nano* **2019**, *13* (5), 5999–6007. https://doi.org/10.1021/acsnano.9b02139.

(16) Iqbal, M. S.; Zhan, W. Electrochemically Triggered Surface Deposition of Polyelectrolytes. *Langmuir* **2018**, *34* (43), 12776–12786. https://doi.org/10.1021/acs.langmuir.8b02671.

(17) Lin, Z.; Zhang, Q.; Qu, Y.; Chen, M.; Soyekwo, F.; Lin, C.; Zhu, A.; Liu, Q. LBL

Assembled Polyelectrolyte Nanofiltration Membranes with Tunable Surface Charges and High Permeation by Employing a Nanosheet Sacrificial Layer. *J. Mater. Chem. A* **2017**, *5* (28), 14819–14827. https://doi.org/10.1039/c7ta03183a.

(18) Reurink, D. M.; te Brinke, E.; Achterhuis, I.; Roesink, H. D. W.; de Vos, W. M. Nafion-Based Low-Hydration Polyelectrolyte Multilayer Membranes for Enhanced Water Purification. *ACS Appl. Polym. Mater.* **2019**, *1* (9), 2543–2551. https://doi.org/10.1021/acsapm.9b00689.

(19) Zhao, L.; Skwarczynski, M.; Toth, I. Polyelectrolyte-Based Platforms for the Delivery of Peptides and Proteins. *ACS Biomater. Sci. Eng.* **2019**, *5* (10), 4937–4950. https://doi.org/10.1021/acsbiomaterials.9b01135.

(20) Li, J.; Wu, S.; Kim, E.; Yan, K.; Liu, H.; Liu, C.; Dong, H.; Qu, X.; Shi, X.; Shen, J.; et al. Electrobiofabrication: Electrically Based Fabrication with Biologically Derived Materials. *Biofabrication* **2019**, *11* (3). https://doi.org/10.1088/1758-5090/ab06ea.

(21) Zhao, X.; Yuan, S.; Jin, Z.; Zhang, B.; Liu, N.; Chen, S.; Liu, S.; Sun, X.; Duan, J. Perfect Combination of LBL with Sol-Gel Film to Enhance the Anticorrosion Performance on Al Alloy under Simulated and Accelerated Corrosive Environment. *Materials (Basel).* **2020**, *13* (1). https://doi.org/10.3390/ma13010111.

(22) Kolibaba, T. J.; Shih, C.-C.; Lazar, S.; Tai, B. L.; Grunlan, J. C. Self-Extinguishing Additive Manufacturing Filament from a Unique Combination of Polylactic Acid and a Polyelectrolyte Complex. *ACS Mater. Lett.* **2020**, *2* (1), 15–19. https://doi.org/10.1021/acsmaterialslett.9b00393.

(23) Iqbal, M. S.; Zhan, W. Electrochemically Triggered Interfacial Deposition/Assembly of Aqueous-Suspended Colloids. *ChemElectroChem* **2020**, *7* (5), 1097–1106.

https://doi.org/10.1002/celc.201902143.

(24) Panfil, Y. E.; Oded, M.; Banin, U. Colloidal Quantum Nanostructures: Emerging Materials for Display Applications. *Angew. Chemie - Int. Ed.* **2018**, *57* (16), 4274–4295. https://doi.org/10.1002/anie.201708510.

(25) Sargent, E. H. Solar Cells, Photodetectors, and Optical Sources from Infrared Colloidal Quantum Dots. *Adv. Mater.* **2008**, *20* (20), 3958–3964. https://doi.org/10.1002/adma.200801153.

(26) Talapin, D. V.; Murray, C. B. Applied Physics: PbSe Nanocrystal Solids for n- and p-Channel Thin Film Field-Effect Transistors. *Science (80-. ).* **2005**, *310* (5745), 86–89. https://doi.org/10.1126/science.1116703.

(27) Lee, J. S.; Shevchenko, E. V.; Talapin, D. V. Au-PbS Core-Shell Nanocrystals: Plasmonic Absorption Enhancement and Electrical Doping via Intra-Particle Charge Transfer. *J. Am. Chem. Soc.* **2008**, *130* (30), 9673–9675. https://doi.org/10.1021/ja802890f.

(28) Grochowski, E.; Halem, R. D. Technological Impact of Magnetic Hard Disk Drives on Storage Systems. *IBM Syst. J.* **2003**, *42* (2), 338–346. https://doi.org/10.1147/sj.422.0338.

(29) Steckel, J. S.; Snee, P.; Coe-Sullivan, S.; Zimmer, J. P.; Halpert, J. E.; Anikeeva, P.; Kim, L. A.; Bulovic, V.; Bawendi, M. G. Color-Saturated Green-Emitting QD-LEDs. *Angew. Chemie - Int. Ed.* **2006**, *45* (35), 5796–5799. https://doi.org/10.1002/anie.200600317.

(30) Anikeeva, P. O.; Halpert, J. E.; Bawendi, M. G.; Bulović, V. Quantum Dot Light-Emitting Devices with Electroluminescence Tunable over the Entire Visible Spectrum. *Nano Lett.* **2009**, *9* (7), 2532–2536. https://doi.org/10.1021/nl9002969.

(31) Patolsky, F.; Weizmann, Y.; Willner, I. Long-Range Electrical Contacting of Redox

Enzymes by SWCNT Connectors. *Angew. Chemie - Int. Ed.* **2004**, *43* (16), 2113–2117. https://doi.org/10.1002/anie.200353275.

(32) Chou, A.; Böcking, T.; Liu, R.; Singh, N. K.; Moran, G.; Gooding, J. J. Effect of Dialysis on the Electrochemical Properties of Acid-Oxidized Single-Walled Carbon Nanotubes. *J. Phys. Chem. C* **2008**, *112* (36), 14131–14138. https://doi.org/10.1021/jp7113785.

(33) Shein, J. B.; Lai, L. M. H.; Eggers, P. K.; Paddon-Row, M. N.; Gooding, J. J. Formation of Efficient Electron Transfer Pathways by Adsorbing Gold Nanoparticles to Self-Assembled Monolayer Modified Electrodes. *Langmuir* **2009**, *25* (18), 11121–11128. https://doi.org/10.1021/la901421m.

(34) Herrera, S. E.; Davia, F. G.; Williams, F. J.; Calvo, E. J. Metal Nanoparticle Enhancement of Electron Transfer to Tethered Redox Centers through Self-Assembled Molecular Films. *Langmuir* **2019**, *35* (19), 6297–6303. https://doi.org/10.1021/acs.langmuir.9b00280.

(35) Lee, S.; Yoon, J. H.; Yoon, S. Adsorption Patterns of Gold Nanoparticles on Methyl-Terminated Self-Assembled Monolayers. *J. Phys. Chem. C* **2011**, *115* (25), 12501–12507. https://doi.org/10.1021/jp202013j.

(36) Allen, T. M.; Cullis, P. R. Liposomal Drug Delivery Systems: From Concept to Clinical Applications. *Adv. Drug Deliv. Rev.* **2013**, *65* (1), 36–48. https://doi.org/10.1016/j.addr.2012.09.037.

(37) Dimov, N.; Kastner, E.; Hussain, M.; Perrie, Y.; Szita, N. Formation and Purification of Tailored Liposomes for Drug Delivery Using a Module-Based Micro Continuous-Flow System. *Sci. Rep.* **2017**, *7* (1), 1–13. https://doi.org/10.1038/s41598-017-11533-1.